LA-12212

MCNP: Neutron Benchmark Problems

Los Alamos
NATIONAL LABORATORY

Los Alamos National Laboratory is operated by the University of California for the United States Department of Energy under contract W-7405-ENG-36.

Prepared by Ann Nagy, Group X-6
Edited by Patricia W. Mendius, Group IS-11

An Affirmative Action/Equal Opportunity Employer

LA-12212

UC-705 and UC-714
Issued: November 1991

MCNP: Neutron Benchmark Problems

Daniel J. Whalen
David A. Cardon
Jennifer L. Uhle
John S. Hendricks

Los Alamos
NATIONAL LABORATORY
Los Alamos, New Mexico 87545

MCNP: NEUTRON BENCHMARK PROBLEMS

by

Daniel J. Whalen
David A. Cardon
Jennifer L. Uhle
John S. Hendricks

ABSTRACT

The recent widespread and increased use of radiation transport codes has produced greater user and institutional demand for assurances that such codes give correct results. Responding to these requirements for code validation, the general purpose Monte Carlo transport code MCNP has been tested on criticality, pulsed sphere, and shielding neutron problem families. Results for each were compared to experimental data. MCNP successfully predicted the experimental results of all three families within the expected data and statistical uncertainties. These successful predictions demonstrate that MCNP can successfully model a broad spectrum of neutron transport problems.

I. INTRODUCTION

A. The MCNP Benchmark Project

This document is the second in a series of reports benchmarking the MCNP[1] Monte Carlo computer code. The first document, LA-12196,[2] demonstrated that MCNP accurately models analytic problems and a wide variety of photon experiments. This report demonstrates that MCNP also models a wide variety of neutron problems well.

For the most part, both this report and its companion report, LA-12196, model the same problems chosen to benchmark the COG Monte Carlo code[3] developed at Lawrence Livermore National Laboratory. The criticality problems reported here are the only serious departures from the set chosen for the COG benchmarks. The COG benchmark set represents a wide variety of radiation transport problems. Furthermore, the COG results provide an indication of what constitutes acceptable accuracy. The calculation of k_{eff} for criticality is considered unacceptable if it deviates more than a fraction of a percent from measurements. But for a deep penetration shielding problem, an answer within a factor of two of the experiment is considered reasonable. In all cases presented here, the MCNP calculated results were as good as or better than those of COG and as accurate as could be reasonably expected in a numerical simulation.

B. Problem Overview

All three families of the neutron benchmark problems presented here were the focus of experimental study. Benchmark one is a set of neutron pulsed-sphere experiments conducted at Lawrence Livermore National Laboratory in the late sixties. These pulsed-sphere experiments were used to validate neutron transport codes (such as SORS or TART) then in operation at Livermore. In these experiments, a nearly-isotropic pulsed deuterium-tritium (D-T) neutron source was placed in the

[1] Judith F. Briesmeister, Editor, "MCNP – A General Monte Carlo Code for Neutron and Photon Transport, Version 3A," Los Alamos National Laboratory report LA-7396-M, Rev. 2 (1986).

[2] Daniel J. Whalen, David E. Hollowell, and John S. Hendricks, "MCNP: Photon Benchmark Problems," Los Alamos National Laboratory report LA-12196 (1991).

[3] Thomas P. Wilcox, Jr., and Edward M. Lent, "COG - A Particle Transport Code Designed to Solve the Boltzmann Equation for Deep Penetration (Shielding) Problems," Vol. 4, "Benchmark Problems," Lawrence Livermore National Laboratory report M-221-4 (12/2/88).

centers of spheres of several different diameters and compositions. The time-of-flight energy spectrum of the neutrons leaving a sphere at a given angle was then measured. Thomas Wilcox and Edward Lent used these pulsed-sphere studies to benchmark the LLNL COG Monte Carlo code in 1987. These experiments were chosen for simulation because they involve neutron scattering over a wide range of energies in many different materials. MCNP was used to compute the neutron spectra of these experiments, and its results were compared to the experimental data.

Benchmark two is one of a series of neutron shielding experiments performed by Santoro et al. at Oak Ridge National Laboratory between 1980 and 1985. These experiments were designed to simulate the D-T fusion neutron spectrum at the first wall of a hypothetical fusion reactor. In these experiments a nearly-isotopic D-T neutron source was placed at one end of an iron pipe. The source and pipe were imbedded in a concrete block shield, and a detector outside the source/shield assembly measured the energy spectra of the neutrons and photons leaving the assembly. The different experiments of this series tested various shielding configurations. MCNP was used to model three stainless steel and polyethylene shielding arrangements. This problem was chosen for study because it involves streaming and deep penetration – a formidable variance reduction task. It also involves neutron-induced photon production and coupled neutron-photon transport.

Benchmark three is a family of critical assembly experiments. These experiments measured the neutron multiplication in several different fissionable systems. Four types of critical assemblies were studied:

1. Fast neutron systems
2. Low-enrichment systems
3. Reflected-neutron systems
4. Interacting systems

These criticals were chosen as benchmarks because they are straightforward and test MCNP's criticality eigenvalue estimators. These three neutron benchmarks are summarized in Tables 1 and 2.

TABLE 1

DESCRIPTION OF MCNP NEUTRON BENCHMARK PROBLEMS

Problem Number	Subcategory	Description	Energy Range
1		A pulsed D-T neutron source which is nearly isotropic is placed at the centers of spheres	
	a-p	of various radii and compositions. The time-of-flight spectrum of the neutrons leaving the spheres is measured.	1.6-15.2 MeV
2		A D-T neutron source is placed at one end of an iron pipe. The pipe and source are imbedded in a concrete shield block, with the other end of the pipe open to the air. The energy spectra of the neutrons and photons penetrating steel and polyethylene are measured. This experiment simulates the neutron spectrum at the first wall of a hypothetical fusion reactor.	15.2 MeV to thermal (neutrons) 15.2 MeV to 1 keV (secondary photons)
3		Four types of critical assemblies were experimented with:	2 MeV to thermal
	a	Fast Neutron Systems 1. Godiva: bare uranium sphere (93.71% ^{235}U) 2. Jezebel: bare plutonium sphere - two cases: 95.5% ^{239}Pu and 80% ^{239}Pu	
	b	Low Enrichment systems 1. uranium cylinder: 10.9% ^{235}U 2. uranium cylinder: 14.11% ^{235}U	
	c	Reflected Neutron Systems 1. uranium sphere (93.5% ^{235}U) surrounded by graphite 2. uranium sphere (97.6% ^{235}U) surrounded by water	
	d	Interacting Units 1. three ^{235}U cylinders 2. 3 x 3 array of plutonium fuel rods	

TABLE 2

DESCRIPTION OF MCNP NEUTRON BENCHMARK PROBLEMS

Problem Number	Quantities Computed	Subcategory	Principal Material Composition	Comments
1	Time-of-flight neutron counts	a	^{6}Li : 0.5/1.6 MFP	Sphere radii are expressed in terms of the mean free pathlength of 14 MeV neutrons in the material of interest. The MCNP model had to adopt a very complicated energy/angle source energy distribution to model the pulsed D-T source.
		b	^{7}Li : 0.5/1.6 MFP	
		c	Be : 0.8 MFP	
		d	C : 0.5/2.9 MFP	
		e	N : 1.1/3.1 MFP	
		f	O : 0.7 MFP	
		g	Mg : 0.7/1.9 MFP	
		h	Al : 0.9/2.6 MFP	
		i	Ti : 1.2/3.5 MFP	
		j	Fe : 0.9/4.8 MFP	
		k	Pb : 1.4 MFP	
		l	H_2O : 1.1/1.9 MFP	
		m	D_2O : 1.2/2.1 MFP	
		n	CH_2 (polyethylene) : 0.8/3.5 MFP	
		o	CF_2 (teflon) : 0.9/2.9 MFP	
		p	concrete : 2.0 MFP	
2	Neutron flux/MeV Photon flux/MeV		Concrete, iron, air, stainless steel, paraffin, polyethylene	Neutron streaming and deep penetration: a difficult variance reduction problem; secondary photons are produced
3	k_{eff}	a	Godiva : ^{235}U, ^{238}U Jezebel : ^{240}Pu, ^{239}Pu	$S(\alpha,\beta)$ thermal neutron treatment was used
		b	^{235}U, ^{238}U	
		c	^{235}U, ^{238}U, C, S, Fe, H_2O	
		d	1. ^{235}U, ^{238}U, O, F, H 2. ^{239}Pu, ^{240}Pu, Fe, C, Al	

II. BENCHMARK PROBLEM ONE: PULSED SPHERES

A. Problem History

In the 1960s researchers at Lawrence Livermore National Laboratory initiated the pulsed spheres program to study nuclear cross sections and to validate neutron transport codes such as SORS and TART. In these experiments a pulsed source of approximately 14-MeV neutrons was placed in the centers of spheres of various materials. The time-of-flight spectrum of the neutrons leaving each sphere was then measured. The pulsed spheres are ideal for benchmarking a code such as MCNP because of the relative simplicity of their geometry and experimental data.

B. Experimental Setup

1. Neutron Source and Target Assembly. The T(d,n)^{4}He reaction was used to create a nearly isotropic source of 14-MeV neutrons. The Livermore Insulated Core Transformer (ICT) accelerator directed 400-keV D+ ions at a tritium-loaded titanium target located approximately at the center of a cubical 12.2 meter (40-ft) target pit. The target was a thin tritiated titanium disk 1.2 cm in diameter. The disk was held in place by a low mass structure made primarily of aluminum and stainless steel. Solid spheres of various materials were constructed. Each had a narrow hole from the outside to the center into which the target assembly could be inserted. Spherical containers with very thin walls were used for liquid materials. Neutron detectors were placed at 30 and 120 degrees with respect to the beam line at distances ranging from 752 cm to 975 cm (see Figs. 1, 2, and 3).

In the center-of-mass frame the T(d,n)^{4}He reaction is isotropic. However, in the laboratory frame the intensity and energy are slightly higher in the direction of the deuteron beam than in the opposite direction. The intensity and most probable energy as a function of angle are known.[4]

2. Neutron Detection. Two types of neutron detectors were used: the Pilot B detector and the NE213. Both detectors were operated at a neutron bias of

[4] C. Wong, J. D. Anderson, P. Brown, L. F. Hansen, J. L. Kammerdiener, C. Logan, and B. Pohl, "Livermore Pulsed Sphere Program: Program Summary Through July 1971", Lawrence Livermore National Laboratory report UCRL-51144 Rev. 1 (1972), p. 7.

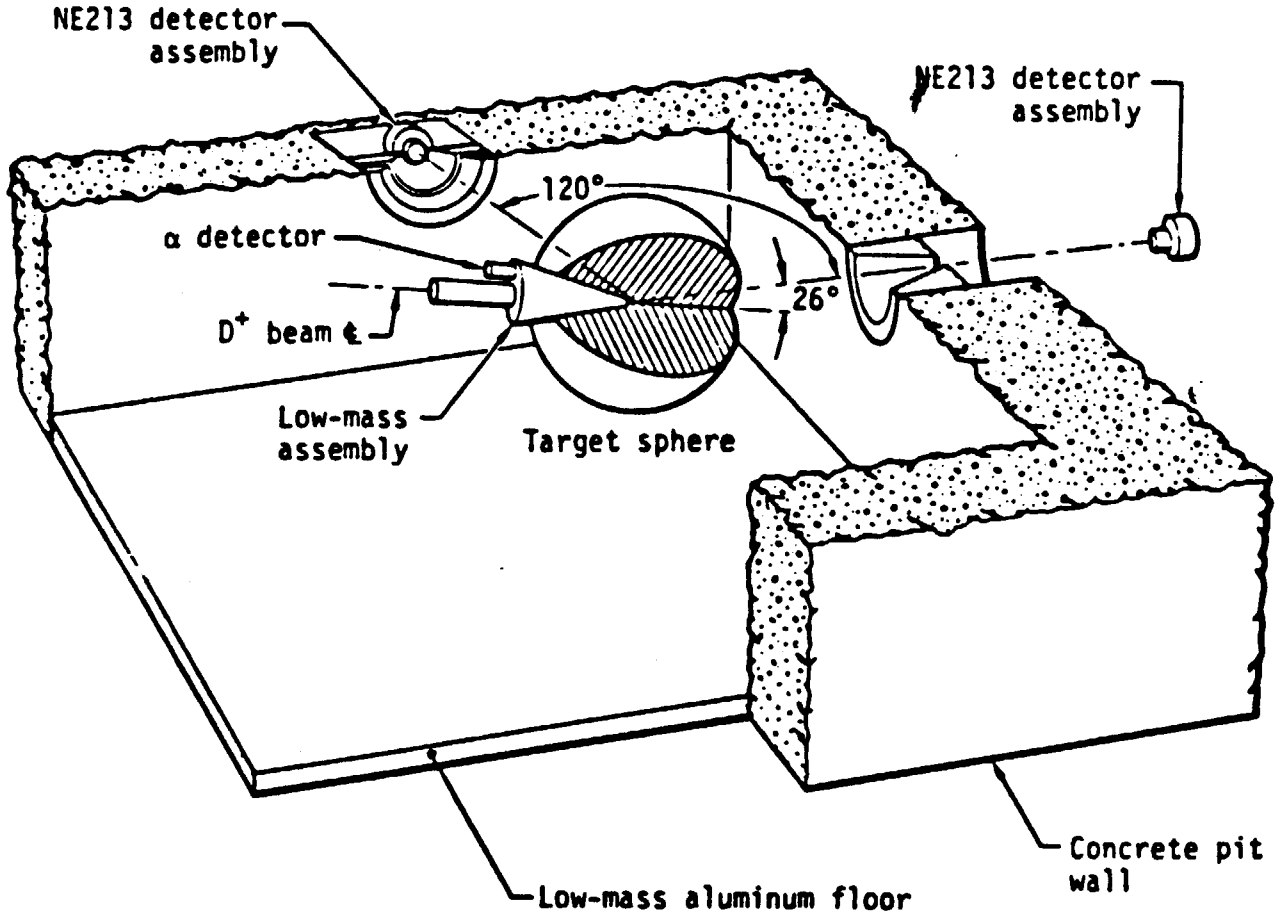

Fig. 1. Time-of-flight geometry of the target sphere and collimated neutron detector in the Livermore pulsed sphere experiments. (Figure taken from Ref. 4.)

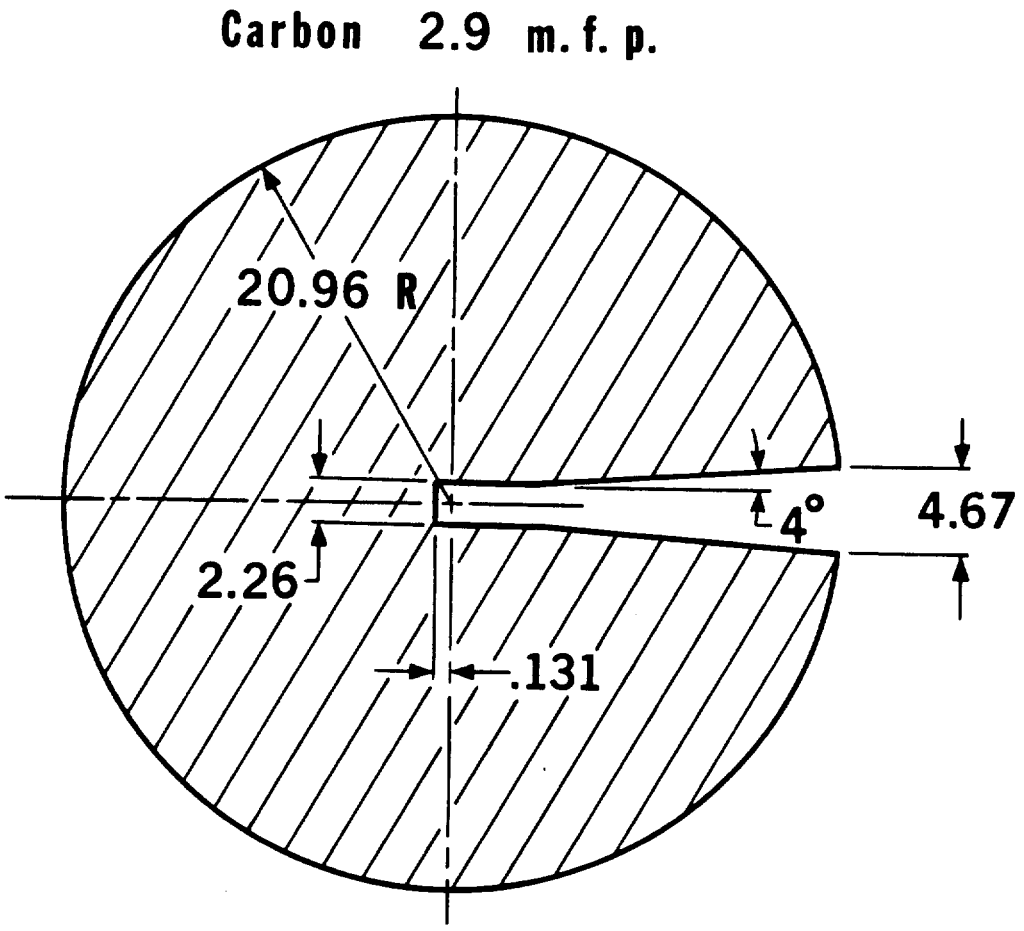

Fig. 2. Diagram showing the specifications of a solid carbon sphere used in the Livermore pulsed sphere experiments. Spheres of other materials were similarly constructed. (Figure taken from Ref. 18.)

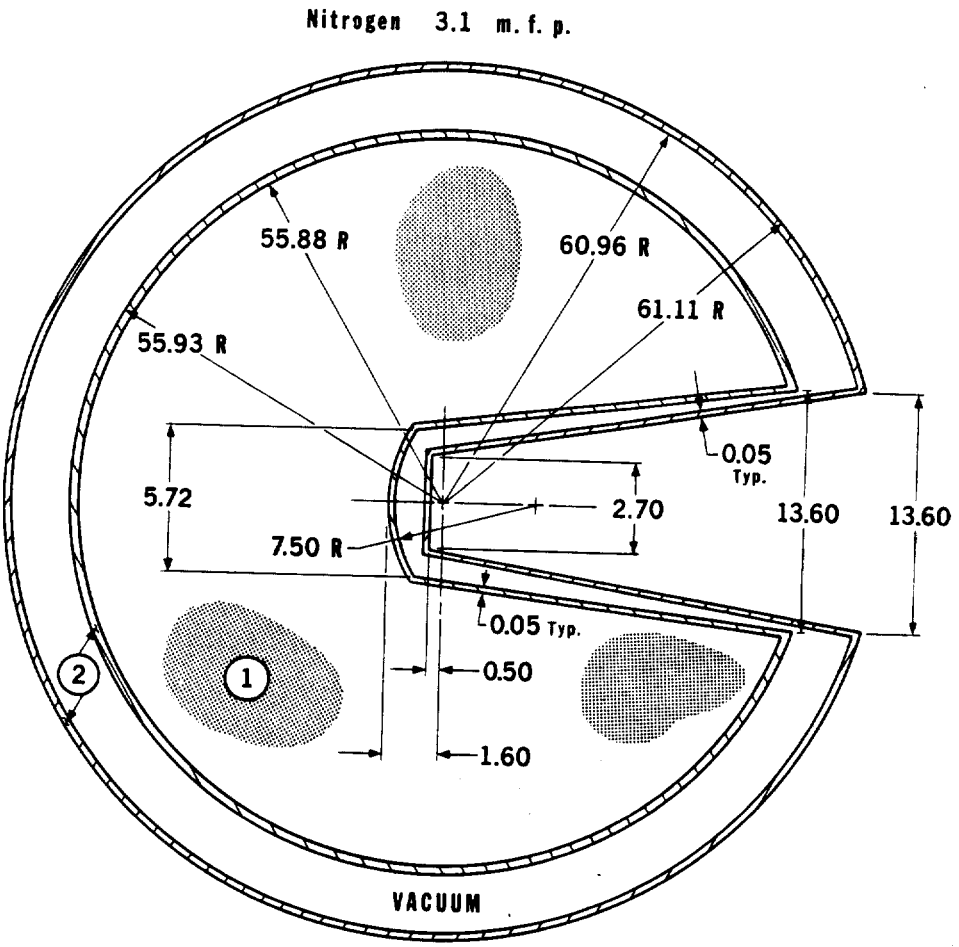

All Dimensions in Centimeters

Zone	Density (g/cm^3)	Material	Atomic %
1	0.808	Liquid N_2	100.0
2	7.9	Fe	68.6
		Cr	20.0
		Ni	8.4
		Si	2.0
		Mn	1.0

Fig. 3. Diagram showing the specifications of the 3.1 mean free path liquid nitrogen sphere used in the Livermore pulsed sphere experiments. Similarly constructed spheres were used for other liquid materials. (Figure taken from Ref. 18.)

1.6 MeV.[5,6,7] Response functions for both detectors at this bias have been measured.[8,9] The detector response functions were not unfolded from the published experimental data.

3. Data. With a sphere of material surrounding the neutron source, the number of detected counts per 2-ns time bin was recorded starting at the beginning of a neutron pulse. The data were then divided by the total number of neutrons recorded from a pulse without the sphere in place. This normalization made the results independent of the accelerator beam intensity.

C. MCNP Problem Model

The MCNP input files for three representative pulsed sphere problem models are in the Appendix in Tables A1-A3.

1. Geometry. The MCNP geometry centers the simulated spherical target assembly at the origin. The spherical assembly is modeled to include the hole into which the tritiated titanium target is inserted in the real experiment (see Fig. 4). The shape and size of the holes vary from material to material. Hence, each input file contains geometry descriptions specific to the sphere being modeled. The spherical target assembly is surrounded by a sphere with a radius of 1000 cm. The region outside the spherical target assembly and inside the large sphere is specified to be air with a standard density of .001288-g/cm^3. The region outside the large sphere is neglected.

---

[5] L. F. Hansen, J. D. Anderson, E. Goldberg, J. Kammerdiener, E. Plechaty, and C. Wong, "Predictions for Neutron Transport in Air, Based on Integral Measurements in Nitrogen and Oxygen at 14 MeV," *Nuclear Science and Engineering* 40, 262-282 (1970), p. 263.

[6] Marion L. Stelts, John D. Anderson, Luisa F. Hansen, Ernest F. Plechaty, and Calvin Wong, "Spectra of Fast Neutrons from Water Pulsed with 14-MeV Neutrons," *Nuclear Science and Engineering* 46, 53-56 (1971), p. 54.

[7] Luisa F. Hansen, John D. Anderson, Eugene Goldberg, Ernest F. Plechaty, Marion L. Stelts, and Calvin Wong, "Time Spectra from Spheres Pulsed with 14-MeV Neutrons," *Nuclear Science and Engineering* 35, 227-239 (1969), p. 228.

[8] Wong et al., pp. 14 and 16.

[9] W. Webster and C. Wong, "Measurement of the Neutron Emission Spectra from Spheres of N, O, W, U-235, U-238, and Pu-239, Pulsed by 14-MeV Neutrons," Lawrence Livermore National Laboratory report UCID-17332 (December 15, 1976), p. 10.

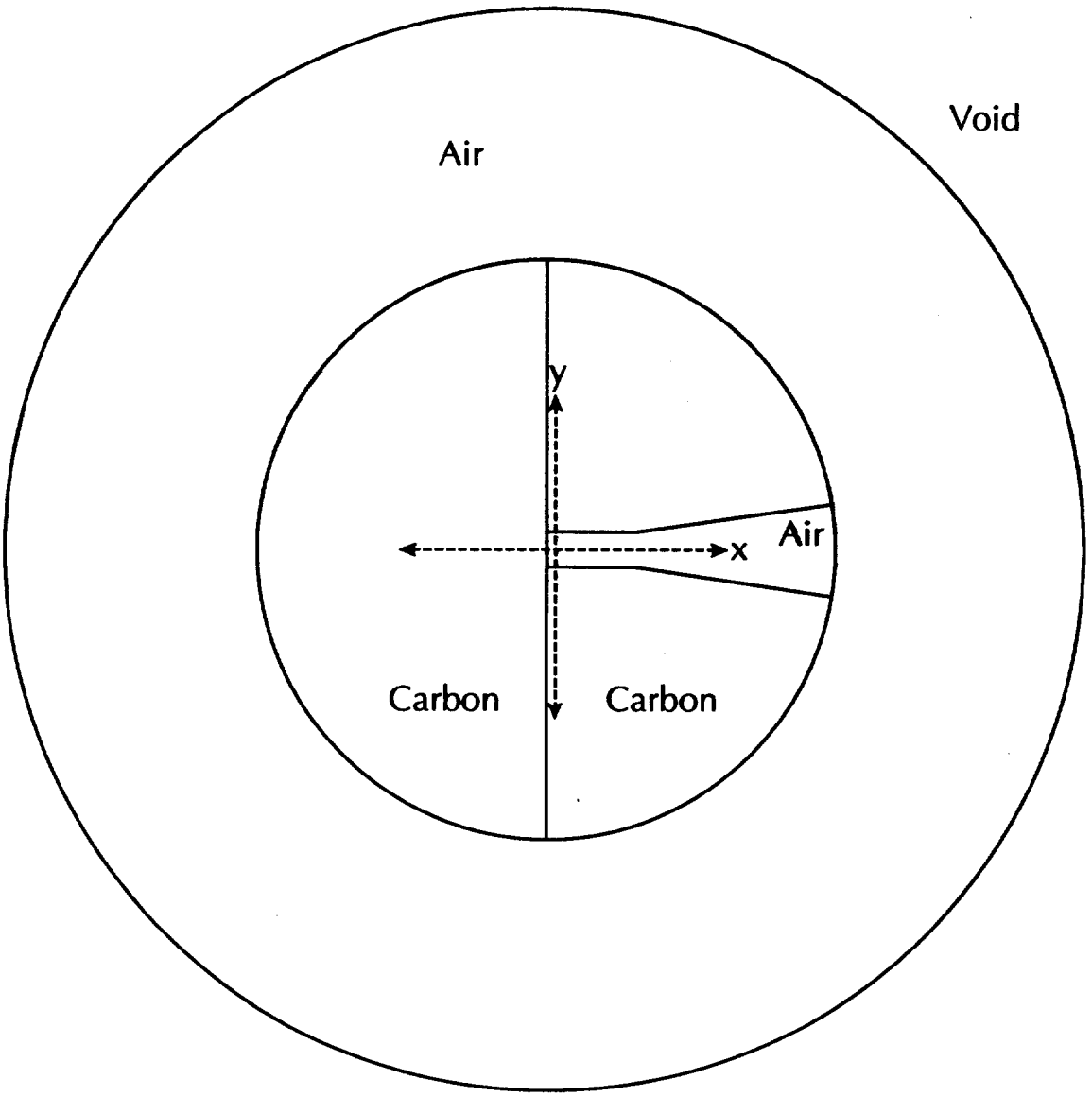

Fig. 4. Cell geometry used for the 2.9 m.f.p. carbon sphere (not to scale). The cell geometries for the other MCNP pulsed sphere calculations are similar.

When the reported dimensions, density, and mass were in conflict, the mass was assumed to be correct. For example, the MCNP model uses an artificially high density for the stainless steel containers in the lithium pulsed sphere experiment to preserve both the reported dimensions and the reported mass.

2. Low Mass Target Assembly. The aluminum-stainless steel structure which holds the titanium-tritide target in place is not included in the model because its mass is small compared to the mass of most of the spherical assemblies. To see if this structure should be included in the models for smaller spheres, a detailed MCNP model of this assembly was created for the .9 mfp iron sphere, but the results were within a percent of the results without the assembly. Therefore, the simpler model has been used in all the pulsed sphere calculations. Also, the room in which the experiment was performed has not been modeled because its effect is assumed to be insignificant.

3. Neutron Source. The most complicated aspect of the MCNP pulsed sphere model is the neutron source specification. The MCNP neutron source produces the intensity and most probable energy as a function of angle. At 0 degrees with respect to the deuteron beam, the most likely neutron energy is 15.11 MeV, and the energy decreases monotonically as a function of the angle to a value of 13.20 MeV at 180 degrees. The intensity also decreases monotonically as a function of angle where intensity is normalized so that I=1.00 at 0 degrees and I=.87 at 180 degrees. The source description, therefore, requires several probability distributions. First, the direction of a neutron is specified on the source definition (SDEF) card with the entries

DIR=D1 VEC=-1 0 0.

The polar angle of a source particle is measured with respect to the vector VEC which points in the direction of the negative x axis. DIR is a variable whose value is the cosine of the angle between the vector VEC and the initial direction of the particle. D1 is a probability distribution defined by the entries on the source information (SI1) and the source probability (SP1) cards. Therefore, distribution 1 is constructed to sample the cosines of the polar angles of the particle's initial direction. The entries on the SI1 card are the cosines of the angles at which the intensity is known. The SP1 card's entries are the intensities corresponding to the angles whose cosines appear on the SI1 card. MCNP linearly interpolates between

the points specified in the SI1 and SP1 cards to form a probability density function from which the values of the cosine are sampled.

The energy is specified on the SDEF card with the entry

ERG=FDIR=D2,

meaning that the values of energy are chosen from probability distribution 2 which itself depends on the already chosen direction. Because the energy distribution depends on the direction distribution, a dependent source (DS2) card must be used. The DS2 card's entries include the cosines of every five degrees where each cosine value is followed by the number of another distribution from which the final energy is taken. For example, the first few entries on the DS2 card are

DS2 Q -.99619 180 -.98481 175 -.96593 170 ... etc.

If a value of the cosine is chosen lying between -.98481 and - .96593 (which are the cosines of 170 and 165 degrees), then the energy will be chosen from distribution 170. Distribution 170 samples uniformly between the most likely energies at 165 and 170 degrees. The energy distributions referred to on the DS2 card above are from the DS2 card on the input file and are numbered according to the angles from 5 to 180 degrees at intervals of 5 degrees. The angular dependence of energy and intensity given in the reference[10] is only accurate to two decimal places. An additional digit was added to these figures by analytically calculating the energy and intensity of an isotropic source moving with respect to the laboratory frame. The values from this analytic calculation were fixed to match the measured energy exactly at 0 and 180 degrees. The recalculated values with three decimal places exactly match the reported values upon truncating or rounding to two places. The final energy spectrum produced by MCNP more closely resembles the actual energy spectrum when the additional digits are used than when they are not.

The actual neutron source is a .6 cm radius titanium tritide disk. Therefore, in the MCNP model the neutrons originate on a disk with .6 cm radius. This is specified by including

RAD=D3 SUR=100

[10] Wong et al., p. 7.

on the source definition card along with the corresponding probability definition

SI3 H 0 .6

SP3 D -21 1 .

The SP3 distribution guarantees that MCNP will uniformly sample the area on a disk of radius .6 cm centered at the origin. This disk is located on surface 100 which is a plane perpendicular to the x axis at the origin.

4. Cross-Section Libraries. ENDF/B-V was used whenever available, including for all major nuclides. Preliminary ENDF/B-VI was also used for nitrogen (see discussion below).

5. Detectors and Data. Because the MCNP model is symmetric with respect to the x-axis, a ring detector about the x-axis was used to calculate the flux at a given polar angle and distance from the detector. The detector response functions were not folded out of the experimental data. Therefore, the MCNP model uses a detector energy (DE) card and a dose function (DF) card which weight the tallies depending on the energy of the detected neutron. The response functions for both the Pilot B and NE213 detectors for a bias at 1.6 MeV neutron energy were modeled by specifying various energy values on the DE card and the corresponding values of the detector response functions on the DF card.[11,12]

Because the experimental results are given in terms of (particles/ns)/(particles detected without the sphere), the MCNP results must be properly normalized. The MCNP tallies give flux/(source particle). Thus, the problem must be rerun with the solid sphere replaced by air to find (flux without sphere in place)/(source particle). The former value is divided by the latter to give values comparable to the experimental results.

6. Special Techniques. Most of the pulsed sphere models contain no variance reduction techniques. However, through trial and error, it was discovered that the MCNP figure of merit for some of the sphere problems with larger radii could be improved by dividing the spherical cell at the origin into several concentric shells. The importance was then increased as the distance from the center of the sphere increased. For the iron sphere with a 4.8 mean free path radius, this increase

[11] Ibid, p. 14, 16.

[12] Webster et al., p. 10.

significantly improved the figure of merit. Another technique that improved the run time for all of the input files was to include an energy cutoff at 1.6 MeV. This cutoff prevented MCNP from tracking particles whose energies dropped below the detector's sensitivity threshold.

D. Results and Discussion

1. MCNP Results. The experimental results and computed results are compared in both plots and tables. Table 3 summarizes the results of the pulsed sphere calculations. For each material the normalized number of counts was integrated in time bins that correspond roughly to neutron energies of 12-16 MeV and 2-16 MeV. It is convenient to discuss the results in this manner because the neutron detectors were not located the same distance from the center of the sphere in each experiment. Determination of the time bins was based on the time a particle of the given energy would take to travel from the center of the sphere to the detector without collision. The table lists the ratio of the calculated value to the experimental value in each energy (time) bin. The results are quite good for most materials. However, there are several notable exceptions, one of which is nitrogen.

With the recent release of the ENDF/B-VI cross sections for nitrogen, it is interesting to compare the results of nitrogen pulsed sphere calculations using both the old and new cross sections. Table 4 contains information for nitrogen spheres with 1.1, 3.1, and 7.7 mean free path radii. Time bins were chosen that correspond roughly to energies of 2-5 MeV, 5-10 MeV, 10-13 MeV, and 13-16 MeV. In general, the agreement between calculated results and experiment is significantly better with the ENDF/B-VI cross sections than it is with the ENDF/B-V cross sections.

The second comparison uses time bins at intervals of 2-ns as in the experiment. Thus, rather than comparing integrated numbers of counts over a broad time range, we compare count rates. Plots of the computed count rate are superimposed on plots of the experimental count rate for comparison of their shapes. This was done for nitrogen, carbon, iron, water, and concrete. See Figs. 5-10.

Note that each of the plots for nitrogen (Figs. 5 and 6) contains two calculated curves: one generated with ENDF/B-V cross sections and one generated with ENDF/B-VI cross sections. The curves generated using ENDF/B-VI cross sections have a better shape and do not exhibit the nonphysical bump at about 210 nanoseconds that is present in the curves generated with the ENDF/B-V cross sections.

TABLE 3

RATIO OF CALCULATED TO EXPERIMENTAL VALUES FOR THE NUMBER OF NEUTRONS DETECTED IN EACH ENERGY RANGE[13]

Material	mfp	12-16 MeV	2-16 MeV
^{6}Li	0.5	.981	.981
	1.6	1.019	1.030
^{7}Li	0.5	.990	.985
	1.6	1.017	1.008
Be	0.8	.937	.997
C	0.5	.974	.990
	2.9	.950	.973
N	1.1	.866	.950
	3.1	.812	.972
O	0.7	.921	.988
Mg	0.7	1.046	1.033
	1.9	.994	.960
Al	0.9	.940	.948
	2.6	.786	.839
Ti	1.2	1.069	.992
	3.5	1.077	.930
Fe	0.9	1.006	1.006
	4.8	.937	.948
Pb	1.4	.873	.851
H_2O	1.1	.881	.946
	1.9	.961	1.066
D_2O	1.2	.865	.914
	2.1	.983	1.025
CH_2	0.8	.973	.999
	3.5	.884	.969
CF_2	0.9	.957	.976
	2.9	.766	.782
Concrete	2.0	.987	1.041

[13] Experimental data is from Ref. 18. All measurements were made at 30 degrees with respect to the deuteron beam except the concrete measurement which was made at 120 degrees.

TABLE 4

RATIO OF THE CALCULATED TO EXPERIMENTAL VALUES FOR NITROGEN USING ENDF/B-V AND ENDF/B-VI CROSS SECTIONS[14]

Nitrogen 1.1 M.F.P

Energy (MeV)	5/meas.	6/meas.
13-16	.872	.910
10-13	1.049	1.195
5-10	1.309	1.271
2-5	1.309	1.084
Total	.959	.975

Nitrogen 3.1 M.F.P

Energy (MeV)	5/meas.	6/meas.
13-16	.815	.899
10-13	.826	1.015
5-10	1.194	1.189
2-5	1.278	1.105
Total	.976	1.009

Nitrogen 7.7 M.F.P.

Energy (MeV)	5/meas.	6/meas.
13-16	.713	.868
10-13	.677	.911
5-10	1.004	1.040
2-5	1.124	1.006
Total	.931	.973

[14] Similar results were obtained by Estes et al. (Ref. 4) in 1982.

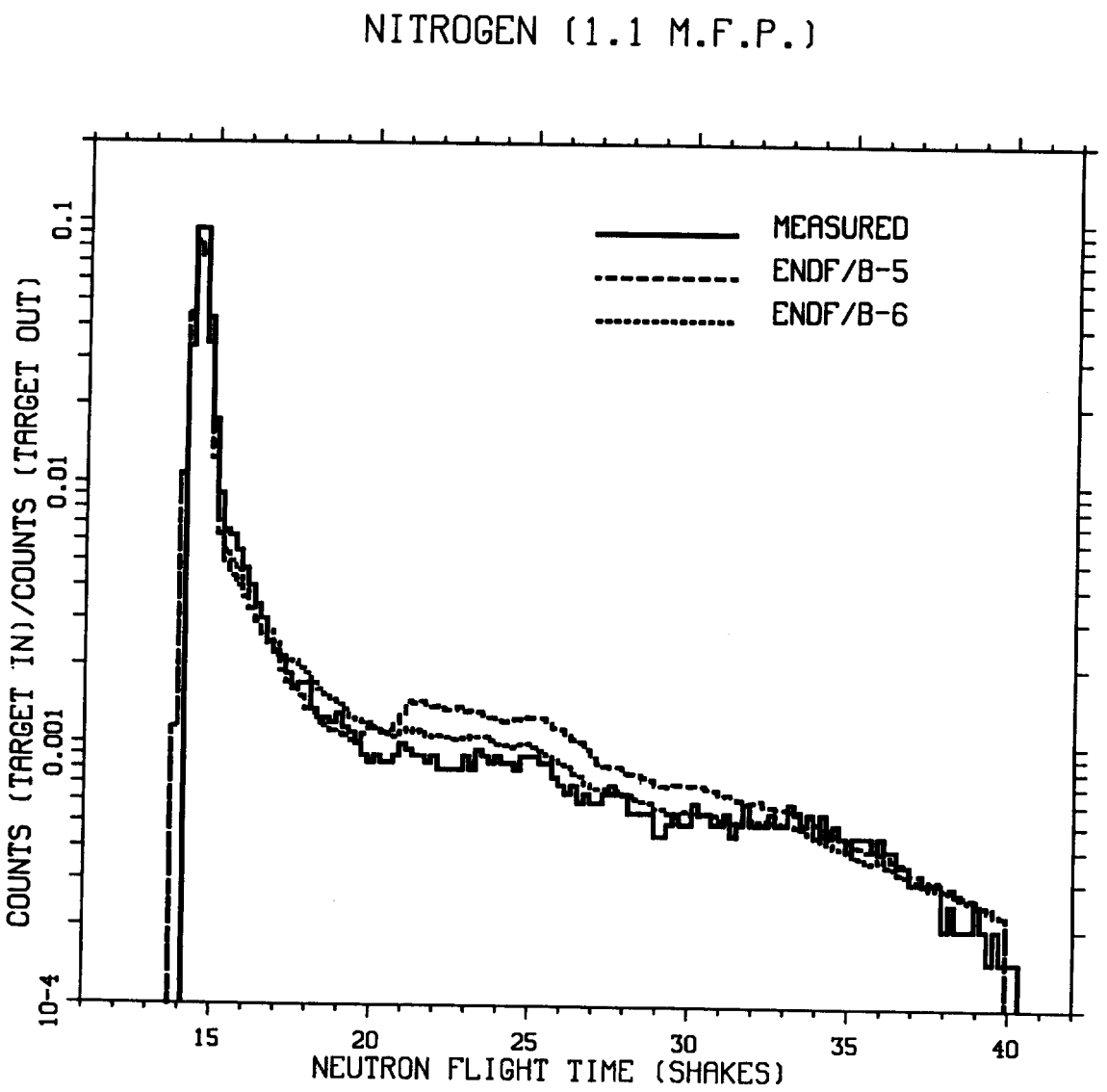

Fig. 5. Plot of experimental and calculated count rates as a function of time for a nitrogen sphere with 1.1 mean free path radius. The detector was located 763.3 cm from the center of the sphere at 30 degrees with respect to the deuteron beam (1 shake = 10 ns).

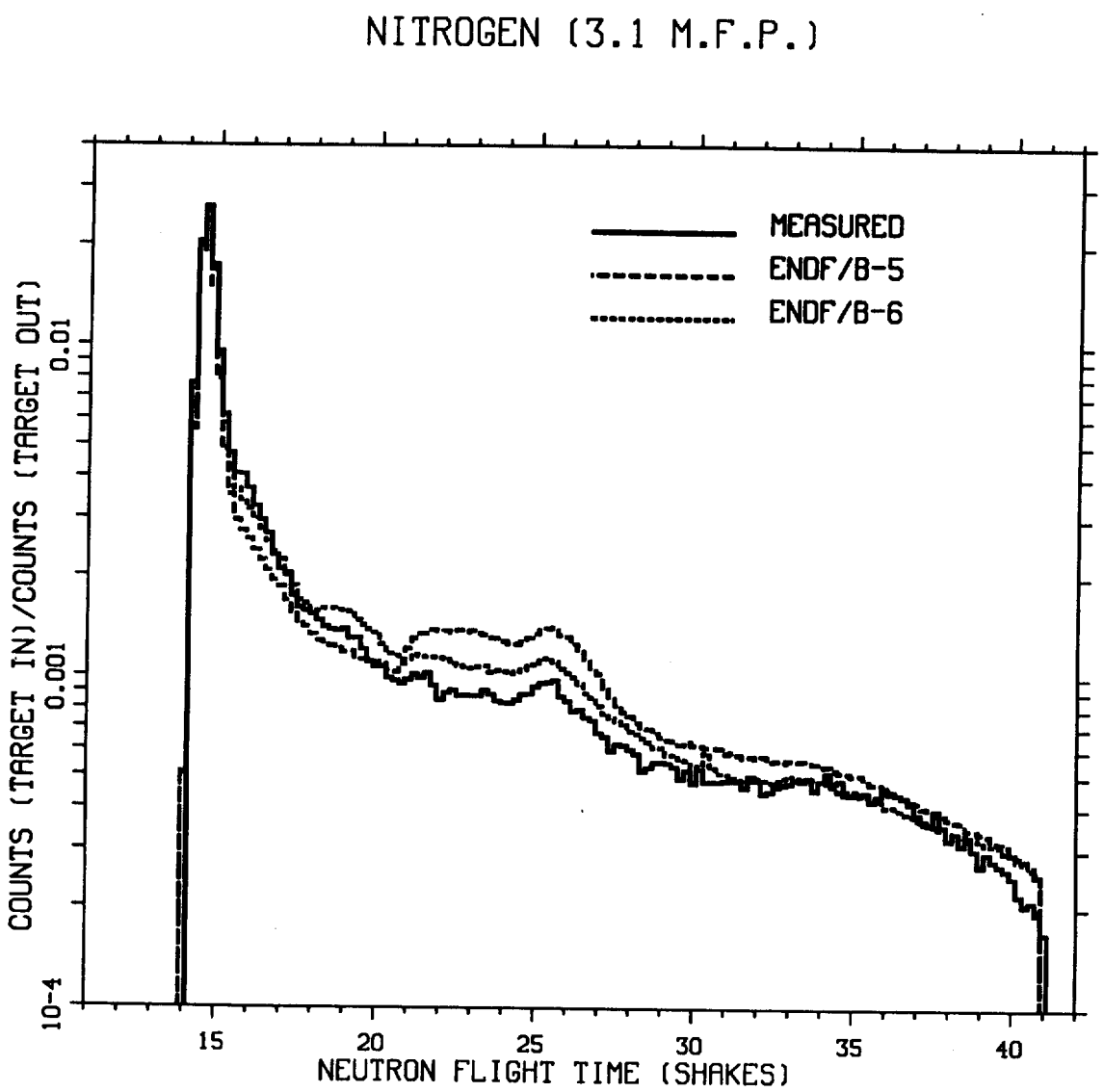

Fig. 6. Plot of experimental and calculated count rates as a function of time for a nitrogen sphere with 3.1 mean free path radius. The detector was located 765.2 cm from the center of the sphere at 30 degrees with respect to the deuteron beam (1 shake = 10 ns).

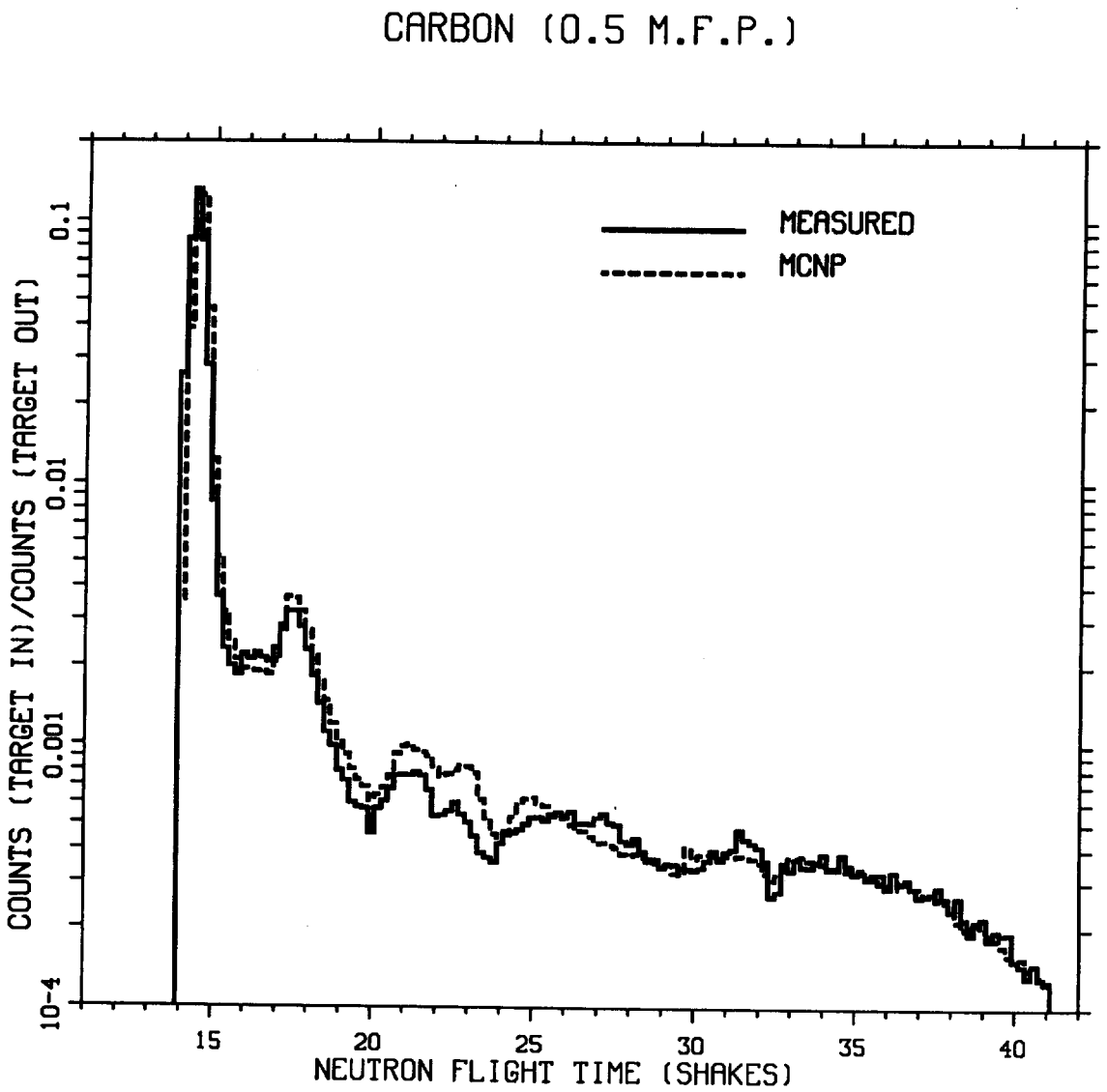

Fig. 7. Plot of experimental and calculated count rates as a function of time for a carbon sphere with 0.5 mean free path radius. The detector was located 766 cm from the center of the sphere at 30 degrees with respect to the deuteron beam (1 shake = 10 ns).

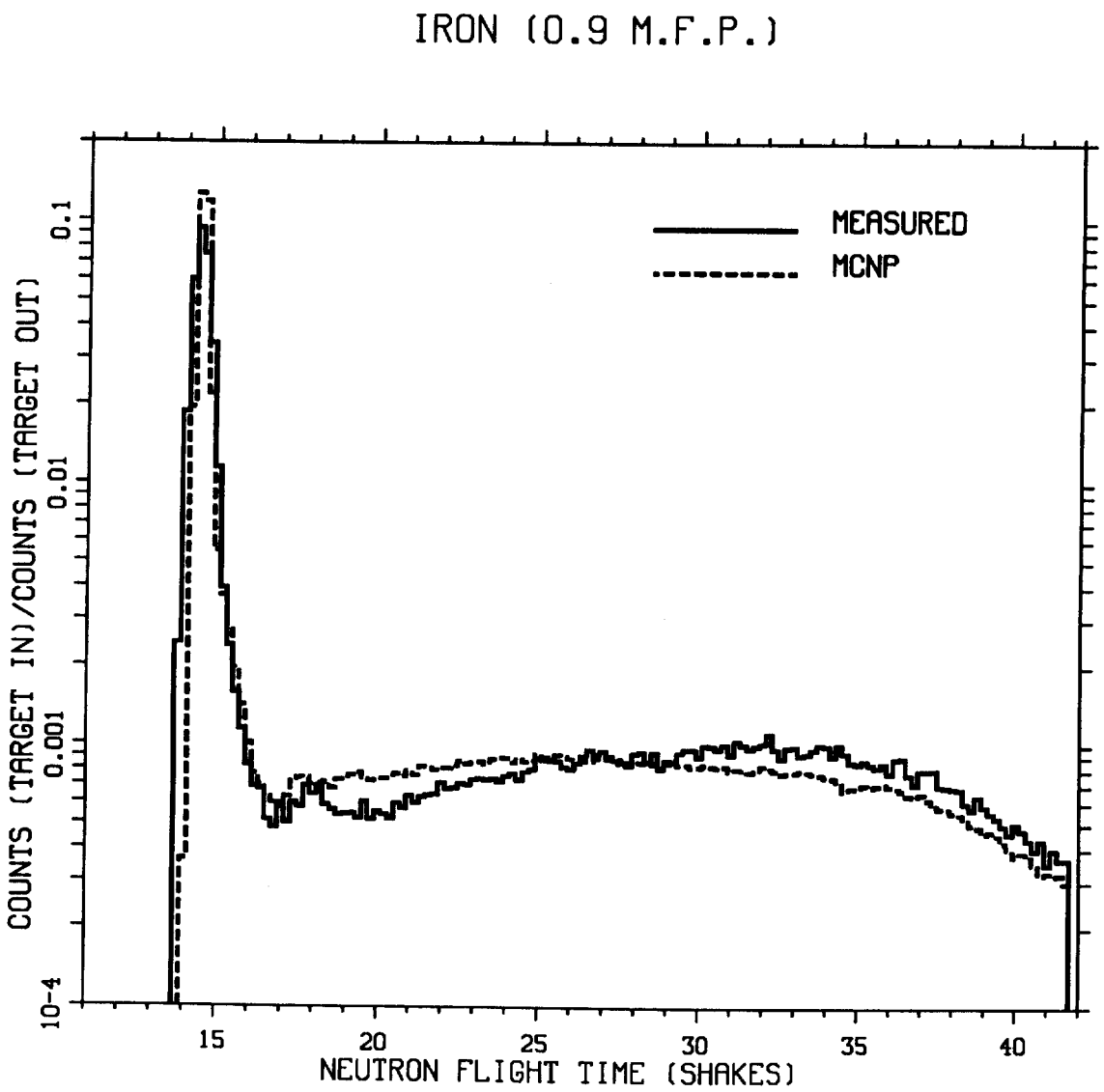

Fig. 8. Plot of experimental and calculated count rates as a function of time for an iron sphere with 0.9 mean free path radius. The detector was located 766 cm from the center of the sphere at 30 degrees with respect to the deuteron beam (1 shake = 10 ns).

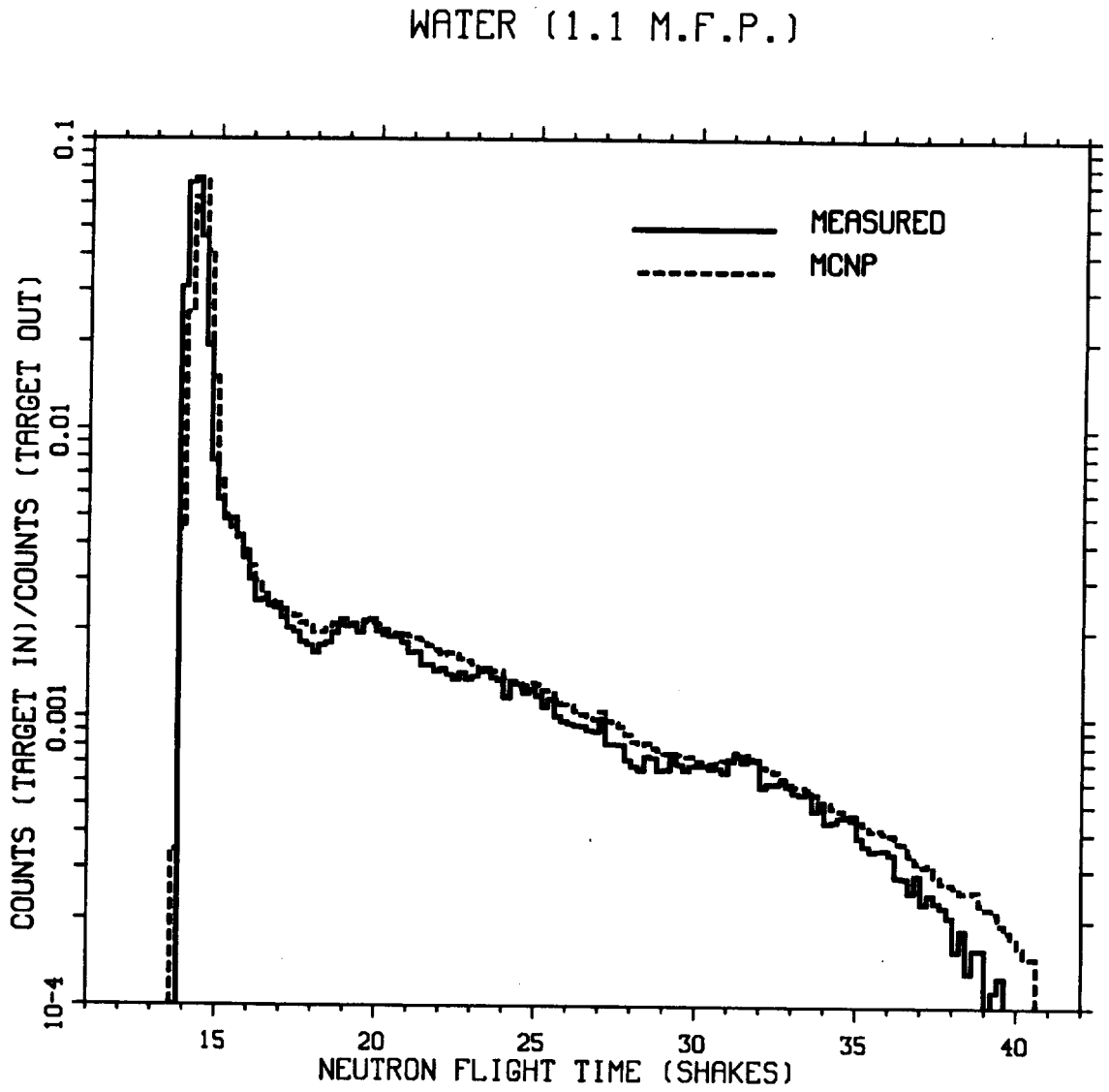

Fig. 9. Plot of experimental and calculated count rates as a function of time for a water sphere with 1.1 mean free path radius. The detector was located 754 cm from center of sphere at 30 degrees with respect to the deuteron beam (1 shake = 10 ns).

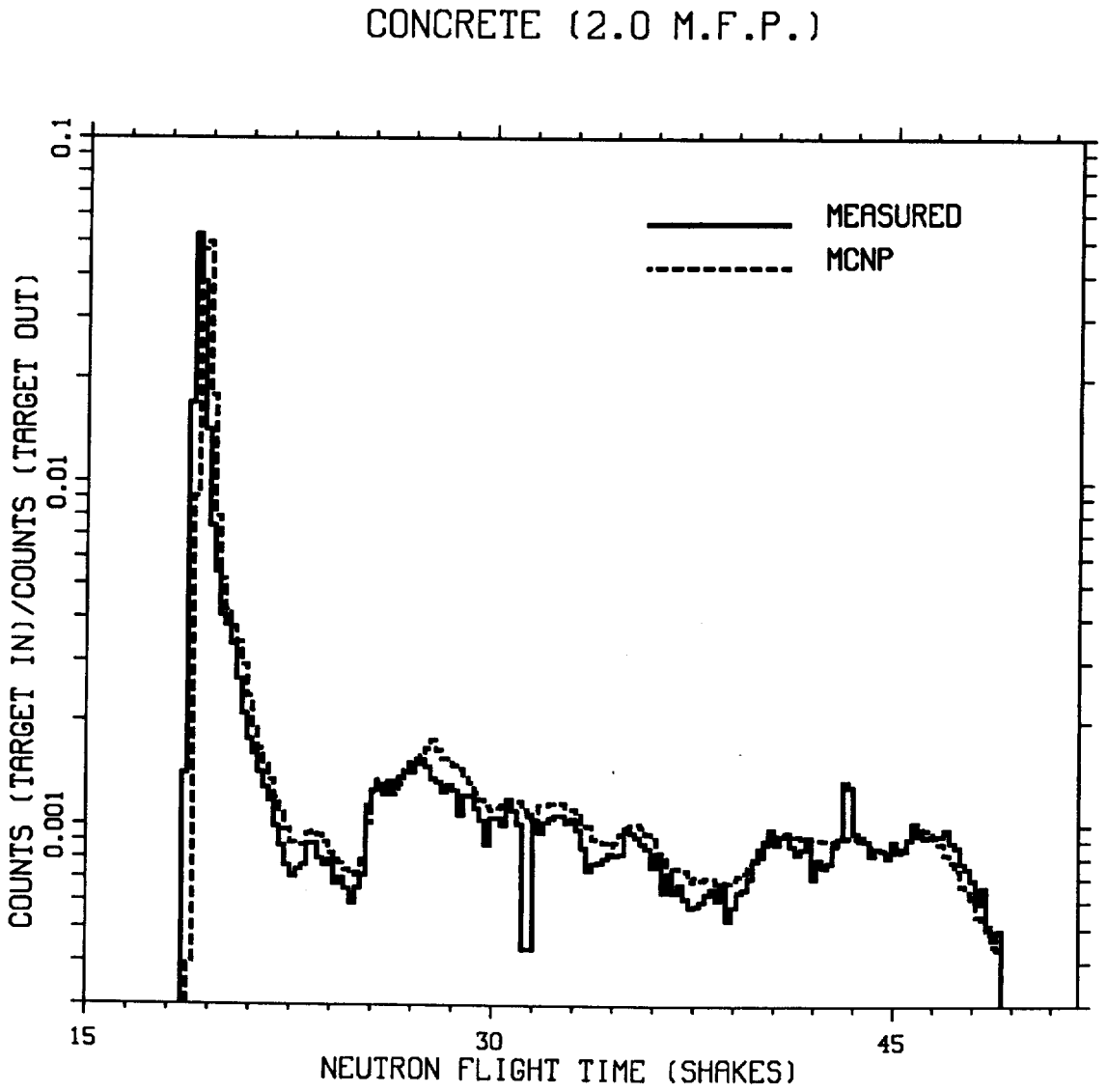

Fig. 10. Plot of experimental and calculated count rates as a function of time for a concrete sphere with 2.0 mean free path radius. The detector was located 975.4 cm from the center of the sphere at 120 degrees with respect to the deuteron beam (1 shake = 10 ns).

E. Conclusion

In cases where MCNP and the measurement disagree, it is reasonable to believe that the disagreement is due to cross section uncertainties as was shown for nitrogen. Also, the disagreements are consistent with those reported for other calculation/experiment comparisons.[15,16] On the basis of the data presented in Tables 3 and 4 and in Figs. 5-10, it is reasonable to conclude that MCNP accurately predicts pulsed sphere results for a wide range of materials.

III. BENCHMARK PROBLEM TWO: FUSION SHIELDING

A. Problem History and Description

How well fusion reactor shields will protect reactor components from radiation damage will have a significant impact on the costs of fusion energy systems. Benchmark two (one of a series of related fusion shielding experiments) was devised and performed by Santoro et al. at Oak Ridge National Laboratory in 1980 to test how well transport codes can predict fusion shield performance.[17] This experiment simulated the deuterium-tritium (D-T) neutron spectrum that would exist at the first wall of a fusion reactor. The experiment also simulated the secondary photon spectrum that would be produced from neutron interactions within this first wall.

The experimental arrangement for this shielding benchmark is shown in Fig. 11.[18] A flat target disk of titanium tritide was positioned at one end of a cylindrical iron duct along its axis. This iron duct, in turn, was imbedded inside a concrete block as shown in Fig. 11. One end of the iron pipe opened to the air outside the concrete block, whereas the other end was capped by an iron can (which held the target assembly). The iron can modified the neutron spectrum from the titanium

---

15 Wilcox and Lent, pp. 48-49.

16 G. P. Estes, R. C. Little, R. E. Seamon, P. D. Soran, "Air Transport in Connection with the Hiroshima-Nagasaki Dose Reevaluation Effort," Los Alamos National Laboratory report LA-9369-MS (July 1982), UC-11 and UC-34c.

17 Philip F. Rose and Robert W. Roussin, editors, "Shielding Benchmark Compilation," Vol. 2, Brookhaven National Laboratory report BNL-19302 (1983), p. S-5.

18 R. T. Santoro, R. G. Alsmiller, J. M. Barnes, and G. T. Chapman, "Calculation of Neutron and Gamma-Ray Spectra for Fusion Reactor Shield Design: Comparison with Experiment," *Nuclear Science and Engineering* **78**, 259-272 (1981), p. 260.

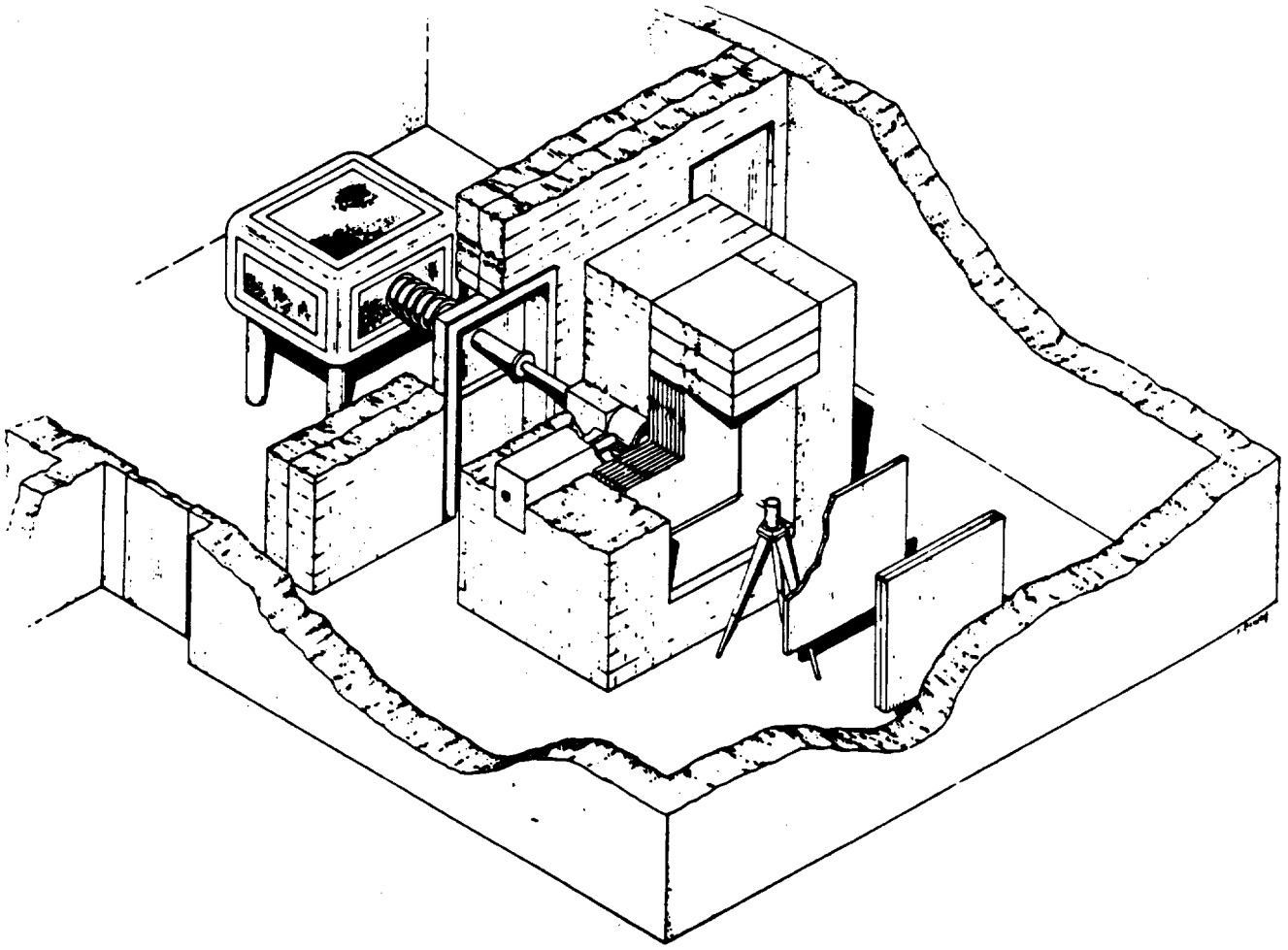

Fig. 11. Artist's rendition of the experimental facility.

target to produce the desired neutron energy profile. A deuteron beam (from the accelerator and beamline shown in Fig. 11) struck the target disk and produced a nearly-isotropic source of 14-MeV neutrons inside the duct by the T(d,n)^{4}He reaction.

Neutron and gamma detectors were placed at several different positions outside the concrete block beyond the open end of the duct. These detectors measured the energy spectra of the neutrons and secondary photons streaming from the duct and concrete assembly. A stainless steel plate was placed between the detectors and the wall to minimize backscatter from the walls, which otherwise would have distorted the spectra the experimenters were attempting to simulate. A neutron/gamma shield was then placed inside the concrete block (see Fig. 11). This shield assembly covered the open end of the iron duct.

Several different shield assemblies were studied in this experiment for their attenuation of the neutron and photon spectra leaving the concrete block.[19] MCNP was used to compute these spectra for the three shield assemblies shown in Fig. 12. The neutron spectrum was computed for one on-axis detector position in configuration 1. Both neutron and photon spectra were computed for on- and off-axis detector positions in configurations 3 and 7 (see Table 5). The fusion shielding experiment was chosen for an MCNP benchmark for several reasons.

First, this experiment was submitted to the 1983 Cross Section Evaluation Working Group Benchmark Report and consequently was very well documented. Next, this experiment is a challenging streaming and deep-penetration shielding problem which heavily tests MCNP's variance reduction abilities. Finally, this experiment has a neutron source that is difficult to model accurately, and the experimental data had response functions folded into them. These complications challenged MCNP's source-modeling and tally-modification features. MCNP's predictions for the neutron and gamma spectra in this problem compared favorably to the corresponding experimental data.

B. MCNP Problem Model

1. MCNP Geometry/Cell Subdivision. The experimental arrangement of the ORNL fusion shielding problem is shown from different angles in Figs. 13 to 15.[20] The dimensions in these diagrams allow a complete and unambiguous MCNP

[19] Rose et al., p. S-15.

[20] Ibid, pp. S-6 to S-8.

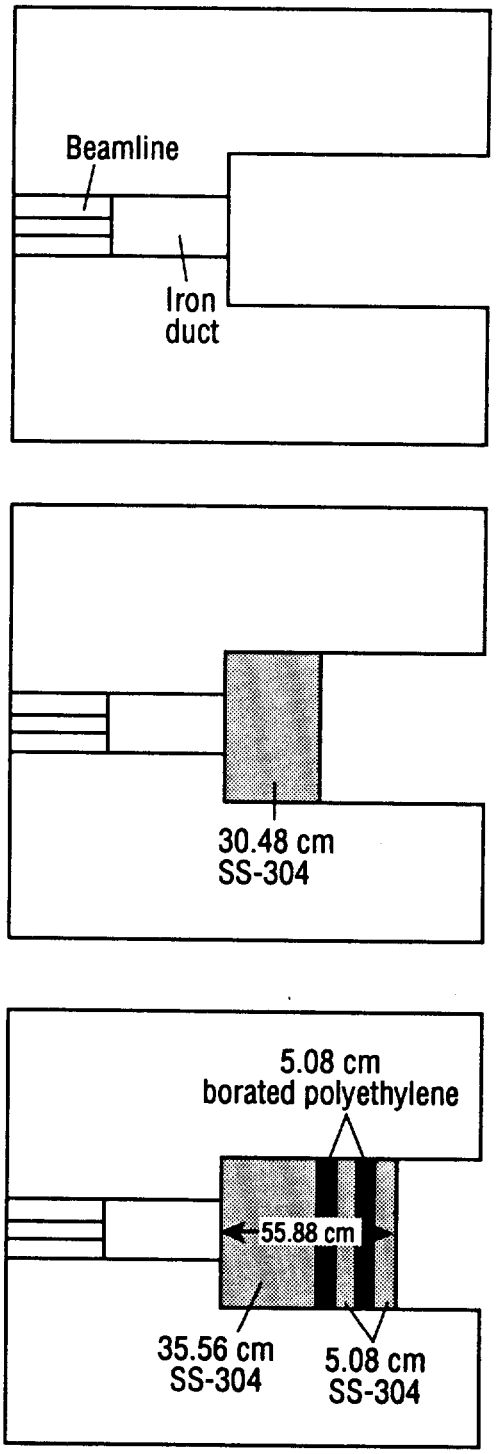

Fig. 12. The three shielding configurations modeled by MCNP.

TABLE 5

MCNP DETECTOR TALLY POSITIONS*

Shielding Configuration	Tally Type	Coordinates (cm)
1	neutron	(x,y,z) = (0, 154.5, 0)
3	neutron	on axis : (0, 154.5, 0)
		off axis : (-100, 159.2, 0)
	photon	on axis : (0, 154.5, 0)
		off axis : (-100, 159.2, 0)
7	neutron	on axis : (0, 154.5, 0)
		off axis : (46, 154.5, 0)
	photon	on axis : (0, 154.5, 0)
		off axis : (46, 154.5, 0)

*The coordinates listed here are relative to the neutron source in the MCNP reference coordinate system. The detector coordinates in the MCNP input files are relative to the reference coordinate system origin.

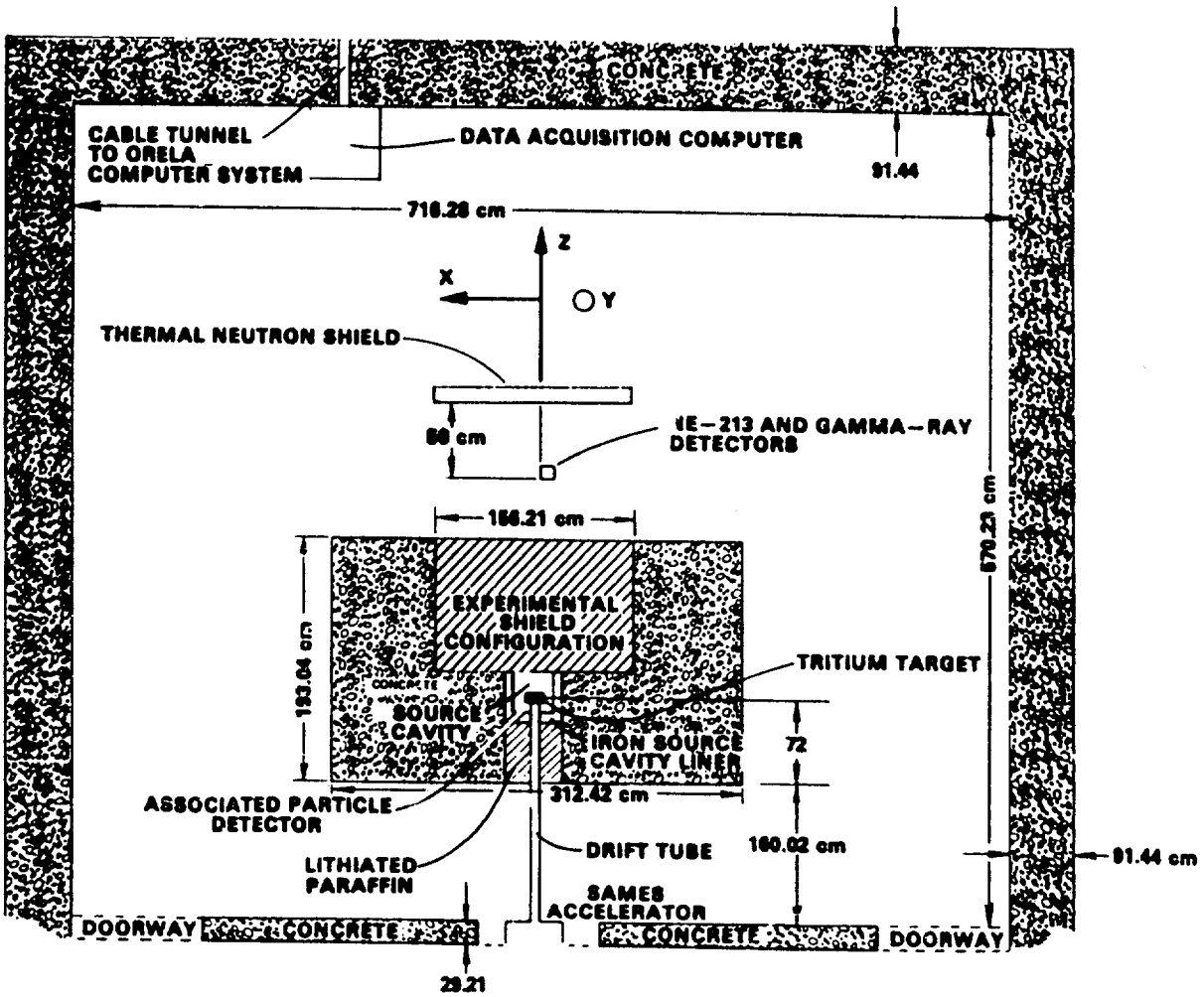

Fig. 13. Horizontal schematic of the experimental enclosure (drawing not to scale).

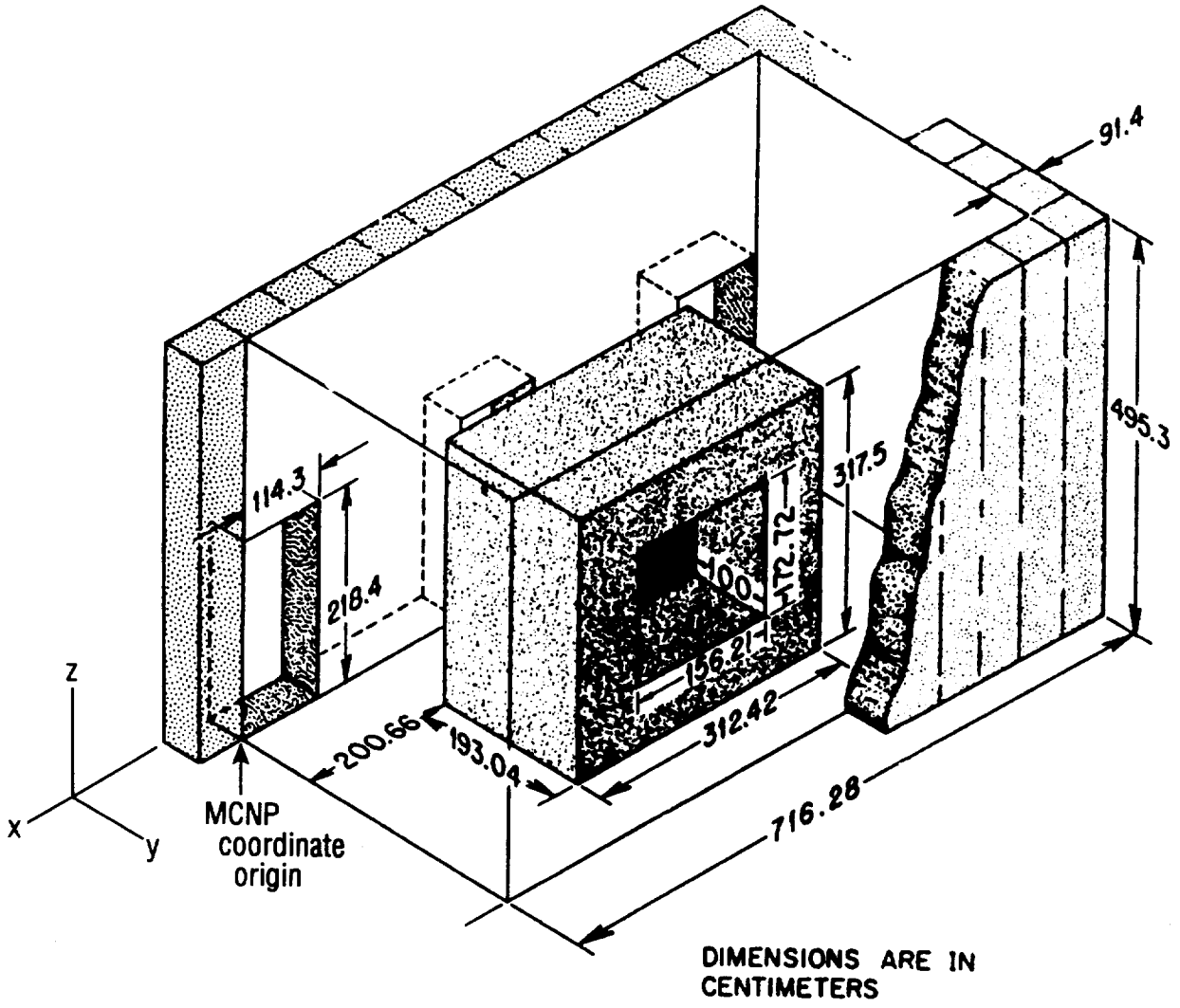

Fig. 14. Three-dimensional view of the experimental enclosure (drawing not to scale).

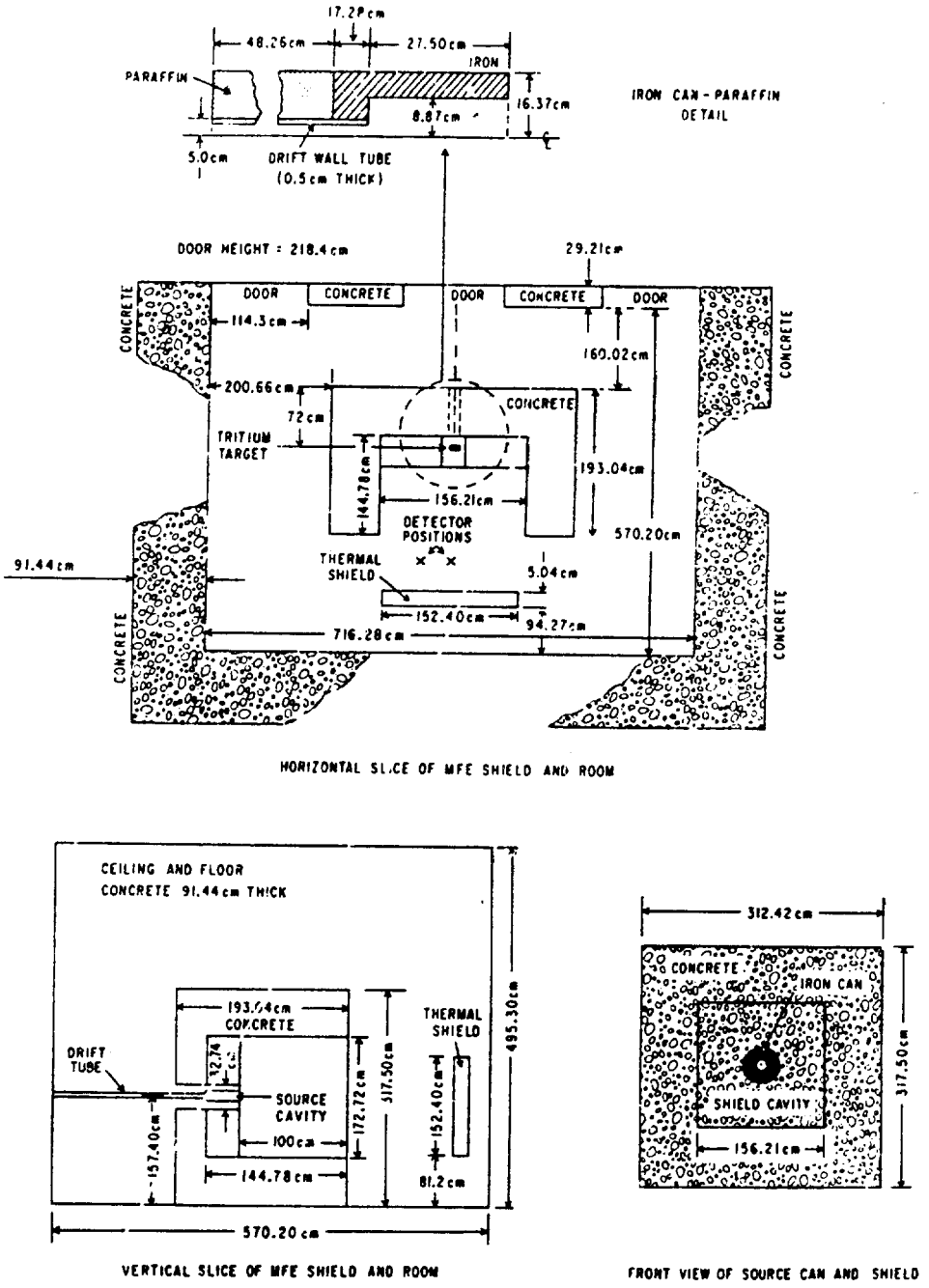

Fig. 15. Additional schematics of the experimental enclosure (drawing not to scale).

geometry of the experiment. The MCNP geometry used in the problem model exactly modeled every detail of the arrangement depicted in Figs. 13 to 15 with a few minor exceptions:

- only the beamline inside the concrete block was included in the geometry - the segment of beamline between the rear wall and the back of the concrete block was ignored.
- the neutron source disk was centered in the iron source can/iron duct assembly - the disk was simply suspended along the assembly axis because no further description of the source was provided. The MCNP source used in this benchmark is identical to that used in benchmark one except for the target radius.
- the MCNP geometry reference coordinate system had a different orientation than that used by the ORNL experimenters in their benchmark report (see Fig. 14). Whenever detector coordinates or component locations are specified in this report, they are in terms of the MCNP coordinate system.

The MCNP geometry of this experiment was subdivided into 175 cells. These cells were all rectangular blocks or slabs, cylinders, or cylindrical shells, and are fully described in the problem input files in Tables A4 and A5 in the Appendix.

2. Material Compositions/Code Tallies. The materials present in the fusion shielding experiment were concrete, air, iron, SS-304 stainless steel, lithiated paraffin, and borated polyethylene. The elemental composition (and atom density of each elemental component) of each material is shown in Table. 6.[21] Where these materials were present in the experiment is seen in Figs. 12-15. ENDF/B-V cross sections were used whenever available.

Point detector (F5) photon and neutron flux tallies were then placed in the MCNP geometry at positions corresponding to where actual fluxes were measured in the experiment. The detector locations for the three shielding configurations that were modeled are listed in Table 5. These tallies were modified to incorporate the gaussian experimental detector response. The FT GEB a b tally modification feature in MCNP allows such an energy-dependent gaussian to be folded into tally estimates, where the FWHM is of the form

[21] Ibid, p. S-11.

TABLE 6

COMPOSITION OF MATERIALS USED IN THE MCNP SHIELDING BENCHMARK MODEL

Nuclide	Number Density (atom/barn-cm)					
	Concrete	Air	Iron	SS-304	BP*	LP**
H	7.86×10^{-3}				7.13×10^{-2}	5.926×10^{-2}
B-10					4.87×10^{-4}	
B-11					1.97×10^{-3}	
C					3.41×10^{-2}	3.338×10^{-2}
N		3.64×10^{-5}				
O	4.39×10^{-2}	9.74×10^{-6}			3.64×10^{-3}	1.125×10^{-2}
Na	1.05×10^{-3}					
Mg	1.40×10^{-4}					
Al	2.39×10^{-3}					
Si	1.58×10^{-2}					
K	6.90×10^{-4}					
Ca	2.92×10^{-3}					
Cr				1.77×10^{-2}		
Mn				1.77×10^{-3}		
Fe	3.10×10^{-4}		8.48×10^{-2}	6.02×10^{-2}		
Ni				7.83×10^{-3}		
Li-6						5.565×10^{-4}
Li-7						6.944×10^{-3}

* BP = Borated Polyethylene

**LP = Lithiated Paraffin

$$FWHM = a + b\sqrt{E}$$

where E is the energy of the particle (in MeV).

However, the experimental gaussian detector responses had a different form. For the neutron detector,[22]

$$FWHM = \sqrt{0.03E^2 + 0.08E} \qquad \text{(E in MeV)}$$

while for the photon detector,

$$FWHM = \sqrt{0.017E^2 + 0.0288E} \qquad \text{(E in MeV)}$$

Therefore, it was necessary to slightly alter MCNP to accept a user-input gaussian energy broadening of the form

$$FWHM = \sqrt{aE^2 + bE} \qquad \text{(E in MeV)}$$

through the FT GEB a b option. How this was done is shown in the patch input file in Table A6 of the Appendix.

Neutron and photon spectra were computed in separate runs, even though when both spectra were computed, they were done at the same position. Separate computations were done for two reasons. First, a neutron spectrum could be calculated in one tenth the CPU time of a photon spectrum. The experimental detector energy cutoffs for neutrons and photons were .85 MeV and .75 MeV, respectively.[23] MCNP could terminate neutron histories below the .85 MeV cutoff and compute an accurate spectrum. To compute photon spectra, the low-energy neutron histories had to be included because they could still produce photons above the .75 MeV cutoff through nuclear reactions. Transporting these low-energy neutrons greatly increased the running time of the problem. Second, it was easier to separately optimize the neutron and photon variance reduction techniques.

3. Variance Reduction. Efficiently simulating the fusion shielding experiment required using strong variance reduction techniques because the model has

[22] Ibid, pp. S-12 to S-13.

[23] Ibid, p. S-13.

streaming and the deep penetration of neutrons and photons into several shielding materials. Each problem was run several times with the MCNP weight window generator[24] to produce a good set of variance reduction weight windows. After two or three such iterations, the figure of merit of each problem increased by a factor of ten or more, which enabled MCNP to converge to low-variance tally results reasonably quickly.

C. Results and Discussion

The experimental data and MCNP results for the neutron and photon spectra for shielding configurations 1, 3, and 7 are shown in Figs. 16-24. In each figure, the MCNP results (solid line) appear with the experimental upper bound data (short dash line) and experimental lower bound data (long dash line). The experimental upper and lower bound data is listed in tabular form in BNL-19302.[25] Agreement between the experimental data and MCNP in the on- and off-axis neutron spectra for all three configurations is good except for between 7.5 and 9.5 MeV where the computational unfolding routines that were used to process the experimental data produce a nonphysical dip in the neutron spectra.

The agreement between MCNP and the experimental data in the photon spectra is not as good as in the neutron spectra, most likely because the neutron-induced photon production cross sections are not well known. Also, processing routines again produce nonphysical fluctuation in the spectra (especially evidenced by the negative flux in Fig. 23). In spite of this, MCNP predicts the main features of the photon spectra well. The 50% or so agreement between MCNP and the measured data is excellent for a deep penetration problem.

---

[24] T. E. Booth and J. S. Hendricks, "Importance Estimation in Forward Monte Carlo Calculations", *Nuclear Technology/Fusion*, 5(1), 90, (1984).

[25] Rose et al., pp. S-31 to S-56.

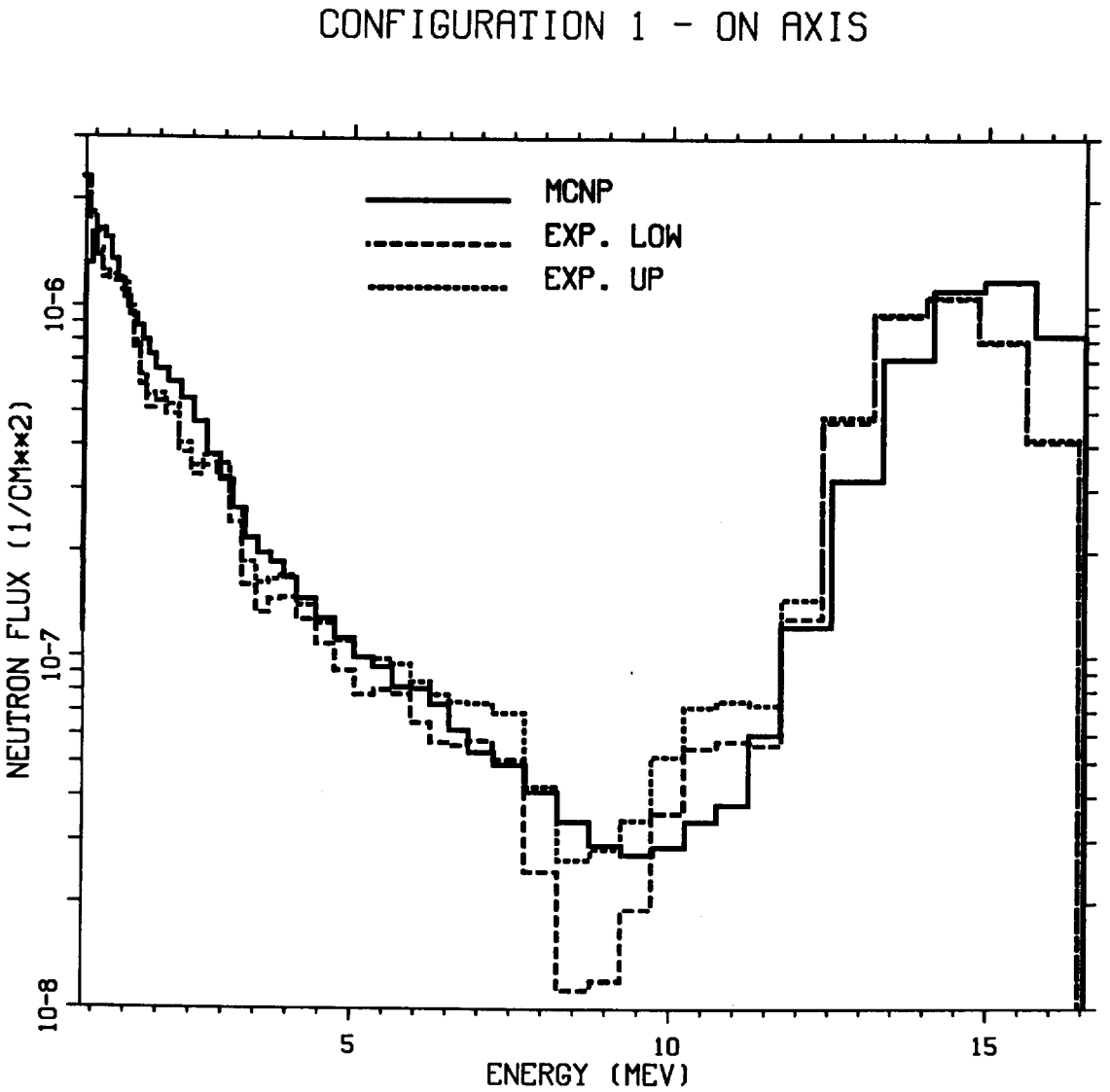

Fig. 16. Neutron spectra for configuration 1: on-axis.

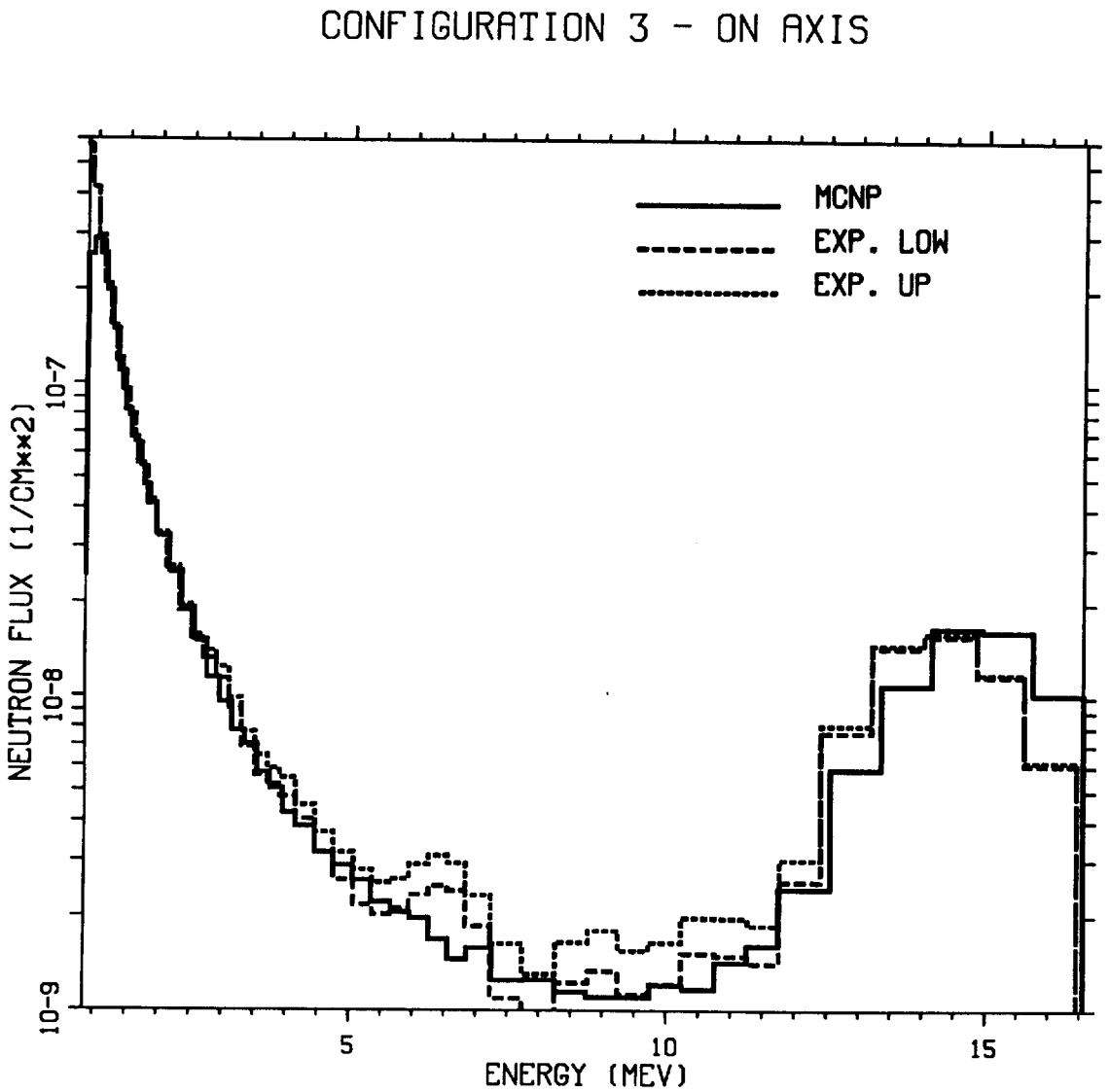

Fig. 17. Neutron spectra for configuration 3: on-axis.

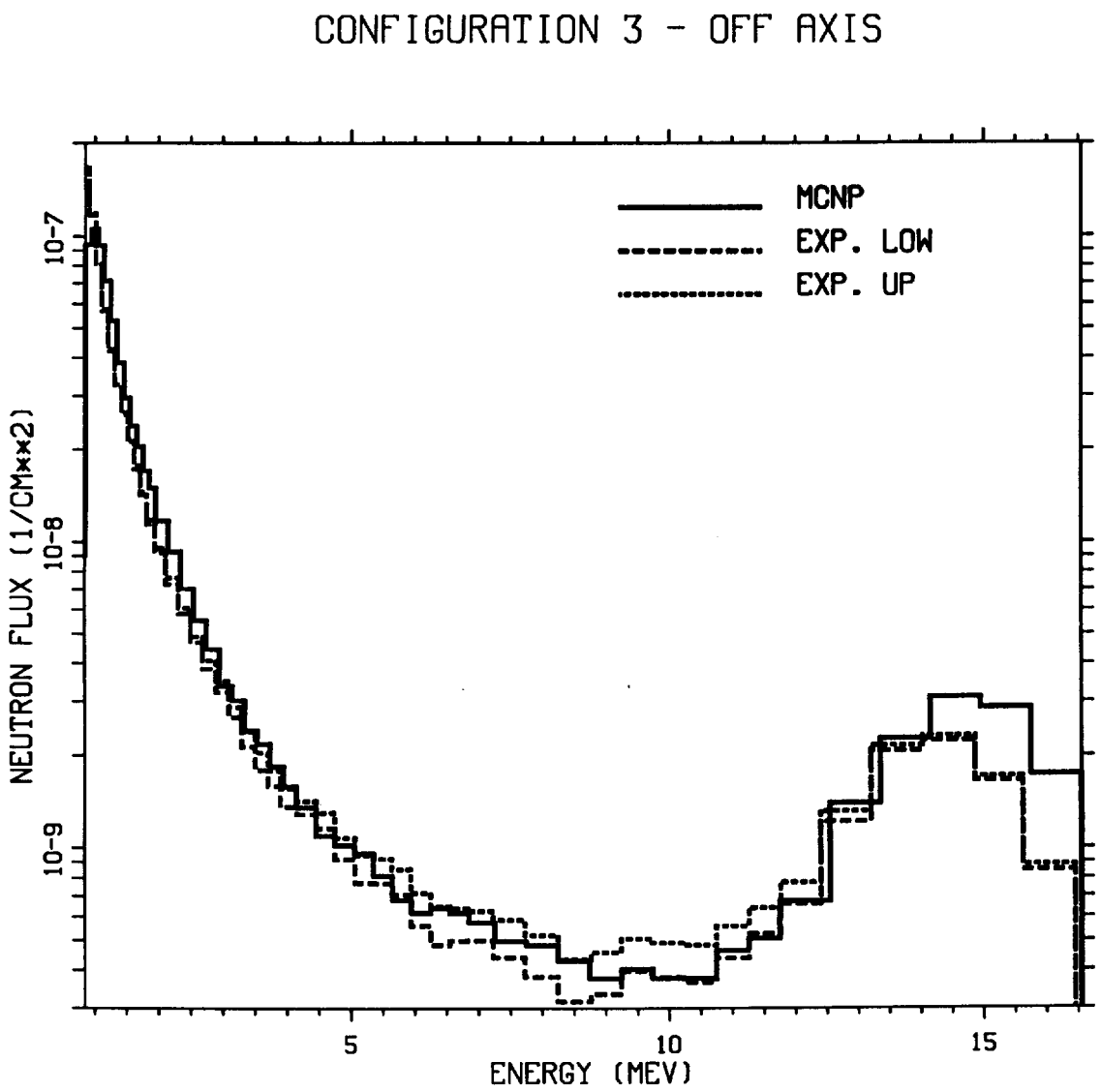

Fig. 18. Neutron spectra for configuration 3: off-axis.

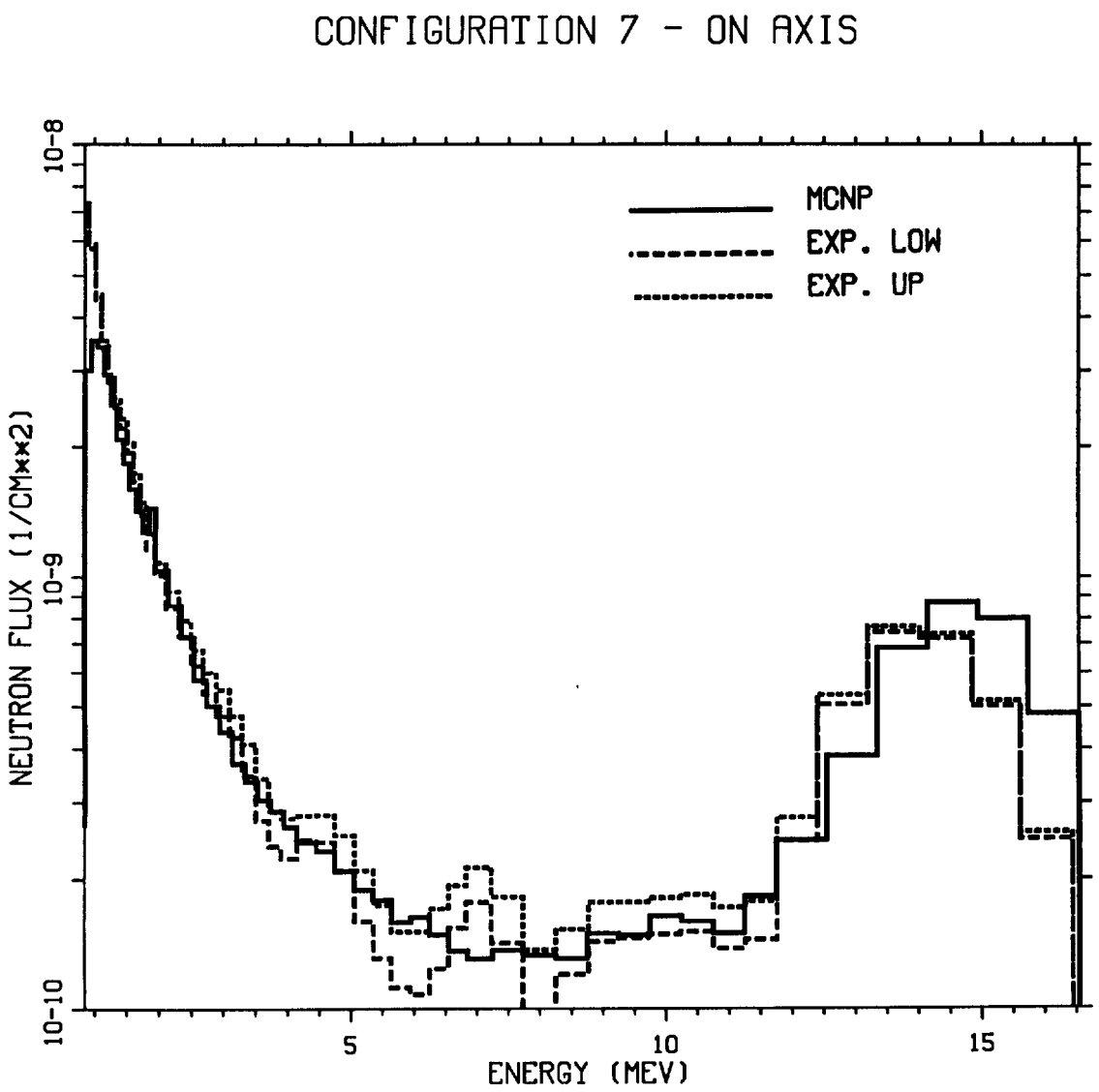

Fig. 19. Neutron spectra for configuration 7: on-axis.

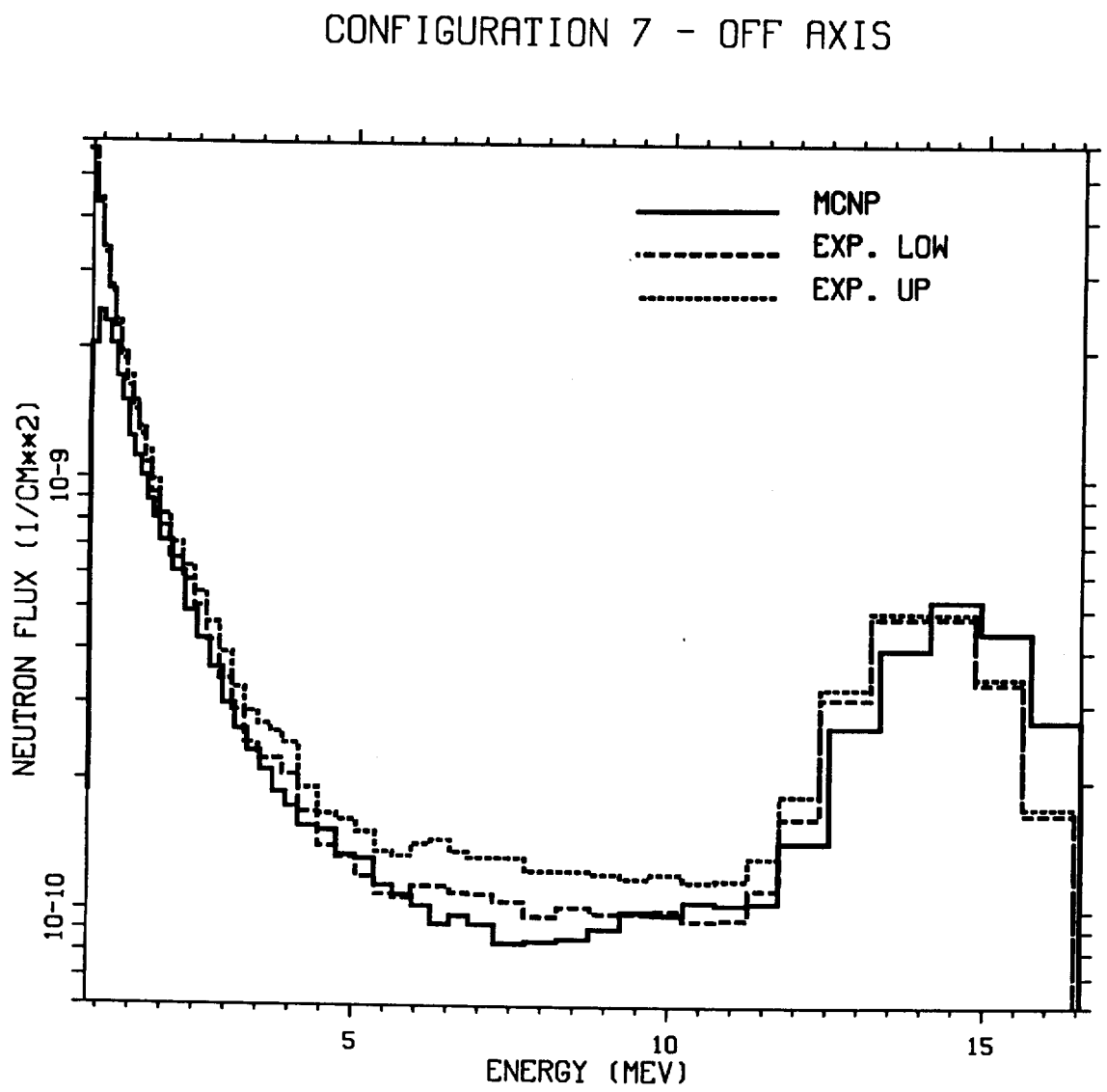

Fig. 20. Neutron spectra for configuration 7: off-axis.

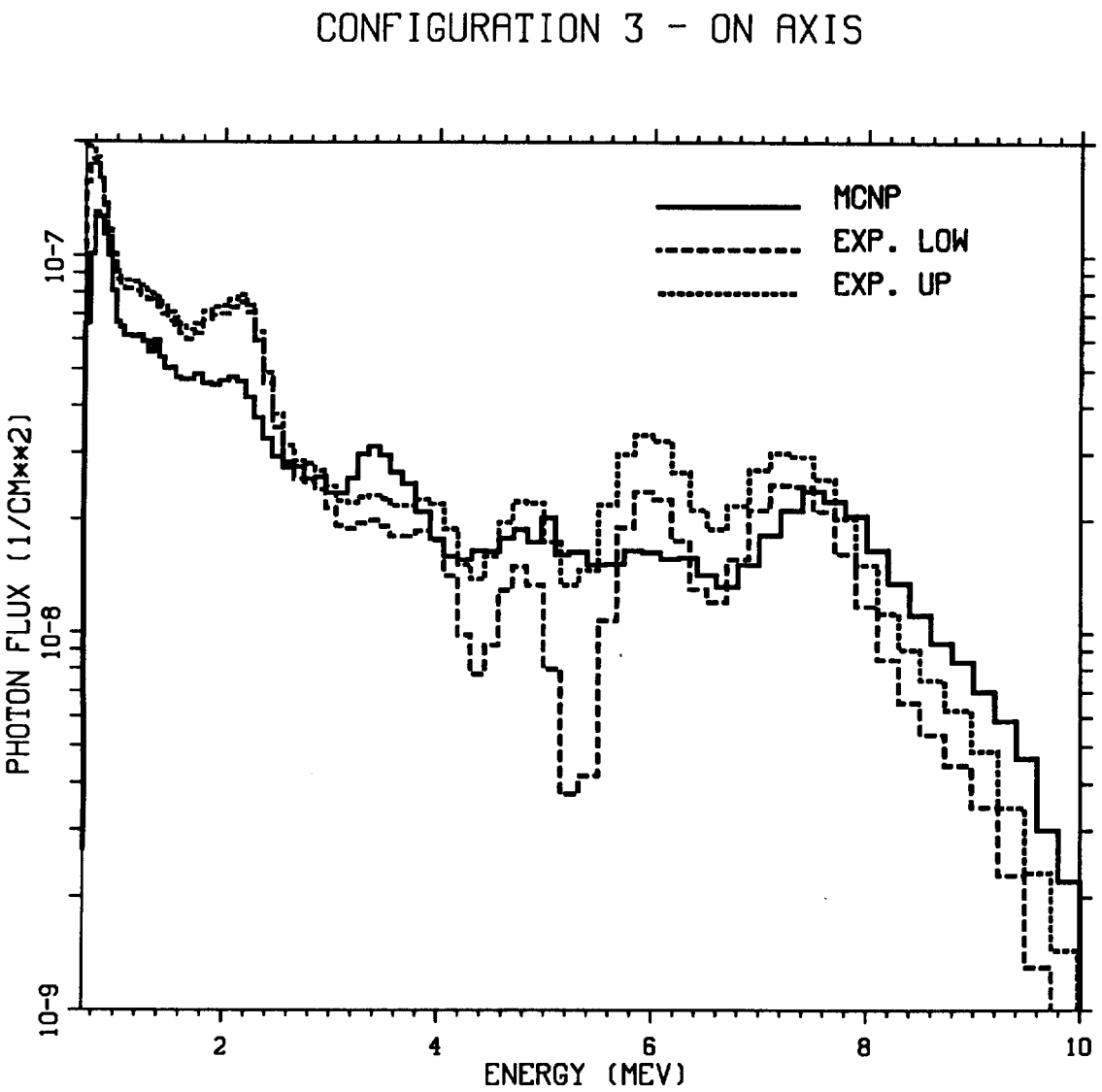

Fig. 21. Photon spectra for configuration 3: on-axis.

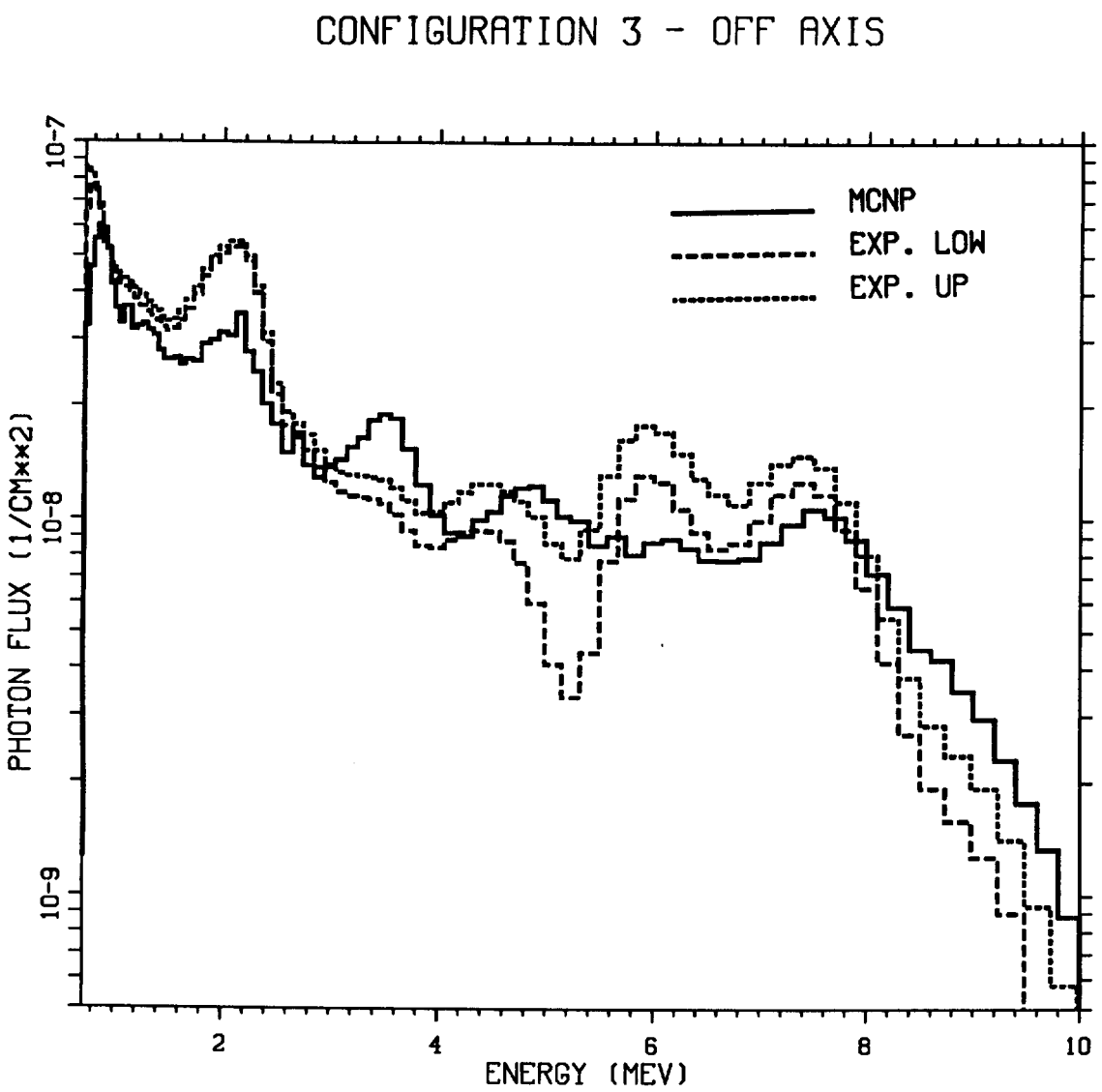

Fig. 22. Photon spectra for configuration 3: off-axis.

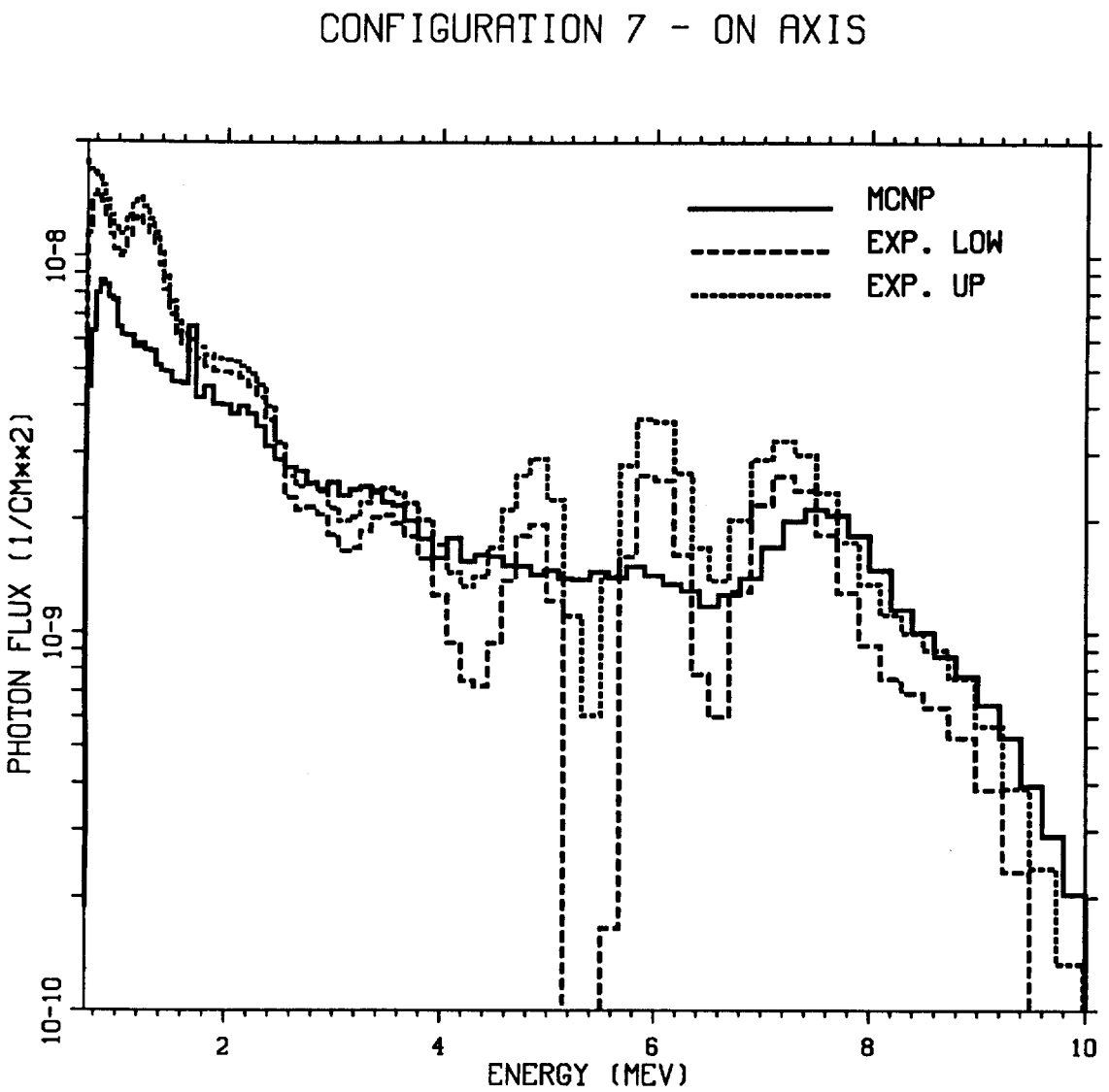

Fig. 23. Photon spectra for configuration 7: on-axis.

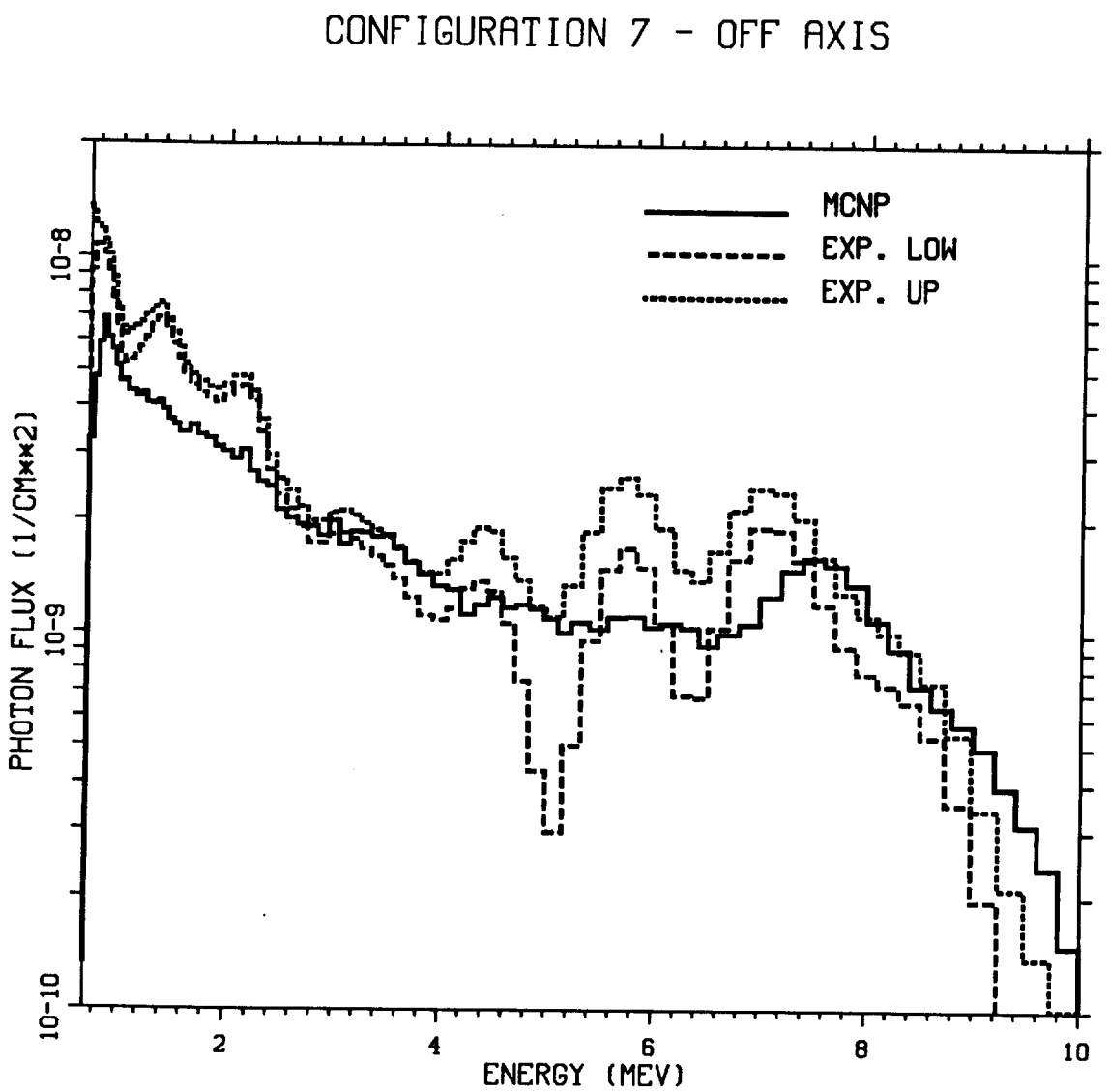

Fig. 24. Photon spectra for configuration 7: off-axis.

IV. BENCHMARK PROBLEM THREE: CRITICAL ASSEMBLIES

A. Problem History

Nuclear criticality has been one of the most important measurements of nuclear systems since the Manhattan Project of World War II. The criticality of a given system is characterized by the multiplication factor, k_{eff}. k_{eff} is the ratio of the number of neutrons in two successive generations of a fission history and is the principal eigenvalue of the Boltzmann transport equation. If a system is critical, then $k_{eff} = 1$, whereas a subcritical and a supercritical condition are characterized by k_{eff} values less than and greater than 1, respectively.

To determine MCNP's ability to calculate the multiplication factor of a critical configuration, nine experimental critical assemblies were analyzed. Each system was modeled, and the simulation results were compared to the experimental data. These nine experiments were carefully chosen so that a good percentage of criticality experimental types were represented in the study. Originally, the study was designed to examine the criticals run by COG,[26] but many turned out to be computational models rather than experiments. Also, adequate documentation for the assemblies was not always available. Therefore, a different set of experiments was modeled, but the systems were similar to those evaluated in the COG document.

This set of nine experiments includes:

I. Fast Neutron Systems
   1. Godiva
   2. Jezebel (Pu-239 95.5%)
   3. Jezebel (Pu-239 80%)

II. Low Enrichment
   1. Uranium cylinder (U-235 10.9%)
   2. Uranium cylinder (U-235 14.11%)

III. Reflected Systems
   1. Graphite-tamped U sphere
   2. Water reflected U sphere

IV. Interacting Units
   1. 3 cylinders of a U solution
   2. 3 x 3 array of Pu fuel rods

[26] Wilcox and Lent, pp. 61-64.

1. Criticality Source Modeling. The choice of criticality source parameter values depends on the settling rate of each problem, the system's dimensions, and the degree of fluctuation seen in the k_{eff} values. For all runs, a k_{eff} value of 1.0 was measured experimentally and was expected from the simulations. A relative error of .003 was assumed to be an acceptable fluctuation in the tally. Therefore, the simulations were run until the k_{eff} value fluctuated about a constant mean value, and the values of subsequent cycles were then averaged until a 0.003 or less relative error was registered. Some simulations, such as Godiva and Jezebel, were allowed to run through more cycles than necessary if the geometry was simple and the computer time was available.

It was found that large geometries required approximately 10,000 initial particles per cycle to yield a converging k_{eff} value, whereas small geometries with simple structural configurations quickly converged with approximately 3000 initial particles. Simple spherical geometries converged using a single source point centrally located, but the remaining systems required a distributed source defined by the SDEF option to yield a constant mean value in an appropriate number of cycles.

2. Cross-Section Libraries. Nuclide cross sections were taken from ENDF/B-V when possible.

3. Criticality Eigenvalue Selection. MCNP offers several options for the k_{eff} value estimate. For this study, the combined average of the absorption, collision, and track-length estimator is quoted as the k_{eff} value. All estimates of k_{eff} are within 1% of the experimental critical value of 1.0. Although a 1% difference in critical systems represents a large discrepancy in overall system behavior, general experimental error restricted the accuracy of the simulation to 1%.

The following sections briefly describe the experimental designs and give the corresponding results of the MCNP simulations. Unless stated otherwise, enrichments, densities, and isotopic fractions are in mass rather than atom units. Further description of the geometries can be found in the cited references. Input files for all nine geometries are in Tables A7-A15 in the Appendix.

B. Fast Neutron Systems

1. Godiva. The specifications used to define a bare uranium sphere were taken from the data of G. E. Hansen and H. C. Paxton, which was originally generated at

Los Alamos National Laboratory and then revised there in 1969.[27] Lady Godiva, as the setup was called, is an example of a fast neutron critical system. It was a simple geometry, consisting of a 52.42 kg sphere of U (93.71)–93.71% U-235 enriched. The density of the system was measured at 18.74 g/cm^3. These data correspond to a sphere of radius equal to 8.741 cm. MCNP calculated a k_{eff} value of 0.9976 with a corresponding relative error of .0011%.

2. Jezebel at 95.5% Pu-239 Enrichment. Jezebel was similar to the Godiva experiment and was reevaluated by G. E. Hansen and H. C. Paxton at Los Alamos National Laboratory in 1969.[28] This system consisted of a bare plutonium sphere. Two different isotopic combinations of Pu-240 and Pu-239 were analyzed—a Pu-239 composition of 95.5% and one of 80%. In both instances, the remaining material was Pu-240. These are "fast" critical assemblies with a relatively hard spectrum.

The 95.5% Pu-239 system was a 17.02 kg sphere with a density of 15.61 g/cm^3 and a radius of 6.385 cm. MCNP calculated a k_{eff} value of 0.9986 ± .0021.

3. Jezebel at 80% Pu-239 Enrichment. The 80% enriched system had a critical mass of 19.46 kg, a density of 15.73 g/cm^3 and a radius of 6.660 cm. The simulation yielded a k_{eff} value of 1.0075 ± .0012.

C. Low Enrichment

1. Uranium Cylinder at 10.9% U-235 Enrichment. To determine MCNP's ability to effectively characterize the behavior of low enrichment systems, two simulations of experiments run by Paxton at LANL in 1975[28] were performed. Both geometries were bare uranium cylinders, but they differed in uranium enrichments. The first was a cylinder of uranium enriched to 10.9% U-235, with a density of 18.63 g/cm^3, a height of 119.392 cm, and a radius of 26.65 cm. MCNP calculated the k_{eff} value of this system to be 1.0024 ± .0013.

2. Uranium Cylinder at 14.11% U-235 Enrichment. The second system was enriched to 14.11% U-235 and had a density of 18.41 g/cm^3. The cylinder had

---

[27] G. E. Hansen and H. C. Paxton, "Reevaluated Critical Specifications of Some Los Alamos Fast-Neutron Systems," Los Alamos National Laboratory report LA–4208 (1969).

[28] H. C. Paxton, "Los Alamos Critical Data," Los Alamos National Laboratory report LA–3067–MS, Rev., (1975).

a radius of 26.65 cm and a height of 44.239 cm. The calculated k_{eff} value was 1.0003 ± .0014.

D. Reflected Assemblies

1. Graphite-Tamped Uranium Sphere. Two simulations of assemblies that were reflected by a tamping material were done. The first experiment, conducted by H. C. Paxton at LANL in 1975,[29] consisted of a uranium sphere reflected by a uniform layer of graphite. The sphere was composed of 93.5%-enriched U-235 with a density of 18.8 g/cm^3. The reflecting layer was 5.1 cm of graphite. The reflector, with a density of 1.67 g/cm^3, consisted of 99.5% (by weight) carbon, .34% iron, and .16% sulfur. The k_{eff} value was calculated to be 0.9981 ± .0010.

2. Water-Reflected Uranium Sphere. The second reflected assembly was measured by Byers et al. at Los Alamos National Laboratory.[30] The setup consisted of a 97.67%-enriched uranium metal sphere immersed in a tank of water, which measured 30 cm in radius and 70 cm in height. The tank represented an effectively infinite water reflector. The sphere density, mass, and radius were 18.794 g/cm^3, 22.160 kg, and 6.5537 cm, respectively. The uranium composition in atoms/b-cm was 0.00053, 0.04703, 0.00010, and 0.00049 for U-234, U-235, U-236, and U-238, respectively. The atomic densities of the hydrogen and oxygen in the water were 0.06679 and 0.03340 atoms/b-cm, respectively. The MCNP-calculated k_{eff} value of this geometry was 0.9956 ± .0022.

In both cases, the S(α,β) thermal treatment was used. This treatment takes into account thermal neutron scattering by molecules, multiatomic molecules, and crystalline structures. To determine the effect of this treatment, the simulations were also run without the S(α,β) thermal treatment. The k_{eff} value computed for the graphite-reflected sphere was 0.9851 ± .0029, whereas the k_{eff} of the water-reflected sphere was 1.0177 ± .0017. Obviously, the implementation of the S(α,β) option radically affects the simulation results of reflected critical systems and should be used whenever possible.

---

[29] Ibid.

[30] C. C. Byers, et al., "Critical Measurements of a Water-Reflected Enriched Uranium Sphere," *Transactions of the American Nuclear Society* **27**, 412-413 (1977).

E. Interacting Units

1. Three Uranium Cylinders. Two interacting units were analyzed. The first experiment, performed by J. K. Fox and L. W. Gilley at Oak Ridge National Laboratory in 1959,[31] consisted of three unreflected aluminum cylinders containing U(93.2) O_2F_2 water solutions. The inside cylinder diameter and critical height measured 20.3 and 41.4 cm, respectively. The aluminum container had a density of 2.71 g/cm^3 and was 0.15 cm thick. The three cylinders were set in an equilateral configuration with a surface separation of 0.38 cm. The solution concentration parameters were 0.090g U-235/cm^3 and a hydrogen to U-235 atomic ratio of 309. Given this data, it was estimated that the solution density was approximately 1.131 g/cm^3 and consisted of 0.0021345 U-235, 0.00015382 U-238, 0.33383 oxygen, 0.65930 hydrogen, and 0.0045756 fluorine in atoms/b-cm. MCNP calculated a k_{eff} value of 0.9991 $\pm$ .0011.

2. 3 x 3 Array of Plutonium Fuel Rods. The most complex setup of the series is a 3 x 3 array of Pu metal fuel rods. This experiment was performed by H. F. Finn at Lawrence Livermore National Laboratory in 1971.[32] In each rod, three cells of Pu were separated by aluminum inner spacers, and therefore, the system was effectively a 3 x 3 x 3 array of Pu metal cells. Table 7 and Figs. 25, 26, and 27 specify the geometrical design and material specifications.

The overall arrangement was nine cylinders in a 3 x 3 configuration with a center-to-center spacing of 9.60 cm set on the surface of a table, modeled as a cylinder with a radius of 80 cm. The assembly table consisted of 2 layers–the top and bottom layers were 2.54 cm of aluminum and 30 cm of steel, respectively. Because hundreds of bolt holes were used to fasten the fuel rods to the table, the density of the aluminum was reduced to 88% of its normal value and that of steel to only 7% of its normal value.

Figure 25 is a cross-sectional cut down the long axis of a cylindrical fuel element. The element consists of three cells of plutonium metal at a vertical center-to-center

---

[31] J. K. Fox, L. W. Gilley, and E. R. Rohrer, "Critical Mass Studies, Part VIII. Aqueous Solutions of U^{233}," Oak Ridge National Laboratory report ORNL–2143 (1959).

[32] H. F. Finn, N. L. Provost, O. C. Kolar, and G. A. Pierce, "Summary of Experimentally Determined Plutonium Array Critical Configurations," Lawrence Livermore National Laboratory report UCRL–51041 (1971).

TABLE 7

MATERIAL SPECIFICATIONS FOR THE PLUTONIUM ARRAY (% MASS)

M1	M2	M3	M4	M5	M6	M7
Cr .20	C .08	N 78.0	Cr .10	Cu .25	C .03	Pu239 93.56
Cu .25	Mn .37	0 21.0	Cu .25	Fe .70	Mn .50	240 5.97
Fe .70	P .015	Ar 1.0	Fe .70	Mg 1.05	P .005	241 .46
Mg 1.0	S .025		Mg 1.025	Mn 1.25	Si .33	242 .01
Mn .15	Si .01		Mn .70	Si .30	S .009	
Si .60	Sn .30		Si .45	Al 96.30	Sn .11	
Ti .15	Fe 99.2		Ti .075		Fe 35.54	
Al 96.7			Al 96.45		Cr .07	
					Cu 2.8	
					Mg .97	
					Al 59.45	

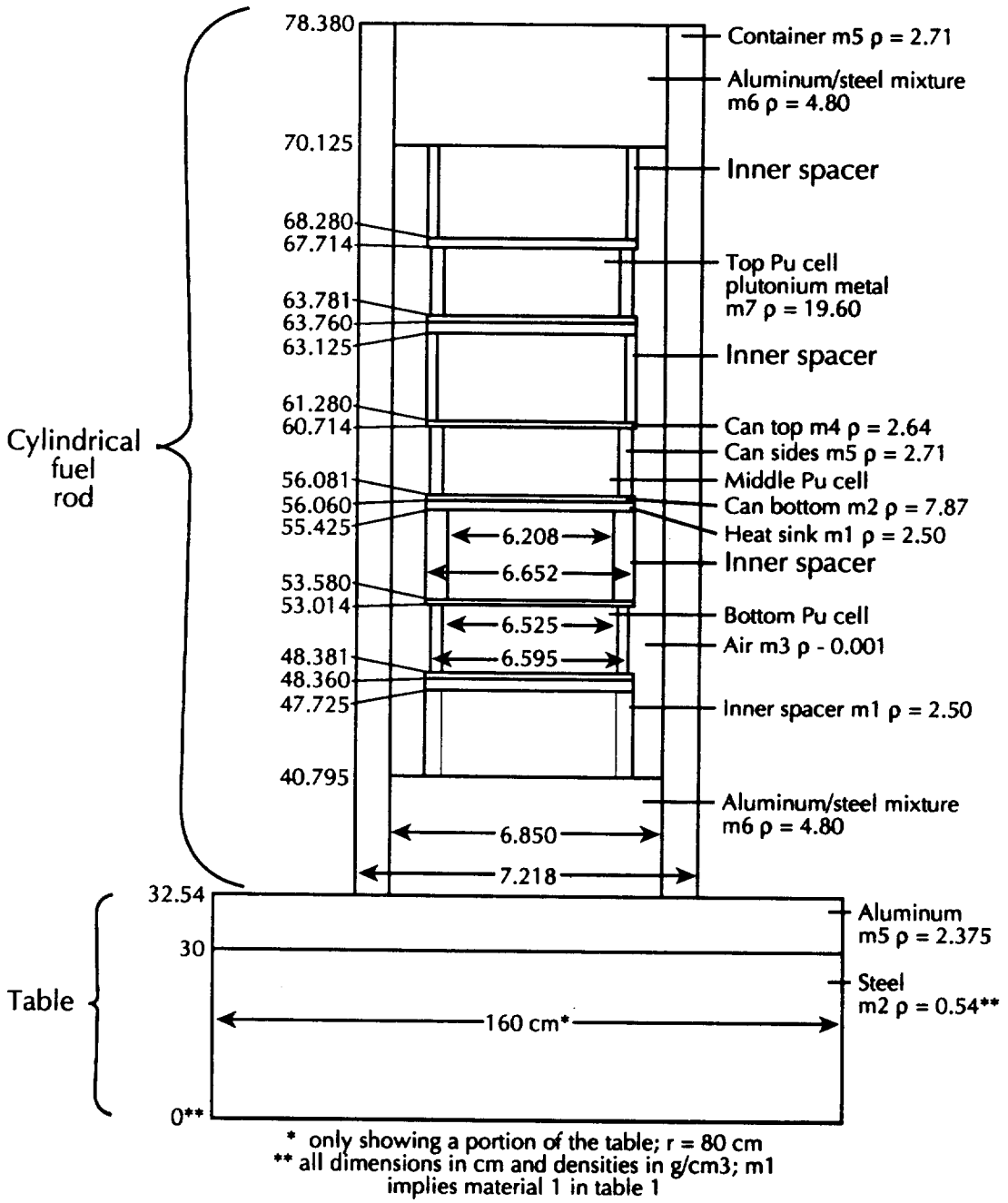

Fig. 25. Cross-sectional cut down the long axis of a cylindrical fuel element containing three cells of plutonium.

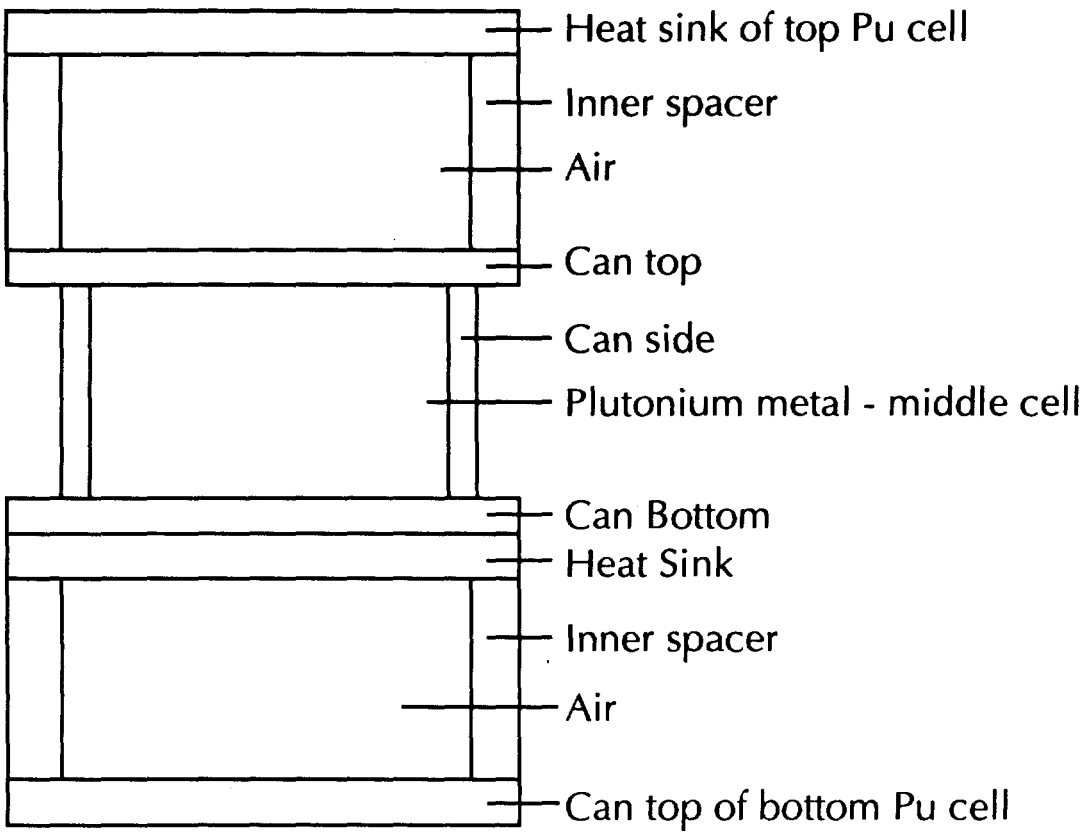

Fig. 26. Repeated structure.

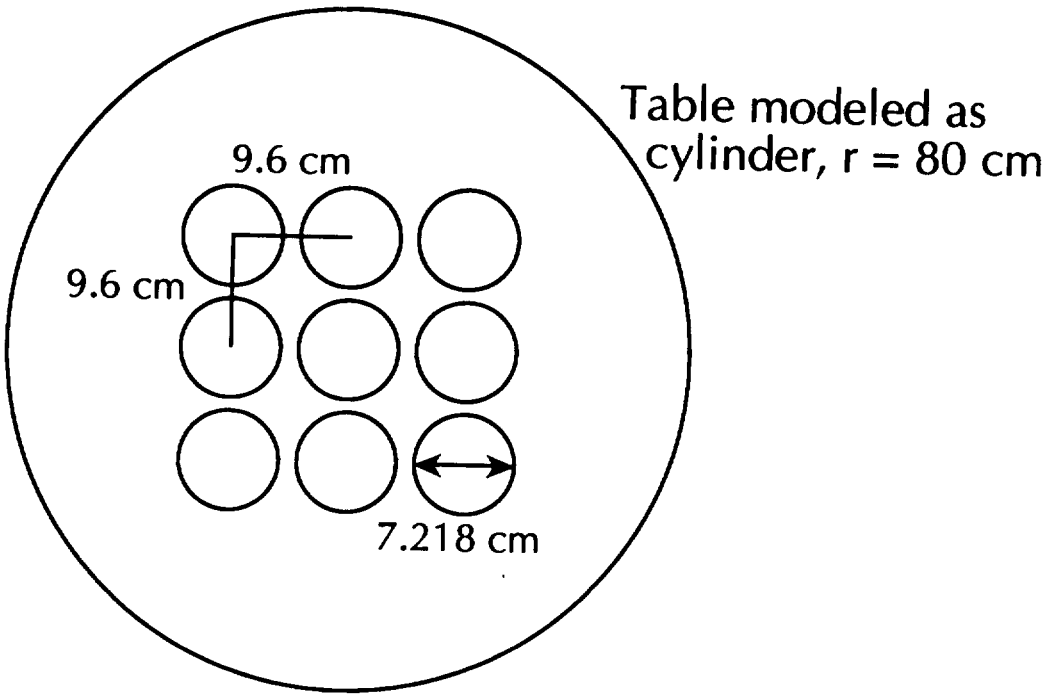

Fig. 27. Top view of the array, depicting the center-to-center separation of 9.6 cm.

spacing of 7.70 cm. The structural integrity of the system arrangement was maintained by the aluminum inner spacers placed between the cells. The plutonium itself was contained in a box fabricated from various aluminum alloys and steel. This structure consisted of an aluminum can top and sides and a steel bottom. Below the can bottom rested an aluminum heat sink. The inner spacers were attached to the bottom of the top plutonium cell's heat sink and the top of the middle cell's can top. The middle and bottom cells were similarly connected. Inner spacers were also placed between the bottom plutonium cell and a region consisting of aluminum and steel, and they connected the top cell to a similar region, which served as the cap to the aluminum cylinder which encased the system. The region inside this cylinder surrounding the plutonium cells and subsequent supporting structures was filled with air.

Figure 26 explicitly shows a plutonium cell and its connection with the other two of the system. Figure 27 depicts the top view of the 3 x 3 array and table arrangement. Table 7 displays the material specifications of the system corresponding to the labels in Fig. 26. MCNP calculated the k_{eff} value at 1.0000 $\pm$ .0019. In comparison, COG published results of 0.991 $\pm$ .0050.

V. SUMMARY

Neutron pulsed sphere, shielding, and criticality problems have been run with MCNP4. These neutron problem families were chosen as benchmarks because they represent a broad spectrum of neutron transport problems and because some of them were also used to validate the COG Monte Carlo code. MCNP predicted the experimental results of all problems in these three families well. This evaluation convincingly demonstrates that MCNP can accurately model a wide class of neutron problems.

REFERENCES

1. Judith F. Briesmeister, Editor, "MCNP – A General Monte Carlo Code for Neutron and Photon Transport, Version 3A," Los Alamos National Laboratory report LA–7396–M, Rev. 2 (1986).

2. T. E. Booth and J. S. Hendricks, "Importance Estimation in Forward Monte Carlo Calculations", *Nuclear Technology/Fusion*, **5**(1), 90 (1984).

3. C. C. Byers, et al., "Critical Measurements of a Water-Reflected Enriched Uranium Sphere," *Transactions of the American Nuclear Society* **27**, 412-413 (1977).

4. G. P. Estes, R. C. Little, R. E. Seamon, P. D. Soran, "Air Transport in Connection with the Hiroshima-Nagasaki Dose Reevaluation Effort," Los Alamos National Laboratory report LA-9369-MS (July 1982).

5. H. F. Finn, N. L. Provost, O. C. Kolar, and G. A. Pierce, "Summary of Experimentally Determined Plutonium Array Critical Configurations," Lawrence Livermore National Laboratory report UCRL–51041 (1971).

6. J. K. Fox, L. W. Gilley, and E. R. Rohrer, "Critical Mass Studies, Part VIII. Aqueous Solutions of U^{233}," Oak Ridge National Laboratory report ORNL–2143 (1959).

7. G. E. Hansen and H. C. Paxton, "Reevaluated Critical Specifications of Some Los Alamos Fast-Neutron Systems," Los Alamos National Laboratory report LA–4208 (1969).

8. L. F. Hansen, J. D. Anderson, P. S. Brown, R. J. Howerton, J. L. Kammerdiener, C. M. Logan, E. F. Plechaty, and C. Wong, "Measurements and Calculations of the Neutron Spectra from Iron Bombarded with 14-MeV Neutrons," *Nuclear Science and Engineering* **51**, 278-295 (1973).

9. L. F. Hansen, J. D. Anderson, E. Goldberg, J. Kammerdiener, E. Plechaty, and C. Wong, "Predictions for Neutron Transport in Air, Based on Integral Measurements in Nitrogen and Oxygen at 14 MeV," *Nuclear Science and Engineering* **40**, 262-282 (1970).

10. Luisa F. Hansen, John D. Anderson, Eugene Goldberg, Ernest F. Plechaty, Marion L. Stelts, and Calvin Wong, "Time Spectra from Spheres Pulsed with 14-MeV Neutrons," *Nuclear Science and Engineering* **35**, 227-239 (1969).

11. H. C. Paxton, "Los Alamos Critical Data," Los Alamos National Laboratory report LA–3067–MS, Rev. (1975).

12. Robert F. Rose and Robert W. Roussin, editors, "Shielding Benchmark Compilation," Vol. 2, Brookhaven National Laboratory report BNL-19302 (1983).

13. R. T. Santoro, R. G. Alsmiller, J. M. Barnes, and G. T. Chapman, "Calculation of Neutron and Gamma-Ray Spectra for Fusion Reactor Shield Design: Comparison with Experiment," *Nuclear Science and Engineering* **78**, 259-272 (1981).

14. Marion L. Stelts, John D. Anderson, Luisa F. Hansen, Ernest F. Plechaty, and Calvin Wong, "Spectra of Fast Neutrons from Water Pulsed with 14-MeV Neutrons," *Nuclear Science and Engineering* **46**, 53-56 (1971).

15. W. Webster and C. Wong, "Measurement of the Neutron Emission Spectra from Spheres of N, O, W, U-235, U-238, and Pu-239, Pulsed by 14-MeV Neutrons," Lawrence Livermore National Laboratory report UCID-17332 (December 15, 1976).

16. Daniel J. Whalen, David E. Hollowell, and John S. Hendricks, "MCNP: Photon Benchmark Problems," Los Alamos National Laboratory report LA–12196 (1991).

17. Thomas P. Wilcox, Jr. and Edward M. Lent, "COG - A Particle Transport Code Designed to Solve the Boltzmann Equation for Deep-Penetration (Shielding) Problems," Volume 4, "Benchmark Problems," Lawrence Livermore National Laboratory report M-221-4 (December 2, 1988).

18. C. Wong, J. D. Anderson, P. Brown, L. F. Hansen, J. L. Kammerdiener, C. Logan, and B. Pohl, "Livermore Pulsed Sphere Program: Program Summary Through July 1971," Lawrence Livermore National Laboratory report UCRL-51144, Rev.1 (1972).

APPENDIX:
MCNP INPUT FILES

```
 1 CARBON SPHERE WITH RADIUS 4.187
 2 1     2 -.001288 1 -2 -3
 3 2     1 -1.8660 (-1:2) -3
 4 3     2 -.001288 3 -4
 5 4     0 4
 6
 7 1     PX -.131
 8 2     CX 1.13
 9 3     SO 4.187
10 4     SO 1000
11 100   PX 0.0
12
13 IMP:N 1 2R 0
14 SDEF POS=0 0 0 DIR=D1 ERG=FDIR=D2 RAD=D3 VEC=-1 0 0
15       SUR=100 TME=D4
16 SI1   A   -1.0000 -.99619 -.98481 -.96593 -.93969
17           -.90631 -.86603 -.81915 -.76604 -.70711
18           -.64279 -.57358 -.50000 -.42262 -.34202
19           -.25882 -.17365 -.08716  .00000  .08716
20            .17365  .25882  .34202  .42262  .50000
21            .57358  .64279  .70711  .76604  .81915
22            .86603  .90631  .93969  .96593  .98481
23            .99619 1.0000
24 SP1        .874 .874 .875 .876 .877
25            .879 .882 .884 .888 .891
26            .895 .899 .904 .909 .914
27            .919 .924 .930 .935 .941
28            .946 .952 .957 .962 .967
29            .972 .976 .981 .985 .988
30            .991 .994 .996 .998 .999
31            1.0 1.0
32 DS2   0   -.99619 180 -.98481 175 -.96593 170 -.93962 165 -.90631 160
33           -.86603 155 -.81915 150 -.76604 145 -.70711 140 -.64279 135
34           -.57358 130 -.50000 125 -.42262 120 -.34202 115 -.25882 110
35           -.17365 105 -.08716 100  0.0000 95   .08716 90   .17365 85
36            .25882 80   .34202 75   .42262 70   .50000 65   .57358 60
37            .64279 55   .70711 50   .76604 45   .81915 40   .86603 35
38            .90631 30   .93969 25   .96593 20   .98481 15   .99619 10
39            1.0000 5
40 SI3   H 0 .6
41 SP3   D -21 1
42 SP4   -41 .4 0
43 SI5   H 15.106 15.110
44 SP5   D 0 1
45 SI10 H 15.095 15.106
46 SP10 D 0 1
47 SI15 H 15.075 15.095
48 SP15 D 0 1
49 SI20 H 15.049 15.075
50 SP20 D 0 1
51 SI25 H 15.015 15.049
52 SP25 D 0 1
53 SI30 H 14.974 15.015
54 SP30 D 0 1
55 SI35 H 14.927 14.974
56 SP35 D 0 1
57 SI40 H 14.873 14.927
58 SP40 D 0 1
59 SI45 H 14.814 14.873
60 SP45 D 0 1
61 SI50 H 14.750 14.814
62 SP50 D 0 1
63 SI55 H 14.681 14.750
64 SP55 D 0 1
65 SI60 H 14.608 14.681
66 SP60 D 0 1
67 SI65 H 14.532 14.608
68 SP65 D 0 1
69 SI70 H 14.453 14.532
70 SP70 D 0 1
71 SI75 H 14.372 14.453
72 SP75 D 0 1
73 SI80 H 14.289 14.372
74 SP80 D 0 1
75 SI85 H 14.206 14.289
76 SP85 D 0 1
77 SI90 H 14.123 14.206
78 SP90 D 0 1
79 SI95 H 14.040 14.123
80 SP95 D 0 1
```

Table A1. Livermore pulsed sphere setup for .5 m.f.p. carbon, representative of the simple sphere problems.

```
 81 SI100 H 13.958 14.040
 82 SP100 D 0 1
 83 SI105 H 13.878 13.958
 84 SP105 D 0 1
 85 SI110 H 13.800 13.878
 86 SP110 D 0 1
 87 SI115 H 13.725 13.800
 88 SP115 D 0 1
 89 SI120 H 13.654 13.725
 90 SP120 D 0 1
 91 SI125 H 13.586 13.654
 92 SP125 D 0 1
 93 SI130 H 13.522 13.586
 94 SP130 D 0 1
 95 SI135 H 13.464 13.522
 96 SP135 D 0 1
 97 SI140 H 13.410 13.464
 98 SP140 D 0 1
 99 SI145 H 13.362 13.410
100 SP145 D 0 1
101 SI150 H 13.320 13.362
102 SP150 D 0 1
103 SI155 H 13.284 13.320
104 SP155 D 0 1
105 SI160 H 13.254 13.284
106 SP160 D 0 1
107 SI165 H 13.230 13.254
108 SP165 D 0 1
109 SI170 H 13.214 13.230
110 SP170 D 0 1
111 SI175 H 13.203 13.214
112 SP175 D 0 1
113 SI180 H 13.200 13.203
114 SP180 D 0 1
115 FC5  NE213 DETECTOR, LOW BIAS, 766.0 CM FLIGHTPATH, 30 DEGREES.
116 F5X:N -663.4 383 0
117 T5    16.0 35.0
118 C     NE213 LOW BIAS RESPONSE FUCTION
119 DE5   LIN 1.6 1.8 1.9 2.0 2.1 2.2 2.3 2.4 2.5 2.75
120       3.0 3.5 4.0 4.5 5.0 5.5 6.0 6.4 6.6 6.8 7.0
121       7.5 8.1 8.5 9.0 10.0 11.0 12.0 12.5 13.0
122       13.5 14.0 15.0 16.0
123 DF5   LIN  0.00 1.46 1.86 2.26 2.58 3.00 3.29 3.42
124       3.63 3.95 4.10 4.25 4.33 4.39 4.40 4.37 4.28
125       4.15 4.20 4.18 4.12 3.97 3.80 3.77 3.65 3.44
126       3.24 3.06 3.01 2.98 2.98 3.01 3.08 3.25
127 FC15  NE213 DETECTOR, LOW BIAS, 766.0 CM FLIGHTPATH, 30 DEGREES.
128 F15X:N -663.4 383 0
129 T15    15.5 17.5 24.9 39.1
130 C      NE213 LOW BIAS RESPONSE FUNCTION
131 DE15  LIN 1.6 1.8 1.9 2.0 2.1 2.2 2.3 2.4 2.5 2.75
132       3.0 3.5 4.0 4.5 5.0 5.5 6.0 6.4 6.6 6.8 7.0
133       7.5 8.1 8.5 9.0 10.0 11.0 12.0 12.5 13.0
134       13.5 14.0 15.0 16.0
135 DF15  LIN  0.00 1.46 1.86 2.26 2.58 3.00 3.29 3.42
136       3.63 3.95 4.10 4.25 4.33 4.39 4.40 4.37 4.28
137       4.15 4.20 4.18 4.12 3.97 3.80 3.77 3.65 3.44
138       3.24 3.06 3.01 2.98 2.98 3.01 3.08 3.25
139 M1    6000 1.00
140 M2    7014 -.7885
141       8016 -.2115
142 CUT:N 39.1 1.6
143 PRINT
144 NPS   200000
```

Table A1. (cont.)

```
 1 IRON SPHERE WITH 4.8 M.F.P.
 2 1     1 -7.85 -1 -3
 3 2     1 -7.85 1 2 -3
 4 3     2 -.001288 1 -2 -3
 5 4     1 -7.85 -1 3 -4
 6 5     1 -7.85 1 2 3 -4
 7 6     2 -.001288 1 -2 3 -4
 8 7     1 -7.85 -1 4 -5
 9 8     1 -7.85 1 2 4 -5
10 9     2 -.001288 1 -2 4 -5
11 10    1 -7.85 -1 5 -6
12 11    1 -7.85 1 2 5 -6
13 12    2 -.001288 1 -2 5 -6
14 13    2 -.001288 6 -7
15 14    0 7
16
17 1     PX -.475
18 2     X 0.0 1.11 22.3 2.67
19 3     SO 6
20 4     SO 12
21 5     SO 18
22 6     SO 22.3
23 7     SO 1000
24 100   PX 0.0
25
26 IMP:N 1 1 1 2 2 2 4 4 4 8 8 8 8 0
27 SDEF  POS=0 0 0 DIR=D1 ERG=FDIR=D2 RAD=D3 VEC=-1 0 0
28       SUR=100 TME=D4
29 SI1   A   -1.0000 -.99619 -.98481 -.96593 -.93969
30           -.90631 -.86603 -.81915 -.76604 -.70711
31           -.64279 -.57358 -.50000 -.42262 -.34202
32           -.25882 -.17365 -.08716  .00000  .08716
33            .17365  .25882  .34202  .42262  .50000
34            .57358  .64279  .70711  .76604  .81915
35            .86603  .90631  .93969  .96593  .98481
36            .99619  1.0000
37 SP1        .874 .874 .875 .876 .877
38            .879 .882 .884 .888 .891
39            .895 .899 .904 .909 .914
40            .919 .924 .930 .935 .941
41            .946 .952 .957 .962 .967
42            .972 .976 .981 .985 .988
43            .991 .994 .996 .998 .999
44            1.0 1.0
45 DS2   Q   -.99619 180 -.98481 175 -.96593 170 -.93962 165 -.90631 160
46           -.86603 155 -.81915 150 -.76604 145 -.70711 140 -.64279 135
47           -.57358 130 -.50000 125 -.42262 120 -.34202 115 -.25882 110
48           -.17365 105 -.08716 100  0.0000 95    .08716 90    .17365 85
49            .25882 80    .34202 75    .42262 70    .50000 65    .57358 60
50            .64279 55    .70711 50    .76604 45    .81915 40    .86603 35
51            .90631 30    .93969 25    .96593 20    .98481 15    .99619 10
52            1.0000 5
53 SI3   H 0 .6
54 SP3   D -21 1
55 SP4   -41 .3 0
56 SI5   H 15.106 15.110
57 SP5   D 0 1
58 SI10  H 15.095 15.106
59 SP10  D 0 1
60 SI15  H 15.075 15.095
61 SP15  D 0 1
62 SI20  H 15.049 15.075
63 SP20  D 0 1
64 SI25  H 15.015 15.049
65 SP25  D 0 1
66 SI30  H 14.974 15.015
67 SP30  D 0 1
68 SI35  H 14.927 14.974
69 SP35  D 0 1
70 SI40  H 14.873 14.927
71 SP40  D 0 1
72 SI45  H 14.814 14.873
73 SP45  D 0 1
74 SI50  H 14.750 14.814
75 SP50  D 0 1
76 SI55  H 14.681 14.750
77 SP55  D 0 1
78 SI60  H 14.608 14.681
79 SP60  D 0 1
80 SI65  H 14.532 14.608
```

Table A2. Livermore pulsed sphere setup for 4.8 m.f.p. iron – the only sphere subdivided for importance sampling.

```
 81 SP65 D 0 1
 82 SI70 H 14.453 14.532
 83 SP70 D 0 1
 84 SI75 H 14.372 14.453
 85 SP75 D 0 1
 86 SI80 H 14.289 14.372
 87 SP80 D 0 1
 88 SI85 H 14.206 14.289
 89 SP85 D 0 1
 90 SI90 H 14.123 14.206
 91 SP90 D 0 1
 92 SI95 H 14.040 14.123
 93 SP95 D 0 1
 94 SI100 H 13.958 14.040
 95 SP100 D 0 1
 96 SI105 H 13.878 13.958
 97 SP105 D 0 1
 98 SI110 H 13.800 13.878
 99 SP110 D 0 1
100 SI115 H 13.725 13.800
101 SP115 D 0 1
102 SI120 H 13.654 13.725
103 SP120 D 0 1
104 SI125 H 13.586 13.654
105 SP125 D 0 1
106 SI130 H 13.522 13.586
107 SP130 D 0 1
108 SI135 H 13.464 13.522
109 SP135 D 0 1
110 SI140 H 13.410 13.464
111 SP140 D 0 1
112 SI145 H 13.362 13.410
113 SP145 D 0 1
114 SI150 H 13.320 13.362
115 SP150 D 0 1
116 SI155 H 13.284 13.320
117 SP155 D 0 1
118 SI160 H 13.254 13.284
119 SP160 D 0 1
120 SI165 H 13.230 13.254
121 SP165 D 0 1
122 SI170 H 13.214 13.230
123 SP170 D 0 1
124 SI175 H 13.203 13.214
125 SP175 D 0 1
126 SI180 H 13.200 13.203
127 SP180 D 0 1
128 FC5  NE213 DETECTOR RESPONSE FUNCTION, 766.0 CM FLIGHTPATH, 30 DEGREES.
129 F5X:N -663.4 383 0
130 T5    16.0 35.0
131 C     NE213 LOW BIAS RESPONSE FUCTION
132 DE5   LIN 1.6 1.8 1.9 2.0 2.1 2.2 2.3 2.4 2.5 2.75
133       3.0 3.5 4.0 4.5 5.0 5.5 6.0 6.4 6.6 6.8 7.0
134       7.5 8.1 8.5 9.0 10.0 11.0 12.0 12.5 13.0
135       13.5 14.0 15.0 16.0
136 DF5   LIN  0.00 1.46 1.86 2.26 2.58 3.00 3.29 3.42
137       3.63 3.95 4.10 4.25 4.33 4.39 4.40 4.37 4.28
138       4.15 4.20 4.18 4.12 3.97 3.80 3.77 3.65 3.44
139       3.24 3.06 3.01 2.98 2.98 3.01 3.08 3.25
140 FC15  NE213 DETECTOR, LOW BIAS, 766.0 CM FLIGHTPATH, 30 DEGREES.
141 F15X:N -663.4 383 0
142 T15    15.5 17.5 24.9 39.1
143 C      NE213 LOW BIAS RESPONSE FUNCTION
144 DE15  LIN 1.6 1.8 1.9 2.0 2.1 2.2 2.3 2.4 2.5 2.75
145       3.0 3.5 4.0 4.5 5.0 5.5 6.0 6.4 6.6 6.8 7.0
146       7.5 8.1 8.5 9.0 10.0 11.0 12.0 12.5 13.0
147       13.5 14.0 15.0 16.0
148 DF15  LIN  0.00 1.46 1.86 2.26 2.58 3.00 3.29 3.42
149       3.63 3.95 4.10 4.25 4.33 4.39 4.40 4.37 4.28
150       4.15 4.20 4.18 4.12 3.97 3.80 3.77 3.65 3.44
151       3.24 3.06 3.01 2.98 2.98 3.01 3.08 3.25
152 M1   26000 .970
153       6000 .012
154      25055 .010
155      19000 .007
156      16032 .001
157 M2    7014 -.7885
158       8016 -.2115
159 CUT:N 39.1 1.6
160 PRINT
```

Table A2. (cont.)

```
NITROGEN SPHERE WITH 3.1 M.F.P.
1     2 -.001288 2 -3 -6
2     3 -7.9 2 3 -4 -6
3     3 -7.9 1 -2 -4
4     1 -.808 1 4 -5
5     1 -.808 -1 -5
6     3 -7.9 1 4 5 -6
7     3 -7.9 -1 5 -6
8     2 -.000001 1 6 -7
9     2 -.000001 -1 6 -7
10    3 -7.9 1 7 -8
11    3 -7.9 -1 7 -8
12    2 -.001288 8 -9
13    0 9

1     PX -1.6
2     PX -1.55
3     X  -1.5 2.86 55.9 6.8
4     X  -1.5 2.91 55.9 6.85
5     SO 55.88
6     SO 55.93
7     SO 60.96
8     SO 61.11
9     SO 1000
100   PX 0.0

IMP:N 1 11R 0
SDEF POS=0 0 0 DIR=D1 ERG=FDIR=D2 RAD=D3 VEC=-1 0 0
     SUR=100 TME=D4
SI1  A  -1.0000 -.99619 -.98481 -.96593 -.93969
        -.90631 -.86603 -.81915 -.76604 -.70711
        -.64279 -.57358 -.50000 -.42262 -.34202
        -.25882 -.17365 -.08716  .00000  .08716
         .17365  .25882  .34202  .42262  .50000
         .57358  .64279  .70711  .76604  .81915
         .86603  .90631  .93969  .96593  .98481
         .99619 1.0000
SP1      .874 .874 .875 .876 .877
         .879 .882 .884 .888 .891
         .895 .899 .904 .909 .914
         .919 .924 .930 .935 .941
         .946 .952 .957 .962 .967
         .972 .976 .981 .985 .988
         .991 .994 .996 .998 .999
         1.0 1.0
DS2  Q  -.99619 180 -.98481 175 -.96593 170 -.93962 165 -.90631 160
        -.86603 155 -.81915 150 -.76604 145 -.70711 140 -.64279 135
        -.57358 130 -.50000 125 -.42262 120 -.34202 115 -.25882 110
        -.17365 105 -.08716 100  0.0000 95   .08716 90   .17365 85
         .25882 80   .34202 75   .42262 70   .50000 65   .57358 60
         .64279 55   .70711 50   .76604 45   .81915 40   .86603 35
         .90631 30   .93969 25   .96593 20   .98481 15   .99619 10
         1.0000 5
SI3  H 0 .6
SP3  D -21 1
SP4  -41 .4 0
SI5  H 15.106 15.110
SP5  D 0 1
SI10 H 15.095 15.106
SP10 D 0 1
SI15 H 15.075 15.095
SP15 D 0 1
SI20 H 15.049 15.075
SP20 D 0 1
SI25 H 15.015 15.049
SP25 D 0 1
SI30 H 14.974 15.015
SP30 D 0 1
SI35 H 14.927 14.974
SP35 D 0 1
SI40 H 14.873 14.927
SP40 D 0 1
SI45 H 14.814 14.873
SP45 D 0 1
SI50 H 14.750 14.814
SP50 D 0 1
SI55 H 14.681 14.750
SP55 D 0 1
SI60 H 14.608 14.681
SP60 D 0 1
```

Table A3. Livermore pulsed sphere setup for 3.1 m.f.p. nitrogen, representative of the liquid spheres.

```
 81 SI65 H 14.532 14.608
 82 SP65 D 0 1
 83 SI70 H 14.453 14.532
 84 SP70 D 0 1
 85 SI75 H 14.372 14.453
 86 SP75 D 0 1
 87 SI80 H 14.289 14.372
 88 SP80 D 0 1
 89 SI85 H 14.206 14.289
 90 SP85 D 0 1
 91 SI90 H 14.123 14.206
 92 SP90 D 0 1
 93 SI95 H 14.040 14.123
 94 SP95 D 0 1
 95 SI100 H 13.958 14.040
 96 SP100 D 0 1
 97 SI105 H 13.878 13.958
 98 SP105 D 0 1
 99 SI110 H 13.800 13.878
100 SP110 D 0 1
101 SI115 H 13.725 13.800
102 SP115 D 0 1
103 SI120 H 13.654 13.725
104 SP120 D 0 1
105 SI125 H 13.586 13.654
106 SP125 D 0 1
107 SI130 H 13.522 13.586
108 SP130 D 0 1
109 SI135 H 13.464 13.522
110 SP135 D 0 1
111 SI140 H 13.410 13.464
112 SP140 D 0 1
113 SI145 H 13.362 13.410
114 SP145 D 0 1
115 SI150 H 13.320 13.362
116 SP150 D 0 1
117 SI155 H 13.284 13.320
118 SP155 D 0 1
119 SI160 H 13.254 13.284
120 SP160 D 0 1
121 SI165 H 13.230 13.254
122 SP165 D 0 1
123 SI170 H 13.214 13.230
124 SP170 D 0 1
125 SI175 H 13.203 13.214
126 SP175 D 0 1
127 SI180 H 13.200 13.203
128 SP180 D 0 1
129 FC5  PILOT B DETECTOR RESPONSE FUNCTION, 765.20 CM FLIGHTPATH, 30 DEGREES.
130 F5X:N -662.7 382.6 0
131 T5    16.0 35.0
132 DE5   LIN 1.6 2.0 13I 16.0
133 DF5   LIN 0.00 2.25 4.10 4.70 4.85 4.85 4.70 4.30
134           4.25 4.05 3.85 3.65 3.55 3.60 3.75 3.85
135 FC15  PILOT B DETECTOR RESPONSE FUNCTION, 765.2 CM FLIGHTPATH, 30 DEGREES.
136 F15X:N -662.7 382.6 0
137 T15    15.5 17.5 24.9 39.1
138 DE15  LIN 1.6 2.0 13I 16.0
139 DF15  LIN 0.00 2.25 4.10 4.70 4.85 4.85 4.70 4.30
140           4.25 4.05 3.85 3.65 3.55 3.60 3.75 3.85
141 M1    7014 1.00
142 M2    7014 -.7885
143       8016 -.2115
144 M3    26000 .686
145       24000 .200
146       28000 .084
147       14000 .020
148       12000 .010
149 CUT:N 39.1 1.6
150 PRINT
151 NPS   400000
```

Table A3. (cont.)

```
FUSION SPECTRA PROBLEM
     1 1 7.506E-2 1 -2 10 -21 -22 29 $ FLOOR CELL $
     2 1 7.506E-2 7 -8 10 -21 -22 29 $ CEILING CELL $
     3 1 7.506E-2 2 -7 10 -21 -22 23 $ LEFT WALL CELL $
     4 1 7.506E-2 2 -7 10 -21 -28 29 $ RIGHT WALL CELL $
     5 1 7.506E-2 2 -7 20 -21 -23 28 $ FRONT WALL CELL $
     6 2 4.614E-5 2 -4 10 -11 -23 32 $ LEFT DOOR CELL $
     7 2 4.614E-5 2 -4 10 -11 -33 34 $ MIDDLE DOOR CELL $
     8 2 4.614E-5 2 -4 10 -11 -35 28 $ RIGHT DOOR CELL $
     9 1 7.506E-2 4 -7 10 -11 -23 32 $ CONCRETE ABOVE LEFT DOOR $
    10 1 7.506E-2 4 -7 10 -11 -33 34 $ CONCRETE ABOVE MIDDLE DOOR
    11 1 7.506E-2 4 -7 10 -11 -35 28 $ CONCRETE ABOVE RIGHT DOOR
    12 1 7.506E-2 2 -4 10 -11 -32 33 $ CONCRETE CELL BETWN L/M DOORS
    13 1 7.506E-2 2 -4 10 -11 -34 35 $ CONCRETE CELL BETWN M/R DOORS
    14 1 7.506E-2 4 -7 10 -11 -32 33 $ WALL CONCRETE ABOVE CELL 12
    15 1 7.506E-2 4 -7 10 -11 -34 35 $ WALL CONCRETE ABOVE CELL 13
    16 2 4.614E-5 2 -4 11 -12 -23 32 $ AIR CELL BTWN LEFT DOOR & BLOCK BACK
    17 2 4.614E-5 2 -4 11 -12 -33 34 $ AIR CELL BTWN MIDDLE DOOR & BLOCK BACK
    18 2 4.614E-5 2 -4 11 -12 -35 28 $ AIR CELL BTWN RIGHT DOOR & BLOCK BACK
    19 2 4.614E-5 2 -4 11 -12 -32 33 $ AIR CELL BTWN CELL12 DOOR & BLOCK BACK
    20 2 4.614E-5 2 -4 11 -12 -34 35 $ AIR CELL BTWN CELL13 DOOR & BLOCK BACK
    21 2 4.614E-5 4 -7 11 -12 -23 32 $ AIR CELL BTWN CELL 9 DOOR & BLOCK BACK
    22 2 4.614E-5 4 -7 11 -12 -33 34 $ AIR CELL BTWN CELL10 DOOR & BLOCK BACK
    23 2 4.614E-5 4 -7 11 -12 -35 28 $ AIR CELL BTWN CELL11 DOOR & BLOCK BACK
    24 2 4.614E-5 4 -7 11 -12 -32 33 $ AIR CELL BTWN CELL14 DOOR & BLOCK BACK
    25 2 4.614E-5 4 -7 11 -12 -34 35 $ AIR CELL BTWN CELL15 DOOR & BLOCK BACK
    26 2 4.614E-5 6 -7 12 -15 -23 32 $ CELLS 26-35: AIR CELLS ABV THE BLOCK
    27 2 4.614E-5 6 -7 12 -15 -32 33
    28 2 4.614E-5 6 -7 12 -15 -33 34
    29 2 4.614E-5 6 -7 12 -15 -34 35
    30 2 4.614E-5 6 -7 12 -15 -35 28
    31 2 4.614E-5 6 -7 15 -17 -23 32
    32 2 4.614E-5 6 -7 15 -17 -32 33
    33 2 4.614E-5 6 -7 15 -17 -33 34
    34 2 4.614E-5 6 -7 15 -17 -34 35
    35 2 4.614E-5 6 -7 15 -17 -35 28
    36 2 4.614E-5 2 -3 12 -15 -23 32 $ CELLS 36-47: AIR CELLS LEFT OF BLOCK
    37 2 4.614E-5 2 -3 12 -15 -32 24
    38 2 4.614E-5 2 -3 15 -17 -23 32
    39 2 4.614E-5 2 -3 15 -17 -32 24
    40 2 4.614E-5 3 -4 12 -15 -23 32
    41 2 4.614E-5 3 -4 12 -15 -32 24
    42 2 4.614E-5 3 -4 15 -17 -23 32
    43 2 4.614E-5 3 -4 15 -17 -32 24
    44 2 4.614E-5 4 -6 12 -15 -23 32
    45 2 4.614E-5 4 -6 12 -15 -32 24
    46 2 4.614E-5 4 -6 15 -17 -23 32
    47 2 4.614E-5 4 -6 15 -17 -32 24
    48 2 4.614E-5 2 -3 12 -15 -27 35 $ CELLS 48-59: AIR CELLS RIGHT OF BLOCK
    49 2 4.614E-5 2 -3 12 -15 -35 28
    50 2 4.614E-5 2 -3 15 -17 -27 35
    51 2 4.614E-5 2 -3 15 -17 -35 28
    52 2 4.614E-5 3 -4 12 -15 -27 35
    53 2 4.614E-5 3 -4 12 -15 -35 28
    54 2 4.614E-5 3 -4 15 -17 -27 35
    55 2 4.614E-5 3 -4 15 -17 -35 28
    56 2 4.614E-5 4 -6 12 -15 -27 35
    57 2 4.614E-5 4 -6 12 -15 -35 28
    58 2 4.614E-5 4 -6 15 -17 -27 35
    59 2 4.614E-5 4 -6 15 -17 -35 28
    60 2 4.614E-5 6 -7 17 -40 -23 32 $ CELLS 60-69: AIR CELLS ABV THERMAL SHIELD
    61 2 4.614E-5 6 -7 17 -40 -32 33
    62 2 4.614E-5 6 -7 17 -40 -33 34
    63 2 4.614E-5 6 -7 17 -40 -34 35
    64 2 4.614E-5 6 -7 17 -40 -35 28
    65 2 4.614E-5 6 -7 40 -20 -23 32
    66 2 4.614E-5 6 -7 40 -20 -32 33
    67 2 4.614E-5 6 -7 40 -20 -33 34
    68 2 4.614E-5 6 -7 40 -20 -34 35
    69 2 4.614E-5 6 -7 40 -20 -35 28
    70 2 4.614E-5 2 -3 17 -40 -23 32 $ CELLS 70-81: AIR CELLS LEFT OF THERMAL SHIELD
    71 2 4.614E-5 2 -3 17 -40 -32 24
    72 2 4.614E-5 2 -3 40 -20 -23 32
    73 2 4.614E-5 2 -3 40 -20 -32 24
    74 2 4.614E-5 3 -4 17 -40 -23 32
    75 2 4.614E-5 3 -4 17 -40 -32 24
    76 2 4.614E-5 3 -4 40 -20 -23 32
    77 2 4.614E-5 3 -4 40 -20 -32 24
    78 2 4.614E-5 4 -6 17 -40 -23 32
    79 2 4.614E-5 4 -6 17 -40 -32 24
```

Table A4. Fusion shielding benchmark setup for configuration 3 with an on-axis neutron detector.

```
 81    80 2 4.614E-5 4 -6 40 -20 -23 32
 82    81 2 4.614E-5 4 -6 40 -20 -32 24
 83    82 2 4.614E-5 2 -3 17 -40 -27 35 $ CELLS 82-93: AIR CELLS RIGHT OF THERMAL SHIELD
 84    83 2 4.614E-5 2 -3 17 -40 -35 28
 85    84 2 4.614E-5 2 -3 40 -20 -27 35
 86    85 2 4.614E-5 2 -3 40 -20 -35 28
 87    86 2 4.614E-5 3 -4 17 -40 -27 35
 88    87 2 4.614E-5 3 -4 17 -40 -35 28
 89    88 2 4.614E-5 3 -4 40 -20 -27 35
 90    89 2 4.614E-5 3 -4 40 -20 -35 28
 91    90 2 4.614E-5 4 -6 17 -40 -27 35
 92    91 2 4.614E-5 4 -6 17 -40 -35 28
 93    92 2 4.614E-5 4 -6 40 -20 -27 35
 94    93 2 4.614E-5 4 -6 40 -20 -35 28
 95    94 4 8.75E-2 3 -5 -25 26 15 -41 $ CELLS 94-103: AIR AND SHIELD CELLS INSIDE
 96    95 4 8.75E-2 3 -5 -25 26 41 -42 $ THE CONCRETE BOX
 97    96 4 8.75E-2 3 -5 -25 26 42 -43
 98    97 2 4.614E-5 3 -5 -25 26 43 -44
 99    98 2 4.614E-5 3 -5 -25 26 44 -45
100    99 2 4.614E-5 3 -5 -25 26 45 -46
101   100 2 4.614E-5 3 -5 -25 26 46 -47
102   101 2 4.614E-5 3 -5 -25 26 47 -48
103   102 2 4.614E-5 3 -5 -25 26 48 -49
104   103 2 4.614E-5 3 -5 -25 26 49 -17
105   104 2 4.614E-5 3 -9 -25 26 17 -18 $ AIR CELL BTWN INNER BOX AND THERMAL SHIELD
106   105 2 4.614E-5 3 -9 -30 31 19 -40 $ CELLS 105-106: AIR CELLS FITTING BETWEEN
107   106 2 4.614E-5 3 -9 -30 31 40 -20 $ THE THERMAL SHIELD AND THE FRONT WALL
108   107 2 4.614E-5 9 -6 -24 27 17 -18 $ CELLS 107-109: AIR CELLS BETWEEN THE UPPER
109   108 2 4.614E-5 9 -6 -24 27 18 -40 $ HORIZONTAL EDGE OF THE CONCRETE BLOCK
110   109 2 4.614E-5 9 -6 -24 27 40 -20 $ AND THE FRONT WALL
111   110 2 4.614E-5 2 -3 -24 27 17 -18 $ CELLS 110-112: AIR CELLS BETWEEN THE
112   111 2 4.614E-5 2 -3 -24 27 18 -40 $ LOWER HORIZONTAL EDGE OF THE CONCRETE
113   112 2 4.614E-5 2 -3 -24 27 40 -20 $ BOX  AND THE FRONT WALL
114   113 2 4.614E-5 3 -9 -24 25 17 -18 $ CELLS 113-118: AIR CELLS BETWEEN THE
115   114 2 4.614E-5 3 -9 -24 25 18 -40 $ RIGHT AND LEFT VERTICAL CONCRETE BOX
116   115 2 4.614E-5 3 -9 -24 25 40 -20 $ WALLS AND THE FRONT WALL
117   116 2 4.614E-5 3 -9 -26 27 17 -18
118   117 2 4.614E-5 3 -9 -26 27 18 -40
119   118 2 4.614E-5 3 -9 -26 27 40 -20
120   119 0 -36 12 -13 $ VACUUM INSIDE BEAMLINE
121   120 0 -36 13 -14 $ VACUUM INSIDE IRON CAN
122   121 0 14 -15 -38 $ VACUUM INSIDE IRON PIPE
123   122 3 8.48E-2 36 -37 12 -13 $ BEAMLINE
124   123 3 8.48E-2 36 -39 13 -14 $ IRON CAN
125   124 3 8.48E-2 38 -39 14 -15 $ IRON PIPE
126   125 5 1.1139E-1 37 -39 12 -13
127   126 1 7.506E-2 5 -6 12 -15 -24 33 $ CELLS 126-134: CONCRETE BOX TOP CELLS
128   127 1 7.506E-2 5 -6 12 -15 -33 34
129   128 1 7.506E-2 5 -6 12 -15 -34 27
130   129 1 7.506E-2 5 -6 15 -45 -24 33
131   130 1 7.506E-2 5 -6 15 -45 -33 34
132   131 1 7.506E-2 5 -6 15 -45 -34 27
133   132 1 7.506E-2 5 -6 45 -17 -24 33
134   133 1 7.506E-2 5 -6 45 -17 -33 34
135   134 1 7.506E-2 5 -6 45 -17 -34 27
136   135 1 7.506E-2 2 -3 12 -15 -24 33 $ CELLS 135-143: CNCR BOX BOTTOM CELLS
137   136 1 7.506E-2 2 -3 12 -15 -33 34
138   137 1 7.506E-2 2 -3 12 -15 -34 27
139   138 1 7.506E-2 2 -3 15 -45 -24 33
140   139 1 7.506E-2 2 -3 15 -45 -33 34
141   140 1 7.506E-2 2 -3 15 -45 -34 27
142   141 1 7.506E-2 2 -3 45 -17 -24 33
143   142 1 7.506E-2 2 -3 45 -17 -33 34
144   143 1 7.506E-2 2 -3 45 -17 -34 27
145   144 1 7.506E-2 -24 25 3 -50 12 -15 $ CELLS 144-149: CONCRETE BOX LEFT
146   145 1 7.506E-2 -24 25 3 -50 15 -45 $ VERTICAL WALL CELLS
147   146 1 7.506E-2 -24 25 3 -50 45 -17
148   147 1 7.506E-2 -24 25 50 -5 12 -15
149   148 1 7.506E-2 -24 25 50 -5 15 -45
150   149 1 7.506E-2 -24 25 50 -5 45 -17
151   150 1 7.506E-2 -26 27 3 -50 12 -15 $ CELLS 150-155: CONCRETE BOX RIGHT
152   151 1 7.506E-2 -26 27 3 -50 15 -45 $ VERTICAL WALL CELLS
153   152 1 7.506E-2 -26 27 3 -50 45 -17
154   153 1 7.506E-2 -26 27 50 -5 12 -15
155   154 1 7.506E-2 -26 27 50 -5 15 -45
156   155 1 7.506E-2 -26 27 50 -5 45 -17
157   156 1 7.506E-2 3 -5 -25 26 39 12 -51 $ CELLS 156-164: INNER CONCRETE BOX CELLS
158   157 1 7.506E-2 3 -5 -25 26 39 51 -52
159   158 1 7.506E-2 3 -5 -25 26 39 52 -53
160   159 1 7.506E-2 3 -5 -25 26 39 53 -54
```

Table A4. (cont.)

```
161    160 1 7.506E-2 3 -5 -25 26 39 54 -55
162    161 1 7.506E-2 3 -5 -25 26 39 55 -56
163    162 1 7.506E-2 3 -5 -25 26 39 56 -57
164    163 1 7.506E-2 3 -5 -25 26 39 57 -58
165    164 1 7.506E-2 3 -5 -25 26 39 58 -15
166 C          165 2 4.614E-5 9 -5 -25 26 18 -40 $ CELLS 165-170: AIR CELLS CENTERED
167 C          166 2 4.614E-5 9 -5 -25 26 40 -20 $ AROUND THE THERMAL SHIELD
168    167 2 4.614E-5 -25 30 3 -9 18 -40
169    168 2 4.614E-5 -25 30 3 -9 40 -20
170    169 2 4.614E-5 -31 26 3 -9 18 -40
171    170 2 4.614E-5 -31 26 3 -9 40 -20
172    171 4 8.75E-2 18 -19 3 -9 -30 31 $ THERMAL SHIELD
173    172 0 -1  $ VOID CELL BELOW THE CONCRETE ROOM
174    173 0  8 $ VOID CELL ABOVE THE CONCRETE ROOM
175    174 0  1 -8 -22 29 -10 $ VOID CELL BEHIND THE REAR WALL
176    175 0  1 -8 -22 29 21  $ VOID CELL IN FRONT OF THE FRONT WALL
177    176 0  1 -8 22 $ VOID CELL LEFT OF THE ROOM
178    177 0  1 -8 -29 $ VOID CELL RIGHT OF THE ROOM
179
180      1 PZ -91.44
181      2 PZ 0 $ UPPER FLOOR PLANE
182      3 PZ 81.2 $ INNER BOX BOTTOM/LOWER THERMAL SHIELD EDGE
183      4 PZ 218.4 $ DOOR UPPER EDGE
184      5 PZ 253.92 $ INNER BOX TOP
185      6 PZ 317.50 $ CONCRETE BOX TOP
186      7 PZ 495.30 $ CEILING PLANE (LOWER)
187      8 PZ 586.74 $ CEILING PLANE (UPPER)
188      9 PZ 233.60 $ UPPER THERMAL SHIELD EDGE
189     10 PY -29.21 $ REAR WALL PLANE (REAR)
190     11 PY 0 $ REAR WALL PLANE (FRONT)
191     12 PY 160.02 $ REAR OF CONCRETE BOX
192     13 PY 208.28 $ END OF PARAFFIN
193     14 PY 225.56 $ REAR EDGE OF IRON CAN
194     15 PY 253.06 $ END OF IRON PIPE/REAR OF INNER BOX
195     16 PY 232.02 $ PLANE OF TARGET
196     17 PY 353.06 $ FRONT OF CONCRETE BOX
197     18 PY 436.52 $ FRONT OF THERMAL SHIELD
198     19 PY 441.60 $ REAR OF THERMAL SHIELD
199     20 PY 570.20 $ FRONT WALL PLANE (INSIDE)
200     21 PY 661.64 $ FRONT WALL PLANE (OUTSIDE)
201     22 PX 91.44  $ LEFT WALL PLANE (OUTSIDE)
202     23 PX 0      $ LEFT WALL PLANE (INSIDE)
203     24 PX -200.66 $ LEFT SIDE OF CONCRETE BOX
204     25 PX -278.76 $ LEFT SIDE OF INNER BOX
205     26 PX -434.97 $ RIGHT SIDE OF INNER BOX
206     27 PX -513.08 $ RIGHT SIDE OF CONCRETE BOX
207     28 PX -716.28 $ RIGHT WALL PLANE (INSIDE)
208     29 PX -807.72 $ RIGHT WALL PLANE (OUTSIDE)
209     30 PX -280.66 $ LEFT EDGE OF THERMAL SHIELD
210     31 PX -433.06 $ RIGHT EDGE OF THERMAL SHIELD
211     32 PX -114.3  $ RIGHT EDGE OF LEFT DOOR
212     33 PX -300.99 $ LEFT EDGE OF MIDDLE DOOR
213     34 PX -415.29 $ RIGHT EDGE OF MIDDLE DOOR
214     35 PX -601.98 $ LEFT EDGE OF RIGHT DOOR
215     36 C/Y -356.87 157.4 4.5   $ BEAMLINE INNER SURFACE
216     37 C/Y -356.87 157.4 5.0   $ BEAMLINE OUTER SURFACE
217     38 C/Y -356.87 157.4 8.87  $ IRON PIPE INNER SURFACE
218     39 C/Y -356.87 157.4 16.37 $ IRON PIPE OUTER SURFACE
219     40 PY 470
220     41 PY 263.06
221     42 PY 273.06
222     43 PY 283.54
223     44 PY 293.06
224     45 PY 303.06
225     46 PY 313.06
226     47 PY 323.06
227     48 PY 333.06
228     49 PY 343.06
229     50 PZ 160
230     51 PY 170
231     52 PY 180
232     53 PY 190
233     54 PY 200
234     55 PY 210
235     56 PY 220
236     57 PY 230
237     58 PY 240
238
239 MODE N
240 WWP:N 4 3 2
```

Table A4. (cont.)

```
241 WWE:N  1.0000E+02
242 WWN 1:N   5.7157E-01  8.2482E-01  1.1366E+00  1.8827E+00  2.3545E-01
243           1.0000E+00  5.00000+00  1.0000E+00  5.0000E+00  1.0000E+01
244           1.0000E+01  5.0000E+00  5.0000E+01  1.0000E+01  1.0000E+01
245           3.4082E+00  1.5581E+00  1.0000E+00  5.0000E+00  4.5422E+00
246           7.8755E-01  2.0160E+00  1.4663E+00  7.2476E-01  1.0350E+00
247           1.8184E+00  2.2603E-01  1.3198E+00  8.3289E-01  3.0384E-01
248           5.6475E-03  1.9888E-01  3.4128E-01  4.1735E-01  2.6609E-01
249           4.6663E-01  2.3017E+00  8.8655E-01  2.5864E+00  1.9168E+00
250           1.2505E+00  3.5393E-01  5.0000E+00  3.7027E-01  4.8900E-01
251           4.6495E-01  6.9928E-01  1.0000E+00  1.0000E+00  2.0362E+00
252           3.0384E-01  6.1182E-01  1.0000E+00  9.1791E-01  3.0384E-01
253           3.5736E-01  8.3125E-01  8.1134E-01  5.5875E-01  5.2973E-01
254           1.5926E-01  3.0755E-01  1.9963E-01  1.2932E-05  1.8919E-01
255           1.9391E-01  4.3654E-01  5.9392E-01  1.0955E+00  3.8491E-01
256           2.9517E-01  2.8659E-01  6.4150E-01  6.3696E-01  7.7681E-01
257           4.8742E-01  1.9254E-01  1.1340E+00  7.7210E-01  8.5872E-01
258           2.0716E-01  7.7957E-01  3.7973E-01  1.2901E-01  1.4179E-01
259           2.8714E-01  1.1002E+00  1.5525E-01  7.1047E-02  9.8868E-02
260           4.6750E-01  1.3068E-01  9.8851E-02  3.3947E-01  1.2105E-01
261           4.7428E-02  6.3136E-02  5.5451E-02  4.7208E-02  4.0007E-02
262           3.5268E-02  3.1338E-02  2.8126E-02  2.8636E-02  2.7712E-02
263           4.8677E-02  5.9129E-02  1.5066E-01  1.4831E-01  6.6109E-02
264           5.4306E-02  9.5399E-02  1.0807E-01  1.1663E-01  8.5825E-02
265           1.0803E-01  6.0931E-02  1.0544E-01  1.0000E+01  1.0910E+00
266           4.9798E-01  4.2069E+00  5.0000E+00  7.8063E-01  1.0000E+01
267           4.5297E+00  1.0000E+01  1.0000E+00  1.6629E-02  1.1417E-01
268           1.5308E-01  8.6710E-02  1.1643E-01  1.1718E-01  6.1331E-01
269           3.8956E+00  4.1442E+00  1.4354E-01  2.2398E-01  8.9739E-02
270           7.6703E-02  5.9417E-02  8.6870E-02  1.5346E-01  2.1836E-01
271           4.8156E-02  5.0000E+00  1.7541E-01  4.6714E-02  4.9562E+00
272           1.2614E-01  6.6703E-02  5.0000E+00  2.1338E-01  6.4126E-02
273           1.0000E+01  1.0000E+01  1.0000E+01  1.0000E+01  1.0000E+01
274           1.0000E+01  5.0000E+00  3.1885E+00  1.0448E+00  6.8880E-02
275           4.7691E-02  1.6627E-02  5.2557E-02  1.7966E-02 -1.0000E+00
276          -1.0000E+00 -1.0000E+00 -1.0000E+00 -1.0000E+00 -1.0000E+00
277 SDEF POS=-356.87 232.02 157.4 DIR=D1 ERG=FDIR=D2 RAD=D3 VEC=0 1 0
278      SUR=16
279 SI1  A   -1.0000 -.99619 -.98481 -.96593 -.93969
280          -.90631 -.86603 -.81915 -.76604 -.70711
281          -.64279 -.57358 -.50000 -.42262 -.34202
282          -.25882 -.17365 -.08716  .00000  .08716
283           .17365  .25882  .34202  .42262  .50000
284           .57358  .64279  .70711  .76604  .81915
285           .86603  .90631  .93969  .96593  .98481
286           .99619  1.0000
287 SP1       .874 .874 .875 .876 .877
288           .879 .882 .884 .888 .891
289           .895 .899 .904 .909 .914
290           .919 .924 .930 .935 .941
291           .946 .952 .957 .962 .967
292           .972 .976 .981 .985 .988
293           .991 .994 .996 .998 .999
294          1.0 1.0
295 DS2  Q   -.99619 180 -.98481 175 -.96593 170 -.93962 165 -.90631 160
296          -.86603 155 -.81915 150 -.76604 145 -.70711 140 -.64279 135
297          -.57358 130 -.50000 125 -.42262 120 -.34202 115 -.25882 110
298          -.17365 105 -.08716 100  0.0000 95   .08716 90   .17365 85
299           .25882 80   .34202 75   .42262 70   .50000 65   .57358 60
300           .64279 55   .70711 50   .76604 45   .81915 40   .86603 35
301           .90631 30   .93969 25   .96593 20   .98481 15   .99619 10
302          1.0000 5
303 SI3  H 0 .64
304 SP3  D -21 1
305 SI5  H 15.106 15.110
306 SP5  D 0 1
307 SI10 H 15.095 15.106
308 SP10 D 0 1
309 SI15 H 15.075 15.095
310 SP15 D 0 1
311 SI20 H 15.049 15.075
312 SP20 D 0 1
313 SI25 H 15.015 15.049
314 SP25 D 0 1
315 SI30 H 14.974 15.015
316 SP30 D 0 1
317 SI35 H 14.927 14.974
318 SP35 D 0 1
319 SI40 H 14.873 14.927
320 SP40 D 0 1
```

Table A4. (cont.)

```
SI45 H 14.814 14.873
SP45 D 0 1
SI50 H 14.750 14.814
SP50 D 0 1
SI55 H 14.681 14.750
SP55 D 0 1
SI60 H 14.608 14.681
SP60 D 0 1
SI65 H 14.532 14.608
SP65 D 0 1
SI70 H 14.453 14.532
SP70 D 0 1
SI75 H 14.372 14.453
SP75 D 0 1
SI80 H 14.289 14.372
SP80 D 0 1
SI85 H 14.206 14.289
SP85 D 0 1
SI90 H 14.123 14.206
SP90 D 0 1
SI95 H 14.040 14.123
SP95 D 0 1
SI100 H 13.958 14.040
SP100 D 0 1
SI105 H 13.878 13.958
SP105 D 0 1
SI110 H 13.800 13.878
SP110 D 0 1
SI115 H 13.725 13.800
SP115 D 0 1
SI120 H 13.654 13.725
SP120 D 0 1
SI125 H 13.586 13.654
SP125 D 0 1
SI130 H 13.522 13.586
SP130 D 0 1
SI135 H 13.464 13.522
SP135 D 0 1
SI140 H 13.410 13.464
SP140 D 0 1
SI145 H 13.362 13.410
SP145 D 0 1
SI150 H 13.320 13.362
SP150 D 0 1
SI155 H 13.284 13.320
SP155 D 0 1
SI160 H 13.254 13.284
SP160 D 0 1
SI165 H 13.230 13.254
SP165 D 0 1
SI170 H 13.214 13.230
SP170 D 0 1
SI175 H 13.203 13.214
SP175 D 0 1
SI180 H 13.200 13.203
SP180 D 0 1
F5:N  -356.87 386.52 157.4 1
FT5   GEB .03 .08
FQ5   E D
WWG  5 121 0 -356.87 386.52 157.4
E5     .85 .95 1.05 1.15 1.25 1.35 1.45 1.55 1.65 1.75 1.85 1.95
       2.15 2.35 2.55 2.75 2.95 3.15 3.35 3.55 3.75 3.95 4.15 4.45
       4.75 5.05 5.35 5.65 5.95 6.25 6.55 6.85 7.25 7.75 8.25 8.75
       9.25 9.75 10.25 10.75 11.25 11.75 12.55 13.35 14.15 14.95
       15.75 16.55
EM5    1 10 10R 5 10R 3.33 8R 2.5 2 8R 1.25 5R
C     F15:P -356.87 386.52 157.4 1
C     E15     .72 .76 .80 .84 .88 .92 .96 1.0 1.04 1.08 1.15 1.2 1.25
C      1.3 1.35 1.4 1.45 1.5 1.55 1.6 1.65 1.72 1.8 1.88 1.96
C      2.04 2.12 2.2 2.28 2.36 2.45 2.55 2.65 2.75 2.85 2.95 3.05
C      3.15 3.25 3.35 3.45 3.55 3.66 3.79 3.93 4.06 4.19 4.32
C      4.45 4.58 4.71 4.84 4.97 5.1 5.23 5.4 5.57 5.74 5.91 6.08
C      6.25 6.42 6.6 6.8 7.0 7.2 7.4 7.6 7.8 8.0 8.2 8.4 8.6 8.8 9.0
C      9.2 9.4 9.6 9.8 10
C     EM15   1 25 8R 14.286 20 9R 14.286 12.5 7R 11.111 10 10R 9.0909 7.6923
C      7.1429 7.6923 9R 5.8824 6R 5.5556 5 16R
CUT:N 1E33 .850 $ IGNORE NEUTRONS BELOW THE DETECTOR RESPONSE
PRDMP  2J 1
M1     1001 7.86E-3
       8016 4.39E-2
```

Table A4. (cont.)

```
401          11023 1.05E-3
402          12000 1.40E-4
403          13027 2.39E-3
404          14000 1.58E-2
405          19000 6.90E-4
406          20000 2.92E-3
407          26000 3.10E-4
408 M3       26000 8.48E-2
409 M4       24000 1.77E-2
410          25055 1.77E-3
411          26000 6.02E-2
412          28000 7.83E-3
413 M2        7014 3.64E-5
414           8016 9.74E-6
415 M5       1001 5.926E-2
416          6000 3.338E-2
417          8016 1.125E-2
418          3006 5.565E-4
419          3007 6.944E-3
420 M6        1001 7.13E-2
421           6000 3.41E-2
422           5010 4.87E-4
423           5011 1.97E-3
424 PRINT
425 NPS      1000000
426
427
```

Table A4. (cont.)

```
FUSION SPECTRA PROBLEM
     1 1 7.506E-2 1 -2 10 -21 -22 29 $ FLOOR CELL $
     2 1 7.506E-2 7 -8 10 -21 -22 29 $ CEILING CELL $
     3 1 7.506E-2 2 -7 10 -21 -22 23 $ LEFT WALL CELL $
     4 1 7.506E-2 2 -7 10 -21 -28 29 $ RIGHT WALL CELL $
     5 1 7.506E-2 2 -7 20 -21 -23 28 $ FRONT WALL CELL $
     6 2 4.614E-5 2 -4 10 -11 -23 32 $ LEFT DOOR CELL $
     7 2 4.614E-5 2 -4 10 -11 -33 34 $ MIDDLE DOOR CELL $
     8 2 4.614E-5 2 -4 10 -11 -35 28 $ RIGHT DOOR CELL $
     9 1 7.506E-2 4 -7 10 -11 -23 32 $ CONCRETE ABOVE LEFT DOOR $
    10 1 7.506E-2 4 -7 10 -11 -33 34 $ CONCRETE ABOVE MIDDLE DOOR
    11 1 7.506E-2 4 -7 10 -11 -35 28 $ CONCRETE ABOVE RIGHT DOOR
    12 1 7.506E-2 2 -4 10 -11 -32 33 $ CONCRETE CELL BETWN L/M DOORS
    13 1 7.506E-2 2 -4 10 -11 -34 35 $ CONCRETE CELL BETWN M/R DOORS
    14 1 7.506E-2 4 -7 10 -11 -32 33 $ WALL CONCRETE ABOVE CELL 12
    15 1 7.506E-2 4 -7 10 -11 -34 35 $ WALL CONCRETE ABOVE CELL 13
    16 2 4.614E-5 2 -4 11 -12 -23 32 $ AIR CELL BTWN LEFT DOOR & BLOCK BACK
    17 2 4.614E-5 2 -4 11 -12 -33 34 $ AIR CELL BTWN MIDDLE DOOR & BLOCK BACK
    18 2 4.614E-5 2 -4 11 -12 -35 28 $ AIR CELL BTWN RIGHT DOOR & BLOCK BACK
    19 2 4.614E-5 2 -4 11 -12 -32 33 $ AIR CELL BTWN CELL12 DOOR & BLOCK BACK
    20 2 4.614E-5 2 -4 11 -12 -34 35 $ AIR CELL BTWN CELL13 DOOR & BLOCK BACK
    21 2 4.614E-5 4 -7 11 -12 -23 32 $ AIR CELL BTWN CELL 9 DOOR & BLOCK BACK
    22 2 4.614E-5 4 -7 11 -12 -33 34 $ AIR CELL BTWN CELL10 DOOR & BLOCK BACK
    23 2 4.614E-5 4 -7 11 -12 -35 28 $ AIR CELL BTWN CELL11 DOOR & BLOCK BACK
    24 2 4.614E-5 4 -7 11 -12 -32 33 $ AIR CELL BTWN CELL14 DOOR & BLOCK BACK
    25 2 4.614E-5 4 -7 11 -12 -34 35 $ AIR CELL BTWN CELL15 DOOR & BLOCK BACK
    26 2 4.614E-5 6 -7 12 -15 -23 32 $ CELLS 26-35: AIR CELLS ABV THE BLOCK
    27 2 4.614E-5 6 -7 12 -15 -32 33
    28 2 4.614E-5 6 -7 12 -15 -33 34
    29 2 4.614E-5 6 -7 12 -15 -34 35
    30 2 4.614E-5 6 -7 12 -15 -35 28
    31 2 4.614E-5 6 -7 15 -17 -23 32
    32 2 4.614E-5 6 -7 15 -17 -32 33
    33 2 4.614E-5 6 -7 15 -17 -33 34
    34 2 4.614E-5 6 -7 15 -17 -34 35
    35 2 4.614E-5 6 -7 15 -17 -35 28
    36 2 4.614E-5 2 -3 12 -15 -23 32 $ CELLS 36-47: AIR CELLS LEFT OF BLOCK
    37 2 4.614E-5 2 -3 12 -15 -32 24
    38 2 4.614E-5 2 -3 15 -17 -23 32
    39 2 4.614E-5 2 -3 15 -17 -32 24
    40 2 4.614E-5 3 -4 12 -15 -23 32
    41 2 4.614E-5 3 -4 12 -15 -32 24
    42 2 4.614E-5 3 -4 15 -17 -23 32
    43 2 4.614E-5 3 -4 15 -17 -32 24
    44 2 4.614E-5 4 -6 12 -15 -23 32
    45 2 4.614E-5 4 -6 12 -15 -32 24
    46 2 4.614E-5 4 -6 15 -17 -23 32
    47 2 4.614E-5 4 -6 15 -17 -32 24
    48 2 4.614E-5 2 -3 12 -15 -27 35 $ CELLS 48-59: AIR CELLS RIGHT OF BLOCK
    49 2 4.614E-5 2 -3 12 -15 -35 28
    50 2 4.614E-5 2 -3 15 -17 -27 35
    51 2 4.614E-5 2 -3 15 -17 -35 28
    52 2 4.614E-5 3 -4 12 -15 -27 35
    53 2 4.614E-5 3 -4 12 -15 -35 28
    54 2 4.614E-5 3 -4 15 -17 -27 35
    55 2 4.614E-5 3 -4 15 -17 -35 28
    56 2 4.614E-5 4 -6 12 -15 -27 35
    57 2 4.614E-5 4 -6 12 -15 -35 28
    58 2 4.614E-5 4 -6 15 -17 -27 35
    59 2 4.614E-5 4 -6 15 -17 -35 28
    60 2 4.614E-5 6 -7 17 -40 -23 32 $ CELLS 60-69: AIR CELLS ABV THERMAL SHIELD
    61 2 4.614E-5 6 -7 17 -40 -32 33
    62 2 4.614E-5 6 -7 17 -40 -33 34
    63 2 4.614E-5 6 -7 17 -40 -34 35
    64 2 4.614E-5 6 -7 17 -40 -35 28
    65 2 4.614E-5 6 -7 40 -20 -23 32
    66 2 4.614E-5 6 -7 40 -20 -32 33
    67 2 4.614E-5 6 -7 40 -20 -33 34
    68 2 4.614E-5 6 -7 40 -20 -34 35
    69 2 4.614E-5 6 -7 40 -20 -35 28
    70 2 4.614E-5 2 -3 17 -40 -23 32 $ CELLS 70-81: AIR CELLS LEFT OF THERMAL SHIELD
    71 2 4.614E-5 2 -3 17 -40 -32 24
    72 2 4.614E-5 2 -3 40 -20 -23 32
    73 2 4.614E-5 2 -3 40 -20 -32 24
    74 2 4.614E-5 3 -4 17 -40 -23 32
    75 2 4.614E-5 3 -4 17 -40 -32 24
    76 2 4.614E-5 3 -4 40 -20 -23 32
    77 2 4.614E-5 3 -4 40 -20 -32 24
    78 2 4.614E-5 4 -6 17 -40 -23 32
    79 2 4.614E-5 4 -6 17 -40 -32 24
```

Table A5. Fusion shielding benchmark setup for configuration 7 with an off-axis photon detector.

```
 81     80 2 4.614E-5 4 -6 40 -20 -23 32
 82     81 2 4.614E-5 4 -6 40 -20 -32 24
 83     82 2 4.614E-5 2 -3 17 -40 -27 35 $ CELLS 82-93: AIR CELLS RIGHT OF THERMAL SHIELD
 84     83 2 4.614E-5 2 -3 17 -40 -35 28
 85     84 2 4.614E-5 2 -3 40 -20 -27 35
 86     85 2 4.614E-5 2 -3 40 -20 -35 28
 87     86 2 4.614E-5 3 -4 17 -40 -27 35
 88     87 2 4.614E-5 3 -4 17 -40 -35 28
 89     88 2 4.614E-5 3 -4 40 -20 -27 35
 90     89 2 4.614E-5 3 -4 40 -20 -35 28
 91     90 2 4.614E-5 4 -6 17 -40 -27 35
 92     91 2 4.614E-5 4 -6 17 -40 -35 28
 93     92 2 4.614E-5 4 -6 40 -20 -27 35
 94     93 2 4.614E-5 4 -6 40 -20 -35 28
 95     94 4 8.75E-2 3 -5 -25 26 15 -41 $ CELLS 94-103: AIR AND SHIELD CELLS INSIDE
 96     95 4 8.75E-2 3 -5 -25 26 41 -42 $ THE CONCRETE BOX
 97     96 4 8.75E-2 3 -5 -25 26 42 -43
 98     97 4 8.75E-2 3 -5 -25 26 43 -44
 99     98 6 .11150 3 -5 -25 26 44 -45
100     99 4 8.75E-2 3 -5 -25 26 45 -46
101    100 6 .11150 3 -5 -25 26 46 -47
102    101 4 8.75E-2 3 -5 -25 26 47 -48
103   1021 2 4.614E-5 3 -5 -25 26 461 -462
104   1022 2 4.614E-5 3 -5 -25 26 462 -463
105   1023 2 4.614E-5 3 -5 -25 26 463 -49
106    102 2 4.614E-5 3 -5 -25 26 48 -461
107    103 2 4.614E-5 3 -5 -25 26 49 -17
108    104 2 4.614E-5 3 -9 -25 26 17 -18 $ AIR CELL BTWN INNER BOX AND THERMAL SHIELD
109    105 2 4.614E-5 3 -9 -30 31 19 -40 $ CELLS 105-106: AIR CELLS FITTING BETWEEN
110    106 2 4.614E-5 3 -9 -30 31 40 -20 $ THE THERMAL SHIELD AND THE FRONT WALL
111    107 2 4.614E-5 9 -6 -24 27 17 -18 $ CELLS 107-109: AIR CELLS BETWEEN THE UPPER
112    108 2 4.614E-5 9 -6 -24 27 18 -40 $ HORIZONTAL EDGE OF THE CONCRETE BLOCK
113    109 2 4.614E-5 9 -6 -24 27 40 -20 $ AND THE FRONT WALL
114    110 2 4.614E-5 2 -3 -24 27 17 -18 $ CELLS 110-112: AIR CELLS BETWEEN THE
115    111 2 4.614E-5 2 -3 -24 27 18 -40 $ LOWER HORIZONTAL EDGE OF THE CONCRETE
116    112 2 4.614E-5 2 -3 -24 27 40 -20 $ BOX  AND THE FRONT WALL
117    113 2 4.614E-5 3 -9 -24 25 17 -18 $ CELLS 113-118: AIR CELLS BETWEEN THE
118    114 2 4.614E-5 3 -9 -24 25 18 -40 $ RIGHT AND LEFT VERTICAL CONCRETE BOX
119    115 2 4.614E-5 3 -9 -24 25 40 -20 $ WALLS AND THE FRONT WALL
120    116 2 4.614E-5 3 -9 -26 27 17 -18
121    117 2 4.614E-5 3 -9 -26 27 18 -40
122    118 2 4.614E-5 3 -9 -26 27 40 -20
123    119 0 -36 12 -13 $ VACUUM INSIDE BEAMLINE
124    120 0 -36 13 -14 $ VACUUM INSIDE IRON CAN
125    121 0 14 -15 -38 $ VACUUM INSIDE IRON PIPE
126    122 3 8.48E-2 36 -37 12 -13 $ BEAMLINE
127    123 3 8.48E-2 36 -39 13 -14 $ IRON CAN
128    124 3 8.48E-2 38 -39 14 -15 $ IRON PIPE
129    125 5 1.1139E-1 37 -39 12 -13
130    126 1 7.506E-2 5 -6 12 -15 -24 33 $ CELLS 126-134: CONCRETE BOX TOP CELLS
131    127 1 7.506E-2 5 -6 12 -15 -33 34
132    128 1 7.506E-2 5 -6 12 -15 -34 27
133    129 1 7.506E-2 5 -6 15 -45 -24 33
134    130 1 7.506E-2 5 -6 15 -45 -33 34
135    131 1 7.506E-2 5 -6 15 -45 -34 27
136    132 1 7.506E-2 5 -6 45 -17 -24 33
137    133 1 7.506E-2 5 -6 45 -17 -33 34
138    134 1 7.506E-2 5 -6 45 -17 -34 27
139    135 1 7.506E-2 2 -3 12 -15 -24 33 $ CELLS 135-143: CNCR BOX BOTTOM CELLS
140    136 1 7.506E-2 2 -3 12 -15 -33 34
141    137 1 7.506E-2 2 -3 12 -15 -34 27
142    138 1 7.506E-2 2 -3 15 -45 -24 33
143    139 1 7.506E-2 2 -3 15 -45 -33 34
144    140 1 7.506E-2 2 -3 15 -45 -34 27
145    141 1 7.506E-2 2 -3 45 -17 -24 33
146    142 1 7.506E-2 2 -3 45 -17 -33 34
147    143 1 7.506E-2 2 -3 45 -17 -34 27
148    144 1 7.506E-2 -24 25 3 -50 12 -15 $ CELLS 144-149: CONCRETE BOX LEFT
149    145 1 7.506E-2 -24 25 3 -50 15 -45 $ VERTICAL WALL CELLS
150    146 1 7.506E-2 -24 25 3 -50 45 -17
151    147 1 7.506E-2 -24 25 50 -5 12 -15
152    148 1 7.506E-2 -24 25 50 -5 15 -45
153    149 1 7.506E-2 -24 25 50 -5 45 -17
154    150 1 7.506E-2 -26 27 3 -50 12 -15 $ CELLS 150-155: CONCRETE BOX RIGHT
155    151 1 7.506E-2 -26 27 3 -50 15 -45 $ VERTICAL WALL CELLS
156    152 1 7.506E-2 -26 27 3 -50 45 -17
157    153 1 7.506E-2 -26 27 50 -5 12 -15
158    154 1 7.506E-2 -26 27 50 -5 15 -45
159    155 1 7.506E-2 -26 27 50 -5 45 -17
160    156 1 7.506E-2 3 -5 -25 26 39 12 -51 $ CELLS 156-164: INNER CONCRETE BOX CELLS
```

Table A5. (cont.)

```
161    157 1 7.506E-2 3 -5 -25 26 39 51 -52
162    158 1 7.506E-2 3 -5 -25 26 39 52 -53
163    159 1 7.506E-2 3 -5 -25 26 39 53 -54
164    160 1 7.506E-2 3 -5 -25 26 39 54 -55
165    161 1 7.506E-2 3 -5 -25 26 39 55 -56
166    162 1 7.506E-2 3 -5 -25 26 39 56 -57
167    163 1 7.506E-2 3 -5 -25 26 39 57 -58
168    164 1 7.506E-2 3 -5 -25 26 39 58 -15
169 C          165 2 4.614E-5 9 -5 -25 26 18 -40 $ CELLS 165-170: AIR CELLS CENTERED
170 C          166 2 4.614E-5 9 -5 -25 26 40 -20 $ AROUND THE THERMAL SHIELD
171    167 2 4.614E-5 -25 30 3 -9 18 -40
172    168 2 4.614E-5 -25 30 3 -9 40 -20
173    169 2 4.614E-5 -31 26 3 -9 18 -40
174    170 2 4.614E-5 -31 26 3 -9 40 -20
175    171 4 8.75E-2 18 -19 3 -9 -30 31 $ THERMAL SHIELD
176    172 0 -1  $ VOID CELL BELOW THE CONCRETE ROOM
177    173 0  8 $ VOID CELL ABOVE THE CONCRETE ROOM
178    174 0  1 -8 -22 29 -10 $ VOID CELL BEHIND THE REAR WALL
179    175 0  1 -8 -22 29 21  $ VOID CELL IN FRONT OF THE FRONT WALL
180    176 0  1 -8 22 $ VOID CELL LEFT OF THE ROOM
181    177 0  1 -8 -29 $ VOID CELL RIGHT OF THE ROOM
182
183      1 PZ -91.44
184      2 PZ 0 $ UPPER FLOOR PLANE
185      3 PZ 81.2 $ INNER BOX BOTTOM/LOWER THERMAL SHIELD EDGE
186      4 PZ 218.4 $ DOOR UPPER EDGE
187      5 PZ 253.92 $ INNER BOX TOP
188      6 PZ 317.50 $ CONCRETE BOX TOP
189      7 PZ 495.30 $ CEILING PLANE (LOWER)
190      8 PZ 586.74 $ CEILING PLANE (UPPER)
191      9 PZ 233.60 $ UPPER THERMAL SHIELD EDGE
192     10 PY -29.21 $ REAR WALL PLANE (REAR)
193     11 PY 0 $ REAR WALL PLANE (FRONT)
194     12 PY 160.02 $ REAR OF CONCRETE BOX
195     13 PY 208.28 $ END OF PARAFFIN
196     14 PY 225.56 $ REAR EDGE OF IRON CAN
197     15 PY 253.06 $ END OF IRON PIPE/REAR OF INNER BOX
198     16 PY 232.02 $ PLANE OF TARGET
199     17 PY 353.06 $ FRONT OF CONCRETE BOX
200     18 PY 436.52 $ FRONT OF THERMAL SHIELD
201     19 PY 441.60 $ REAR OF THERMAL SHIELD
202     20 PY 570.20 $ FRONT WALL PLANE (INSIDE)
203     21 PY 661.64 $ FRONT WALL PLANE (OUTSIDE)
204     22 PX 91.44  $ LEFT WALL PLANE (OUTSIDE)
205     23 PX 0      $ LEFT WALL PLANE (INSIDE)
206     24 PX -200.66 $ LEFT SIDE OF CONCRETE BOX
207     25 PX -278.76 $ LEFT SIDE OF INNER BOX
208     26 PX -434.97 $ RIGHT SIDE OF INNER BOX
209     27 PX -513.08 $ RIGHT SIDE OF CONCRETE BOX
210     28 PX -716.28 $ RIGHT WALL PLANE (INSIDE)
211     29 PX -807.72 $ RIGHT WALL PLANE (OUTSIDE)
212     30 PX -280.66 $ LEFT EDGE OF THERMAL SHIELD
213     31 PX -433.06 $ RIGHT EDGE OF THERMAL SHIELD
214     32 PX -114.3  $ RIGHT EDGE OF LEFT DOOR
215     33 PX -300.99 $ LEFT EDGE OF MIDDLE DOOR
216     34 PX -415.29 $ RIGHT EDGE OF MIDDLE DOOR
217     35 PX -601.98 $ LEFT EDGE OF RIGHT DOOR
218     36 C/Y -356.87 157.4 4.5   $ BEAMLINE INNER SURFACE
219     37 C/Y -356.87 157.4 5.0   $ BEAMLINE OUTER SURFACE
220     38 C/Y -356.87 157.4 8.87  $ IRON PIPE INNER SURFACE
221     39 C/Y -356.87 157.4 16.37 $ IRON PIPE OUTER SURFACE
222     40 PY 470
223     41 PY 263.06
224     42 PY 273.06
225     43 PY 283.54
226     44 PY 288.62
227     45 PY 293.70
228     46 PY 298.78
229     47 PY 303.86
230     48 PY 308.94
231    461 PY 313.06
232    462 PY 323.06
233    463 PY 333.06
234     49 PY 343.06
235     50 PZ 160
236     51 PY 170
237     52 PY 180
238     53 PY 190
239     54 PY 200
240     55 PY 210
```

Table A5. (cont.)

```
    56 PY 220
    57 PY 230
    58 PY 240

MODE N P
FQ15 E D
WWP:N 4 3 2
WWE:N  1.0000E+02
WWN 1:N   2.0095E-02  1.8297E-02  1.7990E-02  2.0387E-02  1.2851E-02
          3.5458E-02  4.9062E-02  2.7750E-02  1.4900E-02  5.0724E-02
          8.1984E-03  5.1868E-02  2.9800E-02  3.4876E-02  3.3713E-02
          2.0850E-02  3.4570E-02  2.3080E-02  3.4280E-02  3.3759E-02
          2.0452E-02  3.3400E-02  1.6036E-02  2.5698E-02  2.7006E-02
          1.5145E-02  1.8960E-02  1.9005E-02  2.0394E-02  2.0230E-02
          1.2365E-02  1.3174E-02  1.1058E-02  1.1972E-02  1.8518E-02
          1.6737E-02  1.3354E-02  1.0041E-02  1.3508E-02  1.7272E-02
          1.4719E-02  9.7106E-03  1.2294E-02  1.6645E-02  1.5639E-02
          9.1845E-03  1.0519E-02  1.2503E-02  2.3776E-02  4.1766E-03
          4.8962E-03  1.6941E-02  8.7442E-03  9.8376E-03  6.9572E-03
          1.9680E-02  1.7259E-02  9.0353E-03  1.4159E-02  1.2960E-02
          1.0844E-02  8.3020E-03  1.0444E-02  1.5688E-02  1.0810E-02
          1.1129E-02  9.4641E-03  1.2360E-02  7.1350E-03  1.1356E-02
          5.1180E-03  1.4116E-02  4.7282E-03  8.5175E-03  6.3173E-03
          9.0316E-03  5.6538E-03  9.6547E-03  6.6240E-03  9.4339E-03
          7.4456E-03  5.7355E-03  1.0871E-02  4.8980E-03  9.0258E-03
          7.5130E-03  7.7076E-03  9.4855E-03  9.5437E-03  9.5587E-03
          1.4105E-02  6.8502E-03  9.6726E-03  3.3084E-01  1.4178E-01
          6.6977E-02  4.3756E-02  2.5004E-02  9.7556E-03  6.4306E-03
          2.0487E-03  2.2281E-03  2.6707E-03  2.7235E-03  1.9927E-03
          2.2858E-03  3.3952E-03  3.6595E-03  4.4616E-03  6.9805E-03
          8.4251E-03  9.5313E-03  3.2920E-03  4.7711E-03  5.4201E-03
          4.2025E-03  2.6823E-03  4.6731E-03  4.8163E-03  3.6405E-03
          7.1145E-03  8.0156E-01  1.1310E+00  5.0000E-01  9.2102E-01
          4.3313E+00  9.2380E-01  2.4301E+00  5.8427E-02  6.9832E-02
          9.4885E-02  1.3553E-02  2.5584E-02  4.2011E-02  6.4868E-03
          3.5495E-03  7.8429E-03  1.3477E-01  8.3048E-01  1.6597E-01
          1.9306E-02  2.3706E-02  9.9729E-02  6.2699E-03  1.8664E-03
          7.6870E-03  2.8462E-01  1.5787E-02  3.0824E-03  1.4005E-01
          1.8673E-02  3.7565E-03  9.3237E-01  5.8835E-02  7.6910E-03
          4.9075E-01  7.5566E-02  5.9833E-03  7.5176E-02  1.5131E-01
          3.2187E-01  1.0449E+00  2.6840E+00  6.3348E+00  5.4851E+00
          3.5436E+00  1.6361E+00  2.3821E-03  1.9917E-03  5.1201E-03
          7.8998E-03  1.7050E-03 -1.0000E+00 -1.0000E+00 -1.0000E+00
         -1.0000E+00 -1.0000E+00 -1.0000E+00
WWP:P 4 3 2
WWE:P  1.0000E+02
WWN 1:P   5.9921E-02  1.          1.7990E-01  2.0387E-01  2.5223E-02
          3.5458E-01  4.9062E-01  2.7750E-01  1.4900E-01  5.0724E-01
          8.1984E-02  5.1868E-01  2.9800E-01  3.4876E-01  3.3713E-01
          1.2702E-02  3.4570E-01  1.          3.4280E-01  3.3759E-01
          2.0452E-01  3.3400E-01  1.6036E-01  2.5698E-01  2.7006E-01
          1.5145E-01  1.8960E-01  8.5269E-03  2.0394E-01  2.0230E-01
          1.2365E-01  1.3174E-01  9.3632E-03  1.          5.9070E-01
          1.          1.3354E-01  1.0041E-01  1.3508E-01  1.2796E-02
          1.          3.3066E-03  2.6466E-03  1.6645E-01  1.5639E-01
          9.1845E-02  1.0519E-01  1.2503E-01  2.3776E-01  4.1766E-02
          4.8962E-02  1.          1.          1.          5.7162E-02
          1.9680E-01  1.          5.9070E-01  1.          1.2960E-01
          1.0844E-01  8.3020E-02  1.0444E-01  6.8184E-03  4.9990E-03
          1.1129E-01  9.4641E-02  2.3175E-01  7.1350E-02  1.1356E-01
          5.1180E-02  2.7990E-03  4.7282E-02  8.5175E-02  6.3173E-02
          1.1981E-02  2.3692E-03  9.6547E-02  6.6240E-02  9.4339E-02
          7.4456E-02  6.6348E-03  8.6149E-05  6.3494E-03  2.5646E-02
          5.4199E-03  1.4629E-02  7.6893E-03  4.0702E-03  1.9072E-02
          1.8812E-02  3.5022E-02  9.6726E-02  1.          8.9318E-01
          9.0313E-02  6.7821E-03  2.1073E-03  1.8369E-03  7.0249E-04
          6.4368E-04  1.3576E-02  2.1587E-02  2.4684E-02  4.9392E-03
          2.7274E-02  7.4889E-03  4.5022E-04  7.9289E-04  6.9805E-02
          3.3233E-03  2.8143E-03  4.1061E-02  4.7711E-02  3.4264E-03
          4.2025E-02  2.2479E-03  3.5523E-03  3.8798E-03  2.1790E-03
          4.5197E-03  8.0156E+00  1.1310E+01  5.9498E+02  9.2102E+00
          4.3313E+01  2.5533E+04  2.4301E+01  5.8427E-01  6.9832E-01
          9.4885E-01  8.2818E-02  4.7811E-03  1.          5.5352E-03
          5.1845E-03  7.5160E-02  1.3477E+00  8.3048E+00  1.6597E+00
          1.          1.5150E-01  1.1108E+00  2.6462E-03  3.1892E-03
          1.8636E-02  6.8808E-01  1.9139E-02  2.0843E-03  1.4005E+00
          3.5037E-02  1.5764E-03  9.3237E+00  1.          1.1226E-02
          4.9075E+00  3.3736E-02  5.7535E-03  7.5176E-01  1.5131E+00
          1.          1.0449E+01  2.6840E+01  1.          1.
          1.          1.          1.3427E-04  1.9917E-02  1.2236E-03
```

Table A5. (cont.)

```
321            1.1834E-03  5.0315E-04 -1.0000E+00 -1.0000E+00 -1.0000E+00
322           -1.0000E+00 -1.0000E+00 -1.0000E+00
323 SDEF POS=-356.87 232.02 157.4 DIR=D1 ERG=FDIR=D2 RAD=D3 VEC=0 1 0
324      SUR=16
325 SI1  A  -1.0000 -.99619 -.98481 -.96593 -.93969
326           -.90631 -.86603 -.81915 -.76604 -.70711
327           -.64279 -.57358 -.50000 -.42262 -.34202
328           -.25882 -.17365 -.08716  .00000  .08716
329            .17365  .25882  .34202  .42262  .50000
330            .57358  .64279  .70711  .76604  .81915
331            .86603  .90631  .93969  .96593  .98481
332            .99619 1.0000
333 SP1        .860 .860 .861 .862 .864
334           .866 .868 .872 .875 .879
335           .883 .888 .893 .898 .904
336           .910 .916 .922 .928 .934
337           .940 .946 .952 .958 .963
338           .969 .974 .978 .983 .987
339           .990 .993 .996 .997 .999
340           1.0  1.0
341 DS2  Q  -.99619 180 -.98481 175 -.96593 170 -.93962 165 -.90631 160
342           -.86603 155 -.81915 150 -.76604 145 -.70711 140 -.64279 135
343           -.57358 130 -.50000 125 -.42262 120 -.34202 115 -.25882 110
344           -.17365 105 -.08716 100  0.0000 95   .08716 90   .17365 85
345            .25882 80   .34202 75   .42262 70   .50000 65   .57358 60
346            .64279 55   .70711 50   .76604 45   .81915 40   .86603 35
347            .90631 30   .93969 25   .96593 20   .98481 15   .99619 10
348           1.0000 5
349 SI3  H 0 .64
350 SP3  D -21 1
351 SI5  H 15.236 15.240
352 SP5  D 0 1
353 SI10 H 15.223 15.236
354 SP10 D 0 1
355 SI15 H 15.201 15.223
356 SP15 D 0 1
357 SI20 H 15.171 15.201
358 SP20 D 0 1
359 SI25 H 15.132 15.171
360 SP25 D 0 1
361 SI30 H 15.086 15.132
362 SP30 D 0 1
363 SI35 H 15.033 15.086
364 SP35 D 0 1
365 SI40 H 14.973 15.033
366 SP40 D 0 1
367 SI45 H 14.906 14.973
368 SP45 D 0 1
369 SI50 H 14.834 14.906
370 SP50 D 0 1
371 SI55 H 14.756 14.834
372 SP55 D 0 1
373 SI60 H 14.647 14.756
374 SP60 D 0 1
375 SI65 H 14.589 14.674
376 SP65 D 0 1
377 SI70 H 14.500 14.589
378 SP70 D 0 1
379 SI75 H 14.409 14.500
380 SP75 D 0 1
381 SI80 H 14.316 14.409
382 SP80 D 0 1
383 SI85 H 14.223 14.316
384 SP85 D 0 1
385 SI90 H 14.130 14.223
386 SP90 D 0 1
387 SI95 H 14.037 14.130
388 SP95 D 0 1
389 SI100 H 13.945 14.037
390 SP100 D 0 1
391 SI105 H 13.856 13.945
392 SP105 D 0 1
393 SI110 H 13.769 13.856
394 SP110 D 0 1
395 SI115 H 13.685 13.769
396 SP115 D 0 1
397 SI120 H 13.605 13.685
398 SP120 D 0 1
399 SI125 H 13.529 13.605
400 SP125 D 0 1
```

Table A5. (cont.)

```
401 SI130 H 13.459 13.529
402 SP130 D 0 1
403 SI135 H 13.393 13.459
404 SP135 D 0 1
405 SI140 H 13.334 13.393
406 SP140 D 0 1
407 SI145 H 13.280 13.334
408 SP145 D 0 1
409 SI150 H 13.233 13.280
410 SP150 D 0 1
411 SI155 H 13.193 13.233
412 SP155 D 0 1
413 SI160 H 13.160 13.193
414 SP160 D 0 1
415 SI165 H 13.134 13.160
416 SP165 D 0 1
417 SI170 H 13.115 13.134
418 SP170 D 0 1
419 SI175 H 13.104 13.115
420 SP175 D 0 1
421 SI180 H 13.100 13.104
422 SP180 D 0 1
423 C      F5:N  -356.87 386.52 157.4 1
424 C      E5      .85 .95 1.05 1.15 1.25 1.35 1.45 1.55 1.65 1.75 1.85 1.95
425 C       2.15 2.35 2.55 2.75 2.95 3.15 3.35 3.55 3.75 3.95 4.15 4.45
426 C       4.75 5.05 5.35 5.65 5.95 6.25 6.55 6.85 7.25 7.75 8.25 8.75
427 C       9.25 9.75 10.25 10.75 11.25 11.75 12.55 13.35 14.15 14.95
428 C       15.75 16.55
429 C      EM5     1 10 10R 5 10R 3.33 8R 2.5 2 8R 1.25 5R
430 F15:P -310.87 386.52 157.4 1
431 FT15   GEB .017 .0288
432 E15     .72 .76 .80 .84 .88 .92 .96 1.0 1.04 1.08 1.15 1.2 1.25
433         1.3 1.35 1.4 1.45 1.5 1.55 1.6 1.65 1.72 1.8 1.88 1.96
434         2.04 2.12 2.2 2.28 2.36 2.45 2.55 2.65 2.75 2.85 2.95 3.05
435         3.15 3.25 3.35 3.45 3.55 3.66 3.79 3.93 4.06 4.19 4.32
436         4.45 4.58 4.71 4.84 4.97 5.1 5.23 5.4 5.57 5.74 5.91 6.08
437         6.25 6.42 6.6 6.8 7.0 7.2 7.4 7.6 7.8 8.0 8.2 8.4 8.6 8.8 9.0
438         9.2 9.4 9.6 9.8 10
439 EM15    1 25 8R 14.286 20 9R 14.286 12.5 7R 11.111 10 10R 9.0909 7.6923
440         7.1429 7.6923 9R 5.8824 6R 5.5556 5 16R
441 PHYS:P  J 1
442 CUT:P 1E33 .750 $ IGNORE PHOTONS BELOW THE DETECTOR RESPONSE
443 WWG   15 121 0 -310.87 386.52 157.4
444 M1     1001 7.86E-3
445        8016 4.39E-2
446       11023 1.05E-3
447       12000 1.40E-4
448       13027 2.39E-3
449       14000 1.58E-2
450       19000 6.90E-4
451       20000 2.92E-3
452       26000 3.10E-4
453 M3    26000 8.48E-2
454 M4    24000 1.77E-2
455       25055 1.77E-3
456       26000 6.02E-2
457       28000 7.83E-3
458 M2     7014 3.64E-5
459        8016 9.74E-6
460 M5    1001 5.926E-2
461       6000 3.338E-2
462       8016 1.125E-2
463       3006 5.565E-4
464       3007 6.944E-3
465 M6     1001 7.13E-2
466        6000 3.41E-2
467        5010 4.87E-4
468        5011 1.97E-3
469 PRINT
470 PRDMP 2J 1
471 NPS   500000
472
```

Table A5. (cont.)

```
 1 */ MCNP4 patch to revise response function for fusion shielding problem.
 2 */              Written by John S. Hendricks, 8/91.
 3 */ Changes FT GEB a b (gaussian energy broadening) response from
 4 */          a + b*sqrt(E)      to      sqrt(a*E**2 + b*E)
 5 */
 6 *ident rrffsp
 7 */ ------------------------------------------------------------ tallyd
 8 *d,td.207 line 23685
 9       erg=erg+.60056120439322*sqrt(tds(l+1)*erg**2+tds(l+2)*erg)*
10 */
11 */ ------------------------------------------------------------  tally
12 *d,ty.68 line 24421
13       erg=erg+.60056120439322*sqrt(tds(l+1)*erg**2+tds(l+2)*erg)*
14 */
15 */ ------------------------------------------------------------ finpht
16 *d,cor4-1.185 line 25172
17       t=t+.60056120439322*sqrt(tds(l+1)*erg**2+tds(l+2)*t)*
```

Table A6. Patch to modify the MCNP gaussian detector response function.

```
 1 GODIVA
 2 1      1 -18.7400  -1  IMP:N=1
 3 2      0  1  IMP:N=0
 4
 5 1      SO 8.741000
 6
 7 M1     92235. -93.7100 92238. -5.27 92234. -1.02
 8 KCODE 3000 1.0 60  150
 9 KSRC  0. 0. 0.
10 PRINT
11
```

Table A7. Lady Godiva fast neutron critical assembly setup, 93.71% U-235 sphere.

```
 1 JEZEBEL 4.5% ENRICHED PU-240
 2 1      1 -15.61 -1 IMP:N=1
 3 2      0 1 IMP:N=0
 4
 5 1      SO 6.385
 6
 7 M1     94240. -4.5 94239. -95.5
 8 KCODE 3000 1.0 80 110
 9 KSRC  0. 0. 0.
10 PRINT
11
```

Table A8. Jezebel fast neutron critical assembly setup, 95.5% Pu-239.

```
 1 JEZEBEL 20% ENRICHED PU-240
 2 1      1 -15.73 -1 IMP:N=1
 3 2      0 1 IMP:N=0
 4
 5 1      SO 6.660
 6
 7 M1     94240. -20 94239 -80
 8 KCODE 3000 1.0 60 150
 9 KSRC  0. 0. 0.
10 PRINT
11
```

Table A9. Jezebel fast neutron critical assembly setup, 80% Pu-239.

```
 1 URANIUM CYLINDER 10.90% ENRICHED
 2 1      1 -18.63 -1 2 -3 IMP:N=1
 3 2      0 -4 #1 IMP:N=1
 4 3      0 4 IMP:N=0
 5
 6 1      CY 26.65
 7 2      PY 0
 8 3      PY 119.392
 9 4      SO 130
10
11 M1     92235. -10.9 92238. -89.1
12 KCODE  9000 1 25 40
13 SDEF   AXS 0 1 0 POS 0 60 0 EXT D1 RAD D2
14 SI1    55
15 SI2    .1 26
16 PRINT
17
```

Table A10. Low-enrichment uranium cylinder critical assembly setup, 10.9% U-235.

```
 1 URANIUM CYLINDER 14.11% ENRICHED
 2 1      1 -18.41 -1 2 -3 IMP:N=1
 3 2      0 -4 #1 IMP:N=1
 4 3      0 4 IMP:N=0
 5
 6 1      CY 26.65
 7 2      PY 0
 8 3      PY 44.239
 9 4      SO 55
10
11 M1     92235. -14.11 92238. -85.89
12 KCODE 9000 1 5 15
13 SDEF   AXS 0 1 0 POS 0 22 0 EXT D1 RAD D2
14 SI1    22
15 SI2    .1 26
16 PRINT
17
```

Table A11. Low-enrichment uranium cylinder critical assembly setup, 14.1% U-235.

```
 1 GRAPHITE REFLECTED URANIUM SPHERE 93.9% ENRICHED
 2 1      1 -18.6 -1 IMP:N=1
 3 2      2 -1.67 1 -2 IMP:N=1
 4 3      0 2 IMP:N=0
 5
 6 1      SO 7.39840
 7 2      SO 12.49840
 8 3      SO 55
 9
10 M1     92235. -93.5
11        92238. -6.5
12 M2     6012. -99.5
13        26000. -.34
14        16032. -.16
15 MT2    GRPH.01T
16 KCODE  3000 1.0 30 50
17 SDEF   AXS 0 1 0  POS 0 0 0 EXT D1 RAD D2
18 SI1    6
19 SI2    6
20 PRINT
21
```

Table A12. Graphite-tamped reflected-uranium sphere critical assembly setup.

```
 1 WATER REFLECTED SPHERE
 2 1      1 0.04815 -1 IMP:N=1
 3 2      2 0.10019 1 -2 -3 4 IMP:N=1
 4 3      0 -5 (2:3:-4) IMP:N=1
 5 4      0 5 IMP:N=0
 6
 7 1      SO 6.5537
 8 2      CY 30
 9 3      PY 35
10 4      PY -35
11 5      SO 50
12
13 M1     92234. .00053 92235. .04703 92236. .0001 92238. .00049
14 M2     1001. .06679 8016. .0334
15 MT2    LWTR
16 KCODE 3000 1.0 30 90
17 KSRC   0. 0. 0.
18 PRINT
19
```

Table A13. Water-reflected uranium sphere critical assembly setup.

```
 1 U CYLINDERS U-93.2 IN AIR
 2 1      1 -1.131 -1 3 -4 IMP:N=1 U=-1
 3 2      2 -2.71 1:-3:4 IMP:N=1  U=1
 4 7      0 -2 8 -9 FILL=1 IMP:N=1
 5 5      0 -7 #7 #8 #9 IMP:N=1
 6 6      0 7 IMP:N=0
 7 8      LIKE 7 BUT TRCL=1
 8 9      LIKE 7 BUT TRCL=2
 9
10 1      CY 10.15
11 2      CY 10.30
12 3      PY 0.0
13 8      PY -.15
14 9      PY 41.55
15 4      PY 41.40
16 7      SO 150
17
18 M1     92235. .000383
19        92238. .0000276
20        9019. .000821
21        1001. .1183
22        8016. .05990
23 M2     13027. 1.0
24 TR1    20.98 0 0
25 TR2    10.49 0 18.169
26 KCODE 10000 .7 30 90
27 SDEF   AXS 0 1 0 POS D1 RAD D2 EXT D3
28 SP1    0.33 .33 .34
29 SI1    L 0 20.7 0  20.98 20.7 0. 10.49 20.7 18.169
30 SI2    8
31 SI3   15
32 PRINT
33
```

Table A14. Three interacting uranium cylinders critical assembly setup.

```
 1 3X3X3 PLUTONIUM ARRAY
 2 1      6 -2.710 -1 2 5 -27 IMP:N=1 U=-1
 3 2      2 -.5400 3 -4 -38  IMP:N=1
 4 3      6 -2.375 4 -44 -38   IMP:N=1
 5 4      7 -4.800 -2 5 -6  IMP:N=1 U=-1
 6 5      1 -2.5000 6 -7 -8 9  IMP:N=1 U=-1
 7 6      4 -.001 6 -7 -9  IMP:N=1 U=-1
 8 7      1 -2.5000 -8 7 -10  IMP:N=1 U=-1
 9 8      2 -7.870 -8 10 -11  IMP:N=1 U=-1
10 9      8 -19.6 -12 11 -14  IMP:N=1 U=-1
11 10     6 -2.710 12 -13 11 -14  IMP:N=1 U=-1
12 11     5 -2.640 -8 14 -15  IMP:N=1 U=-1
13 12     1 -2.5000 -8 9 15 -16  IMP:N=1 U=-1
14 13     4 -.001 8 -2 -16 14  IMP:N=1 U=-1
15 14     4 -.001 13 -2 -14 11 IMP:N=1 U=-1
16 15     4 -.001 8 -2 -11 6  IMP:N=1 U=-1
17 16     4 -.001 -9 15 -16  IMP:N=1 U=-1
18 17     0       37  IMP:N=0
19 19     4 -.001 -37 #2 #3 #41 #51 #52 #53 #54 #55 #56 #57 #58  IMP:N=1
20 20     1 -2.5000 -8 16 -17 IMP:N=1 U=-1
21 21     2 -7.870  -8 17 -18 IMP:N=1 U=-1
22 22     8 -19.6   -12 18 -19 IMP:N=1 U=-1
23 23     5 -2.640  -8 19 -20 IMP:N=1 U=-1
24 24     4 -.001   -9 20 -21 IMP:N=1 U=-1
25 25     1 -2.5000 -8 21 -22 IMP:N=1 U=-1
26 26     2 -7.870   -8 22 -23   IMP:N=1 U=-1
27 27     8 -19.6  -12 23 -24 IMP:N=1 U=-1
28 28     5 -2.640 -8 24 -25 IMP:N=1 U=-1
29 29     4 -.001 -9 25 -26 IMP:N=1 U=-1
30 30     7 -4.810 -2 26 -27 IMP:N=1 U=-1
31 32     6 -2.710 -13 12 -19 18 IMP:N=1 U=-1
32 33     1 -2.500 -8 9 20 -21 IMP:N=1 U=-1
33 34     6 -2.710 -13 12 -24 23  IMP:N=1 U=-1
34 35     1 -2.500 -8 9 25 -26 IMP:N=1 U=-1
35 36     4 -.001 8 -2 -26 24 IMP:N=1 U=-1
36 37     4 -.001 13 -2 23 -24 IMP:N=1 U=-1
37 38     4 -.001 8 -2 -23 19 IMP:N=1 U=-1
38 39     4 -0.001 13 -2 -19 18 IMP:N=1 U=-1
39 40     4 -.001 8 -2 -18 16 IMP:N=1 U=-1
40 41     0    -42 -43 44  FILL=1 IMP:N=1
41 42      0 (1:27:-5)  U=1 IMP:N=1
42 51      LIKE 41 BUT TRCL=1
43 52      LIKE 41 BUT TRCL=2
44 53      LIKE 41 BUT TRCL=3
45 54      LIKE 41 BUT TRCL=4
46 55     LIKE 41 BUT TRCL=5
47 56     LIKE 41 BUT TRCL=6
48 57     LIKE 41 BUT TRCL=7
49 58     LIKE 41 BUT TRCL=8
50
51 1      C/Y 3.609 3.609 3.609
52 2      C/Y 3.609 3.609 3.425
53 3      PY 0.0
54 4      PY 30.0
55 5      PY 32.540
56 6      PY 40.795
57 7      PY 47.725
58 8      C/Y 3.609 3.609 3.326
59 9      C/Y 3.609 3.609 3.104
60 10     PY 48.360
61 11     PY 48.381
62 12     C/Y 3.60900 3.609 3.26250
63 13     C/Y 3.60900 3.609 3.29950
64 14     PY 53.014
65 15     PY 53.580
66 16     PY 55.425
67 38     C/Y 3.609 3.609 80
68 37     SO 500
69 17     PY 56.060
70 18     PY 56.081
71 19     PY 60.714
72 20     PY 61.280
73 21     PY 63.125
74 22     PY 63.760
75 23     PY 63.781
76 24     PY 67.714
77 25     PY 68.280
78 26     PY 70.125
79 27     PY 78.380
80 42     C/Y 3.609 3.609 3.6100
```

Table A15. 3 x 3 array of plutonium fuel rods critical assembly setup.

```
 81 43    PY 78.3810
 82 44    PY 32.539
 83
 84 TR1   9.6 0. 0.
 85 TR2   19.2 0. 0.
 86 TR3   0. 0. 9.6
 87 TR4   9.6 0 9.6
 88 TR5   19.2 0 9.6
 89 TR6   0 0 19.2
 90 TR7   9.6 0 19.2
 91 TR8   19.2 0 19.2
 92 M3    7014. -0.78 8016. -0.21 18000. -0.01
 93 M1    24000. -.002 29000. -.0025  26000. -.007 12000. -.010 25055. -.0015
 94       14000. -.006 22000. -.0015 13027. -.9670
 95 M2    6012. -.0008 25055. -.0037 15031. -.00015 14000. -.0001 16032.
 96       -.00025 50000. -.0030 26000. -.992
 97 M5    29000. -.0025  26000. -.007 12000. -.0105 25055. -.0125 14000. -.003
 98         13027. -.9630
 99 M4    24000. -.001 29000. -.0025  26000. -.007 12000. -.01025 25055. -.007
100       14000. -.0045   22000. -.00075 13027. -.9645
101 M7    94239. -.9356
102       94240. -.0597
103       94241. -.0046
104       94242. -.0001
105 M6    6012. -.0003 25055. -.005 15031. -.00005 14000. -.0033 16032.
106       -.00009 50000. -.0011 26000. -.3554 24000. -.0007 29000. -.028
107       12000. -.0097 13027. -.5945032
108 KCODE 3000 0.5 60 150
109 SDEF  AXS= 0 1 0 POS=16.4 50 16.4 EXT=D1 RAD=D2
110 SI1   14
111 SI2   .001 16
112 PRINT
113
```

Table A15. (cont.)

Los Alamos
NATIONAL LABORATORY
Los Alamos, New Mexico 87545